PREPARATION AND CHARACTERIZATION OF RICE HUSK ASH FILLED NATURAL RUBBER FILM: EFFECT OF CROSS-LINKING AGENTS ON MECHANICAL AND ELECTRICAL PROPERTIES

Miss Praewpakun Sintharm

จุฬาลงกรณ์มหาวิทยาลัย
CHULALONGKORN UNIVERSITY

A Dissertation Submitted in Partial Fulfillment of the Requirements
for the Degree of Doctor of Engineering in Chemical Engineering
Department of Chemical Engineering
FACULTY OF ENGINEERING
Chulalongkorn University
Academic Year 2020

การเตรียมและการศึกษาสมบัติของฟิล์มยางธรรมชาติที่เติมเถ้าแกลบ: ผลของสารเชื่อมขวางต่อสมบัติเชิงกลและด้านไฟฟ้า

น.ส.แพรวพกุล ศิลธรรม

วิทยานิพนธ์นี้เป็นส่วนหนึ่งของการศึกษาตามหลักสูตรปริญญาวิศวกรรมศาสตรดุษฎีบัณฑิต
สาขาวิชาวิศวกรรมเคมี ภาควิชาวิศวกรรมเคมี
คณะวิศวกรรมศาสตร์ จุฬาลงกรณ์มหาวิทยาลัย
ปีการศึกษา 2563
ลิขสิทธิ์ของจุฬาลงกรณ์มหาวิทยาลัย

Thesis Title	PREPARATION AND CHARACTERIZATION OF RICE HUSK ASH FILLED NATURAL RUBBER FILM: EFFECT OF CROSS-LINKING AGENTS ON MECHANICAL AND ELECTRICAL PROPERTIES
By	Miss Praewpakun Sintharm
Field of Study	Chemical Engineering
Thesis Advisor	Professor MUENDUEN PHISALAPHONG, Ph.D.

Accepted by the FACULTY OF ENGINEERING, Chulalongkorn University in Partial Fulfillment of the Requirement for the Doctor of Engineering

.... Dean of the FACULTY OF ENGINEERING
(Professor SUPOT TEACHAVORASINSKUN, D.Eng.)

DISSERTATION COMMITTEE

.... Chairman
(Associate Professor Sarute Ummartyotin, Ph.D.)

.... Thesis Advisor
(Professor MUENDUEN PHISALAPHONG, Ph.D.)

.... Examiner
(Professor ARTIWAN SHOTIPRUK, Ph.D.)

.... Examiner
(Assistant Professor PIMPORN PONPESH, Ph.D.)

.... External Examiner
(Assistant Professor Suchata Kirdponpattara, D.Eng.)

จุฬาลงกรณ์มหาวิทยาลัย

CHULALONGKORN UNIVERSITY

แพรวพกุล ศิลธรรม : การเตรียมและการศึกษาสมบัติของฟิล์มยางธรรมชาติที่เติมเถ้าแกลบ: ผลของสารเชื่อม
ขวางต่อสมบัติเชิงกลและด้านไฟฟ้า. (PREPARATION AND CHARACTERIZATION
OF RICE HUSK ASH FILLED NATURAL RUBBER FILM: EFFECT
OF CROSS-LINKING AGENTS ON MECHANICAL AND
ELECTRICAL PROPERTIES) อ.ที่ปรึกษาหลัก : ศ. ดร.เหมือนเดือน พิศาลพงศ์

      ยางธรรมชาติ (NR) เป็นหนึ่งในพอลิเมอร์จากพืชที่สำคัญมากที่สุด ซึ่งถูกนำไปใช้อย่างแพร่หลายสำหรับเป็น
วัตถุดิบของผลิตภัณฑ์หลายประเภทเนื่องจากมีความยืดหยุ่นดีเยี่ยม เถ้าแกลบ (RHA) เป็นหนึ่งในวัสดุเหลือทิ้งทางการเกษตร
ที่สำคัญจากโรงสีข้าว เพื่อเป็นการเพิ่มมูลค่าให้กับยางธรรมชาติและเถ้าแกลบ การศึกษานี้จึงมีวัตถุประสงค์นำเถ้าแกลบชนิด
ต่าง ๆ (เถ้าแกลบดำ (BRHA), เถ้าแกลบขาว (WRHA) และเถ้าแกลบดำที่ผ่านการปรับสภาพด้วยกรด
(BRHAT)) มาใช้เป็นสารตัวเติมในยางธรรมชาติ ด้วยการเติมอัลจิเนตเป็นสารปรับความข้นหนืดและเป็นสารช่วยการ
กระจายตัวของเถ้าแกลบ ปริมาณเถ้าแกลบสูงสุดที่ 100 ส่วนเทียบกับยาง 100 ส่วนโดยน้ำหนัก (phr) สามารถเติมลงไป
ในเนื้อยางธรรมชาติโดยไม่มีการแยกส่วน นอกจากนี้ในงานวิจัยยังศึกษาผลของการเชื่อมขวางคอมโพสิตยางธรรมชาติด้วย
แคลเซียมคลอไรด์เปรียบเทียบกับกระบวนการเชื่อมขวางที่ใช้ทั่วไปโดยการวัลคาไนซ์ด้วยกำมะถัน ต่อสมบัติเชิงกลและสมบัติ
ทางไฟฟ้าของคอมโพสิตยางธรรมชาติ สมบัติเชิงกลของคอมโพสิตยางธรรมชาติที่เติมเถ้าแกลบในส่วนของความทนต่อแรงดึง
มอดูลัสของยัง และความยืดสูงสุด ณ จุดขาดมีค่าเพิ่มขึ้นเมื่อเทียบกับแผ่นฟิล์มยางธรรมชาติล้วน สมบัติเชิงกลของคอมโพสิต
ยางธรรมชาติที่เสริมแรงด้วยเถ้าแกลบขาวมีค่าสูงกว่าสมบัติเชิงกลของคอมโพสิตยางธรรมชาติที่เสริมแรงด้วยเถ้าแกลบดำและ
เถ้าแกลบดำที่ผ่านการปรับสภาพด้วยกรดตามลำดับ การเชื่อมขวางด้วยแคลเซียมคลอไรด์ให้ผลสำเร็จในคอมโพสิตยางที่เติมเถ้า
แกลบขาว โดยสามารถปรับปรุงสมบัติความทนต่อแรงดึงและความทนทานต่อสารเคมีของคอมโพสิตได้เทียบเท่ากับสมบัติของ
ฟิล์มยางธรรมชาติที่ผ่านการวัลคาไนซ์ด้วยกำมะถัน คอมโพสิตยางธรรมชาติสามารถย่อยสลายทางชีวภาพได้ในดิน โดยมี
น้ำหนักที่หายไปร้อยละ 7.6 ถึง 18.3 เมื่อเทียบกับน้ำหนักเริ่มต้นหลังจากฝังดินเป็นระยะเวลา 3 เดือน ค่าคงที่ไดอิเล็ก
ตริก แฟกเตอร์การสูญเสียไดอิเล็กตริก และค่าการนำไฟฟ้าของคอมโพสิตเพิ่มขึ้นตามปริมาณของเถ้าแกลบ อย่างไรก็ตาม
ค่าคงที่ไดอิเล็กตริก แฟกเตอร์การสูญเสีย ไดอิเล็กตริกและค่าการนำไฟฟ้าของคอมโพสิตยางธรรมชาติที่เติมเถ้าแกลบลดลงอย่าง
มีนัยสำคัญหลังจากเชื่อมขวางคอมโพสิตด้วยแคลเซียมคลอไรด์และวัลคาไนซ์ด้วยกำมะถัน นอกจากนี้ยังได้พัฒนาแบคทีเรีย
เซลลูโลส (BC) ที่เสริมแรงด้วยหางน้ำยางธรรมชาติและน้ำยางธรรมชาติสด (SNRL/FNRL) โดยเป็นการรวมสมบัติ
เชิงกลที่โดดเด่นของโครงสร้างตาข่ายเส้นใยขนาดนาโนเมตรของแบคทีเรียเซลลูโลสที่ซ้อนกันหลายชั้นและสมบัติความยืดหยุ่น
สูงของยางธรรมชาติ โดยเมื่อเทียบกับน้ำยางธรรมชาติสด หางน้ำยางธรรมชาติสามารถแพร่ผ่านรูของโครงตาข่ายแบคทีเรีย
เซลลูโลสได้ง่ายกว่า ข้อดีมากมายที่ได้จากการเสริมแรงด้วยหางน้ำยางธรรมชาติ คือ มีสมบัติเชิงกลและความทนทานต่อสารเคมี
ที่ดี และมีสมบัติไดอิเล็กทริกตริกที่ดีขึ้นอย่างเห็นได้ชัด ฟิล์มแบคทีเรียเซลลูโลสที่เสริมแรงด้วยหางน้ำยางธรรมชาติสามารถย่อย
สลายได้ทางชีวภาพและสามารถย่อยสลายได้ในดินเป็นส่วนใหญ่หรือย่อยสลายทั้งหมดภายใน 6 สัปดาห์ ฟิล์มคอมโพสิตที่ถูก
พัฒนาขึ้นในการศึกษานี้แสดงศักยภาพการนำไปประยุกต์ต่อไปเป็นฟิล์มพอลิเมอร์กึ่งตัวนำและอุปกรณ์อิเล็กทรอนิกส์ที่ยืดหยุ่น
ได้สำหรับใช้ในงานด้านอิเล็กทรอนิกส์

สาขาวิชา	วิศวกรรมเคมี	ลายมือชื่อนิสิต ....
ปีการศึกษา	2563	ลายมือชื่อ อ.ที่ปรึกษาหลัก ....

5971437521 : MAJOR CHEMICAL ENGINEERING
KEYWORD: Rice husk ash, Natural rubber latex, Alginate, crosslinking, Skim natural rubber latex, Fresh natural rubber latex, Bacterial cellulose, Mechanical properties, dielectric properties, Electrical properties

Praewpakun Sintharm : PREPARATION AND CHARACTERIZATION OF RICE HUSK ASH FILLED NATURAL RUBBER FILM: EFFECT OF CROSS-LINKING AGENTS ON MECHANICAL AND ELECTRICAL PROPERTIES . Advisor: Prof. MUENDUEN PHISALAPHONG, Ph.D.

Natural rubber (NR) is one of the most important polymers produced by plants and is widely utilized as raw material for many products due to its excellent flexibility. Rice husk ash (RHA) is one of the major agricultural residues generated from the rice milling plant. In order to add value to NR and RHA, this study aims to use different types of RHA (black rice husk ash (BRHA), white rice husk ash (WRHA) and BRHA treated by acid washing (BRHAT)) as filler in NR composites. By the addition of alginate as a thickening and dispersing agent, a maximum of 100 per hundred rubbers (phr) of RHA could be integrated in NR matrix without phase separation. In addition, this study investigated the effects of crosslinking NR composite by $CaCl_2$ compared to the common crosslinking process by sulfur vulcanization on mechanical and electrical properties of NR composites. Mechanical properties of the composite films with RHAs in terms of tensile strength, Young's modulus and elongation at break were considerably enhanced, compared to the neat NR film. The composite films reinforced with WRHA demonstrated relatively better mechanical properties than those reinforced with BRHA and BRHAT, respectively. The crosslinking by $CaCl_2$ was achieved on NR–WRHA, in which tensile strength and chemical resistance of the composite films were improved close to properties of sulfur vulcanized NR films. The NR composites were biodegradable in soil, with weight loss of 7.6–18.3% of the initial dry weight after 3 months. Dielectric constant, dielectric loss factors and electrical conductivity of the composites were enhanced with RHAs loading. However, dielectric constant, dielectric loss factor and electrical conductivity of NR composites with RHAs had dropped significantly after crosslinking the composites by $CaCl_2$ or by sulfur vulcanization. Moreover, bacterial cellulose (BC) reinforced with skim/fresh natural rubber latex (SNRL/FNRL) were future developed by combining the prominent mechanical properties of multilayer BC nanofibrous structural networks and the high elasticity of NR. As compared to FNRL, SNRL could easily diffuse through the pores of a BC network. Many good benefits were obtained for the reinforcement with SNRL, including good mechanical properties, chemical resistance and noticeably improved dielectric properties. The SNRL-BC films are biodegradable and could be mostly or totally decomposed in soil within 6 weeks. The composite films developed in this study display potential for further application as semiconducting polymer films and flexible electronic devices for electronic applications.

Field of Study:	Chemical Engineering	Student's Signature	
Academic Year:	2020	Advisor's Signature	

ACKNOWLEDGEMENTS

<div align="right">Praewpakun Sintharm</div>

TABLE OF CONTENTS

Page

LIST OF FIGURES

LIST OF TABLES

จุฬาลงกรณ์มหาวิทยาลัย

CHULALONGKORN UNIVERSITY

LIST OF ABBREVIATIONS

BRHA	Black rice husk ash from rice milling plant
BRHAT	Black rice husk ash treated by acid washing
WRHA	White rice husk ash that obtains from controlled combustion of rice husk
RHA	Rice husk ash
NRL	Natural rubber latex
Phr	Parts per hundred of rubber
DRC	Dry rubber content
BC	Bacterial cellulose
SNRL	Skim natural rubber latex
FNRL	Fresh natural rubber latex
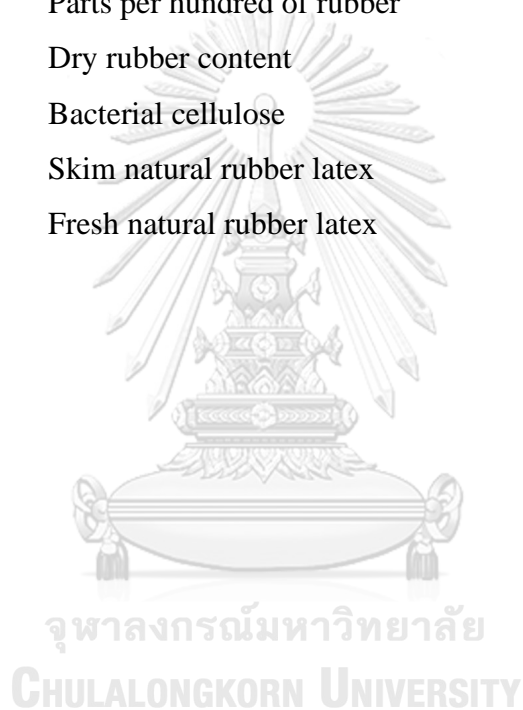
CHAPTER I
INTRODUCTION

1.1 Motivations

Thailand is the world's largest producer and exporter of natural rubber because the environment of Thailand is highly conducive to rubber tree cultivation. In 2017, over 4.5 million tons of natural rubbers were produced in the country (about 37% of global production) [1]. Rubber is exported in several basic forms including ribbed smoked sheets, concentrated latex and compound rubber. Thailand natural rubber prices have been falling for several years because of oversupply from major rubber producing countries and weak global economy. Therefore, the Thailand government has the policy to increase the value of natural rubber by using a variety of technologies for improving natural rubber properties or transforming natural rubber latex to high value products.

Natural rubber is one of the important elastomers and it is widely utilized to prepare many rubber products such as vehicle tires to belts, condoms, gloves, health equipment and accessories, coatings and floor covering [2]. Natural rubber is non-saturated rubber because its structural unit contains double bond. Natural rubber has very low aging resistance because ozone and oxygen can react with double bond very easily. Therefore, the chemical structure of natural rubber is often modified by vulcanization process and/or it has been reinforced by adding filler for improved properties [3]. Carbon black and silica are synthetic fillers, commonly used as reinforcing fillers in rubber industries. Currently, natural fillers become a good choice of reinforcing agent in natural rubber because they are biodegradable, environment friendly, inexpensive and reducing domestic waste [4].

In agricultural countries, rice husk is one of the major agricultural residues generated from the rice milling process. Rice husk is mostly used as a biomass fuel in the milling plants and power plant. A by-product from burnt rice husk is called rice husk ash [5]. Rice husk ash is mainly composed of silica (SiO_2) (over 80-90%) and carbon black. Rice husk ash has been studied to be used as reinforcing filler in natural rubber composites. Previously, natural rubber composites were produced from natural

rubber mixed with rice husk ash in solid form by two-roll mill (conventional process). The limitations of this method are the low filler loading (not over 60 phr) and inferior dispersion of filler in natural rubber composite [6-9]. The latex compounding method was then developed to solve the problem of incompatibility between rubber and filler and to improve the dispersion of fillers in the natural rubber matrices. Moreover, the latex compounding method had lower energy consumption during mixing when compared to the conventional process [10].

Alginate is a polysaccharide and has widespread applications in the food and drinks, cosmetic, pharmaceutical and bioengineering industries because it has unique structure, biocompatibility and biodegrade-ability [11]. Alginate has been commonly used as thickening agent and gelling agent. It is soluble in water and becomes hydrogel at various temperatures. Each amount of its usage for applications is lower in comparison to other substances. Modification by crosslinking is expected to widen its application [12].

Silica as dielectric metal oxide semiconductor has dielectric constant about 3-9 and is used in micro and nano electronic industries [13]. Recently, the electric and dielectric properties have attracted much interest because they are important in predicting the behavior of the product as material for the application in microelectronics, batteries, sensors, fuel cells and super capacitors [14].

The aims of this study are to improve mechanical and chemical properties of natural rubber composite films reinforced with different types of rice husk ash via a latex aqueous micro-dispersion process. In order to obtain good dispersion of polar fillers in a nonpolar NR matrix, sodium alginate, one of the most commonly used natural polysaccharides, was employed as a thickening and dispersing agent in the mixture. Through the use of this technique, high concentrations of fillers can be added into the NR matrix without phase separation. The effects of reinforcing NR composites with RHAs and different crosslinking agent on the chemical, mechanical, biodegradation and dielectric properties were investigated for further development of the composite films.

1.2 Objectives

- To prepare and investigate chemical and mechanical properties of natural rubber composites filled with different types of rice husk ash prepared via a latex aqueous micro-dispersion process

- To compare electrical properties of the fabricated natural rubber composites treated with different cross-linking agents

1.3 Scopes of this research

- Rice husk ashes in this research are

    1) BRHA is original black rice husk ash from rice milling plant.

    2) BRHAT is BRHA that is treated by acid washing, using hydrochloric acid for removing impurities.

    3) WRHA is obtained from the controlled combustion of rice husk under the burning temperature at 500°C for a period of ≈ 2 hours.

- Preparation of natural rubber composites via a latex aqueous micro-dispersion process.

- Utilization of alginate for filler dispersion.

- Investigation for effects of types of fillers (BRHA, BRHT and WRHA) and the amount of filler loading at 0, 20, 60 and 100 phr.

- Investigation for effects of crosslink agents in natural rubber crosslinking processes (sulfur vulcanized and alginate crosslinked with $CaCl_2$).

- Characterization of chemical and mechanical properties of natural rubber composites:

    1) Chemical properties

        ▪ Morphology

        ▪ Overall components

        ▪ Particle size distribution

        ▪ Structural information

        ▪ Functional groups and possible interaction between fillers and natural rubber

        ▪ The solvent uptake

        ▪ Water absorption

        ▪ Biodegradation in soil

2) Mechanical properties

- Tensile strength
- Young modulus
- Elongation at the break

3) Electrical conductivity, dielectric constant and dielectric loss of natural rubber composite were studied.

CHAPTER II
BACKGROUND AND LITERATURE REVIEWS

2.1 Natural rubber

The major commercial source of natural rubber latex (NRL) is *Hevea brasiliensis* which originated from Amazon Forest in South America. Generally, fresh natural rubber latex (FNRL) is composed of about 30-40 wt% dry rubber content (DRC) and non-rubber components of small amounts of proteins, carbohydrate and lipids as shown in Table 2.1. Non-rubber components in NRL causes latex destabilization due to promotes the growth of bacteria. To ensure long term storage, ammonia is often added to the latex in very small amounts to maintain physical properties and prevent coagulation during transportation and storage [15, 16]. The fresh NR latex is often modified to concentrated natural rubber latex (CNRL) with about 60 wt% DRC by centrifugation as Figure 2.1. After the centrifugation process, the leftover suspension, or skim natural rubber latex (SNRL), is composed of about 4-6 wt% DRC, and typically used to produce lower grade products such as car mats and bicycle wheels. Besides the DRC contents, the latex particle sizes also affect the mechanical properties of NRL [17-19].

Table 2. 1 Composition of fresh natural rubber latex [18]

Compositions	Content (%)
Rubber hydrocarbon	30 - 40
Protein	1.5
Carbohydrate	1.5
Lipids	1.3
Organic solutes	0.5
Inorganic substances	0.5
Water	55 - 60

NR latex is colloidal suspension of rubber particles dispersed in water. Latex colloids from Hevea tree commonly shows a bimodal particle size distribution, which can be classified into small rubber particles (SRP: particle size between 10 and 250 nm) and large rubber particles (LRP: particle size between 250 nm and 3 μm). Specific weight of fresh NR latex is 0.96 – 0.98 g/cm3 and its pH is varying within 6.5 – 7.0.
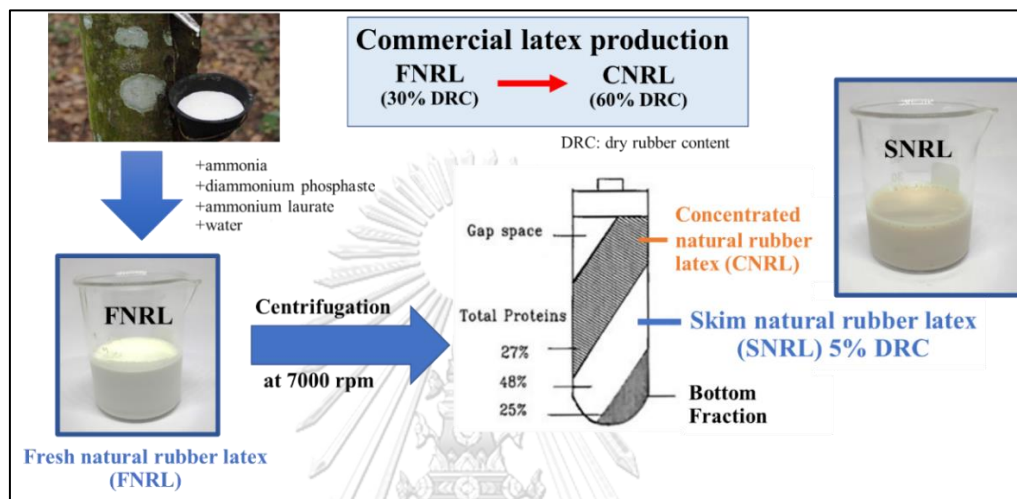
Figure 2. 1 Production of concentrated natural rubber latex

From the centrifugal process, the supernatant SNRL contains mostly small particles (81 wt% SRP + 19 wt% of LRP), whereas FNRL is most composed of large particles (24 wt% SRP + 76 wt% LRP) [17]. The difference in particle size distribution also results in branch point structures after drying, leading to the different characteristics and properties [17, 20].
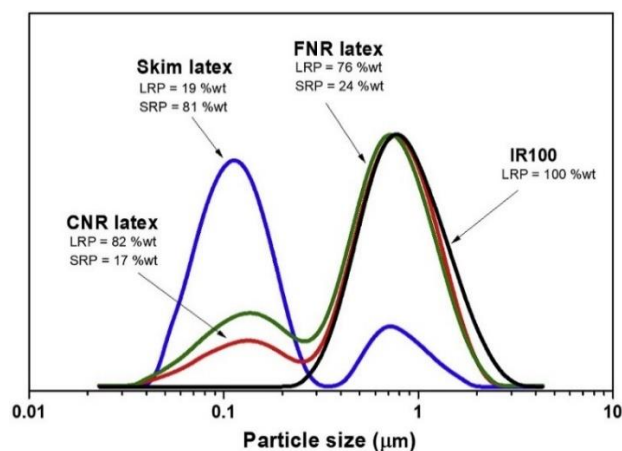
Figure 2. 2 Particle size distributions of FNRL, CNRL, and SNRL compared with synthetic polyisoprene (IR100).

NR has many advantageous properties, such as high elasticity, flexibility at low temperatures, resistance to abrasion, to impact and corrosion, facile adhesion to textiles, insulating properties and ability to disperse heat. The properties of NR are suitable for requirements of multiple products. Therefore, NR is used extensively in many applications and products such as glove, adhesives, health equipment and accessories, coatings, condoms, and floor [21].

NR is a biopolymer of cis-1,4-polyisoprene. The chemical structure of NR is shown in figure 2.3. NR rubber is a highly non-saturated rubber because each its structural unit contains an unsaturated bond or double bond. Thus, it is easy to react with ozone, oxygen and ultraviolet light, which cause its very low aging resistance [3]. For this reason, the properties of NR need to be improved by a process, such as vulcanization and/or another reinforcement process.
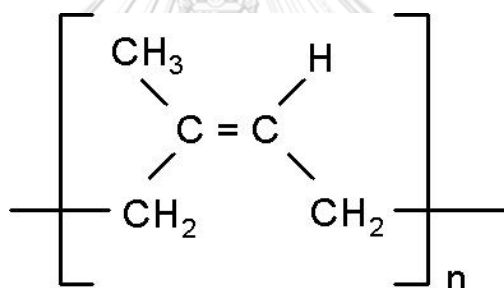
Figure 2. 3 Chemical structure of cis-1,4-polyisoprene

Vulcanization is a reaction that leads to the formation of crosslinks between polymer chains. This process can improve NR mechanical properties such as tensile strength. The vulcanizing agent is originally referred to elemental sulfur. It now also includes non-sulfur systems such as peroxides and metal oxide. A crosslink may be a group of sulfur atoms in a short chain, a single sulfur atom, a carbon-to-carbon bond, a polyvalent organic radical, an ionic cluster, or a polyvalent metal ion [22]. Network formation in vulcanization process is shown in Figure 2.4
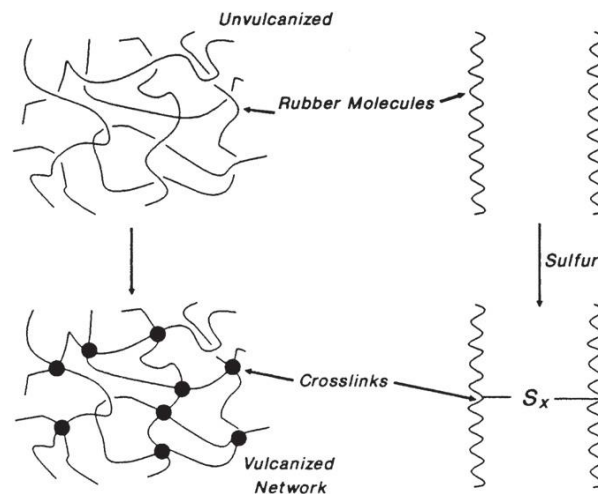
Figure 2. 4 Network formation in vulcanization process

Types of Crosslinking system are described below:

    1) Sulfur system

        The crosslinks depend on sulfur level, accelerator type, accelerator /sulfur ratio and cure time. High accelerator, sulfur ratio and longer cure time increase the mono-and di–sulfidic linkages. Mono and di-sulfidic crosslinks have better solvent and heat resistance, set resistance, reversion resistance but are generally stiffer, hence lower tensile strength, crack resistance. Polysulfidic crosslinks have a better tensile strength, softer, crack resistance but lower set resistance, heat and solvent resistance [22, 23].

    2) Peroxide system

        Unlike sulfur vulcanization, peroxide curing does not require carbon-carbon double bonds to form crosslinks. This system is suitable for both rubbers with or without double bonds. Carbon-carbon crosslinks formed by peroxide give the rubber a stiffer structure (high modulus) [23].

    3) Metal oxide system

        Polychloroprene and carboxylate acrylonitrile rubbers can be crosslinked with metal oxides such as zinc oxide and magnesium oxide. The crosslinks in chloroprene rubber by zinc oxide is covalent bonding while the nitrile rubber is ionic bonding.

        The mechanism of high strength in polysulfidic crosslinks is thought to be the ability to interchange with one another and redistribute local stress. Sulfur, peroxide

and radiation curing systems could produce more intra-molecular C-C links which do not contribute to the mechanical properties [24].

2.2 Rice husk and rice husk ash

Asia is the world's important rice-growing region with approximately 90% of total world output. Thailand has rice plantation area around 60 million rai, which yields output of around 20 million tons of milled rice. Domestic rice consumption in Thailand is around 10 million tons of milled rice (50% of all rice). Export markets include China, the United States, ASEAN countries, and Africa. Export rice are generally of white rice, parboiled rice, and Thai jasmine rice [25].

Rice husk is the outer layer of rice grain, which is an agriculture by-product of the rice milling industry. It is reported that chemical content of rice husk consists of 50% cellulose, 25-30% lignin, and 15-20% silica [26]. The rice husk is also used as a biomass fuel in steam boiler to generate hot steam in the power plant and rice milling plant. Burning rice husk as fuel results in the production of rice husk ash as a waste material.

Rice husk ash produced from burning rice husks at a temperature of 400ºC - 500ºC is in form of amorphous silica. But, by burning at temperatures greater than 1,000ºC, rice husks will turn into crystalline silica. The resulting amorphous silica from rice husk ash is suspected as an important source to produce pure silicon, silicon carbide, and silicon nitride flour [27]. Rice husk ash is rich in silica (SiO_2) over

80-90%. Silica is used in many applications such as in pharmaceutical products, vegetable oil refining, detergents, chromatograph column packing, ceramics etc.[28]. Many research have been developed to produce high purity silica with large surface area using rice husk or rice husk ash such as:

Sankar et al.(in 2016) produced nanosilica powder from three kinds of rice husks. Their methods were: 1) combustion of rice husk in the open, 2) acid leaching and 3) incineration at 700ºC under atmospheric conditions. The results showed that spherical and completely amorphous silica particles with large specific surface area and composed only by Si and O were obtained from all kinds of rice husks [29].

Bakar (in 2016) investigated the conditions to obtain high purity silica from rice husk by acid leaching and incineration at different temperatures under atmospheric conditions. The result indicated that rice husk leached with HCl produced the highest content of amorphous silica (99.6%) at 600 ºC [30] .

Yalçin and Sevinç(in 2001) reported that the highest purity silica from rice husk was obtained with prior acid treatment and incineration in oxygen atmosphere. Silica from this study was amorphous silica particles with maximum specific surface area of 321 m^2/g and 99.7% purity [31].

Fernandes et al. (in 2017) showed that it is possible to produce silica from rice husk ash with purity above 98%, by using simple methods. The treatments that afforded the best results were acid leaching followed by thermal treatment at 800ºC, and alkaline extraction at low temperature, in which products with silica purity of 99.3% and 99.6%, respectively could be obtained [32].

Several studies might use different chemical and thermal treatment approaches, but they all reported that by acid leaching pretreatment followed by oxygen-rich incineration, the combustion of rice husk produced the highest silica content. The atmosphere with the highest partial pressure of oxygen induced the chemical reduction of carbon and was more efficient than the other atmosphere settings [33].

Rice husk ash has high silica contents, and it is available in abundant with low cost. In recent years, rice husk ash has been widely used as construction material such as pozzolana in concrete, or as adsorbent to adsorb organic dye, inorganic metal ions and insulation boards [34]. In addition, rice husk ash is wildly used as natural filler in rubber industry. It can be used as an additive agent for improved tensile strength of natural rubber. Moreover, it is also used to reduce the cost of rubber compounding and reduce wastes from landfills.

2.3 Alginate

Alginates are present in nature as one of the constituents of brown algae (*Phaeophyceae*) and as capsular polysaccharides in soil bacteria. The commercial alginates are currently obtained from algal sources. Alginate is the most abundant

marine biopolymer and occurs in the intercellular mucilage and algal cells of brown seaweeds in the form of calcium, sodium and magnesium salts of alginic acid [11].

The structure of sodium alginate is represented in Figure 2.5. Alginate is a binary linear heteropolysaccharides containing 1,4-linked α-l-guluronic acid and β-d-mannuronic acid. Alginate has been widely used in the field of controlled release, ion exchange, and in the vapor-permeation membrane-separation technique [35, 36]. To make stable water-insoluble alginate products, alginic acid is transformed by incorporating different salts. This produces Na-, K-, NH_4-, Mg-, and Ca- alginate.
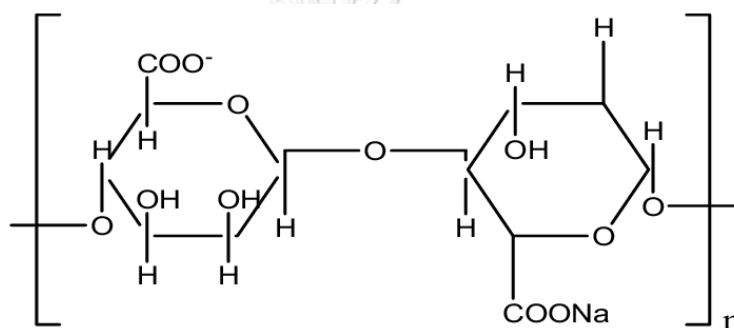
Figure 2. 5 Chemical structure of sodium alginate

Alginate has widespread applications in the food and drinks, pharmaceutical and bioengineering industries [37]. In addition, the crosslinked sodium alginate was highly stable, flexible and easy to use. When sodium alginate is put into a solution of calcium ions, the calcium ions replace the sodium ions in the polymer. Each calcium ion can attach to two of the polymer strands that is called cross-linking alginate. The crosslinking is achieved by the ionic interaction between calcium ions and the carboxyl groups of the blocks of guluronic acid residues of two neighboring alginate chains, resulting in formation of stable three-dimensional network [38, 39]. Ca^{2+} is preferred to crosslink alginate for biomedical applications due to the mild reaction conditions. Calcium salts suitable for crosslinking alginate include $CaCl_2$, $CaSO_4$, $CaCO_3$, calcium acetate, calcium ascorbate etc. [40]. There are a few research studies about blending alginate with natural rubber such as below:

Riyajan and Tangboriboonrat (in 2014) studied about blending NR with sodium alginate solution and coconut waste used as a cofiber for absorption of lead

ions (Pb^{2+}). After being cross-linked by calcium chloride, the beads were highly stable, flexible and easily used in the environment. The cofiber increased the porosity and contact. The adsorption efficiency of the composite beads was up to 99.6% of the Pb^{2+} [41].

Riyajan (in 2017) investigated novel bead of modified starch for encapsulating 2,4-dichlorophenoxy acetate (2,4 DA) was made from NR-graft-cassava starch and sodium alginate in a water-based system. The results suggested that NR with sodium alginate matrix was a good polymer membrane for encapsulating 2,4 DA in a water medium and the beads were also easily decomposed in the natural environment after use [42].

However, no studies so far have investigated the use of alginate as a dispersing agent and binder for the fabrication of rice husk ash filled-NR composite films and the effect of crosslinking by $CaCl_2$ on the NR composite films.

2.4 Improvement properties of natural rubber composites with fillers

2.4.1 Reinforcing agents for NR

Fillers are solid substances that are added to rubbers for many reasons, such as modification physical properties, modification processing performance, reinforcement and reducing production costs. The two types of common fillers are reinforcing and diluent (or non-reinforcing) fillers [43]. Silica and carbon black are widely used for reinforcement in NR because it can improve the mechanical and other related rubber product properties. Carbon black has been used as reinforcing material in tire industries for long times, whereas silica is only limited to colored rubber products.

1) Silica

Silica is a strongly polar and hydrophilic reinforcing filler. The conventional silica is white in color. Many researchers reported that adding silica into rubber compounds can improve mechanical properties such as hardness, tensile strength and tearing energy. Silica contains high silanol groups on its surface and these polar groups promote strong particle–particle interaction leading to high degree of aggregation and agglomeration of silica particles and low compatibility with non-polar rubbers, which result in poor dispersion. The structure of silica aggregates in

rubbers can be adjusted by modifying the filler surface to increase the compatibility of silica with hydrocarbon rubbers in order to improve the filler dispersion [44].

For unvulcanized NR with silica, the lipid and protein in natural rubber may induce hydrogen bonding between rubber and silanol group on surface of silica as shown in Figure 2.6. The proteins in natural rubber have a similar effect as silane on the silica surfaces, although not as strong [45, 46].
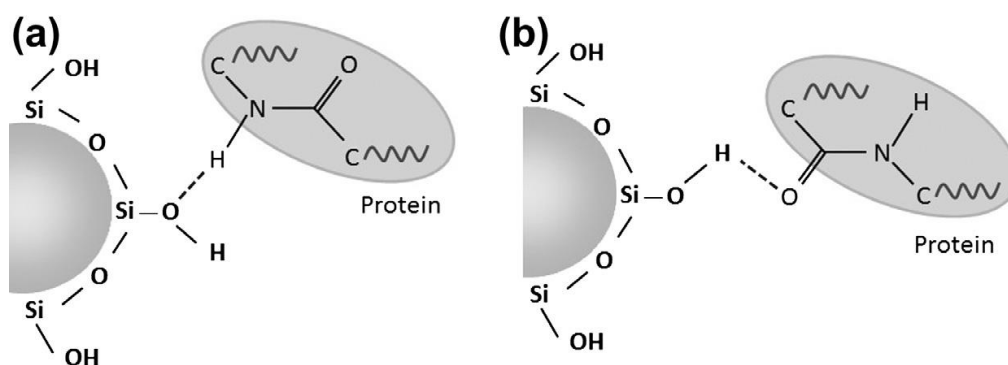
Figure 2. 6 The interactions between silanol groups of silica and proteins in NR via hydrogen bonding with functional groups: (a) amino group and (b) carboxyl group.

Successful use of silica for rubber reinforcement therefore requires commonly silane coupling agents to enhance silica–rubber interaction and silica dispersion as well as to prevent accelerator adsorption on the silica surface. Silane coupling agents in rubber systems are TESPT28 and bis(triethoxysilylpropyl) disulphide (TESPD) [47].

2) Carbon black

Carbon black is the most traditional and commonly used reinforcing filler because of the hydrophobic surface of carbon black filler matched to hydrophobic surface of NR. The size of carbon black aggregate of 0.1-0.2 µm is also important in determining the carbon black reinforcement in natural rubber. The agglomeration of carbon black can form aggregate of 10-1000 µm in size. The filler–filler interaction of carbon black is due mainly to weak Van der Waals forces that degrade easily during mixing [48, 49].

M Kardan (*in 2004*) indicated that the active carbon black was more effective when the rubber was originally in cis-conformation as opposed to trans-

conformation. In addition, reinforcing carbon black did not participate in any crosslinks within the elastomer network. The carbon black reinforced the rubber structure by means of the formation of a network of entanglements or mechanical interlocking forces [50].

However, the production and use of carbon black may cause environmental problems because carbon dioxide is released into the atmosphere during the production of carbon black. Many researchers involved replacing the carbon black with other eco -friendly fillers such as fly ash and wastes from agricultural biomass.

3) Fly ash

Fly ash is a byproduct of the power generation industries. The main component of fly ash is silica. For many years, fly ash can be used as a potential reinforcing filler to improve the mechanical properties of rubber compound.

Panitchakarn et al. (in 2019) developed composite films composed of uncured NR combined with coal fly ash that obtained from pulping facility in Prachinburi province, Thailand. The results indicated that mechanical properties and structural stability of NR composite film were improved at coal fly ash content of 20 phr. The tensile strength, elongation at break and Young's modulus of composite film increased to 10.5 MPa, 222% and 126 MPa, respectively, which were 8.7, 2.2, and 52.5 folds when compared to the original NR [51].

Arti Maan et al. (in 2014) found that the particle size of fly ash had significant effect on mechanical properties of NR composite. The composite had higher tensile strength,
density, hardness, abrasion resistance, skid resistance and water absorption at small particle size (25 µm) of fly ash. This is due to lower surface area of higher particle size fly ash available for interaction with rubber matrix than lower particle size fly ash at same loading [52].

Yangthong et al. (in 2019) studied novel epoxidized natural rubber (ENR) composites with geopolymers (GP) from fly ash waste. The result indicated that the ENR/GP composites with 15 phr GP were the highest tensile strength because of the maximal chemical linkages of hydroxyl groups and metal oxides on GP surfaces and epoxide groups in ENR. The possible reaction mechanism of the polar functional

groups on GP surfaces is shown in Figure 2.7. The silanol groups on the GP surfaces interacted with the polar functional groups in epoxide rings and with the opened ring products of ENR during vulcanization [53]. Their results showed that fly ash can be used as reinforcing filler to improve mechanical properties of NR composites.
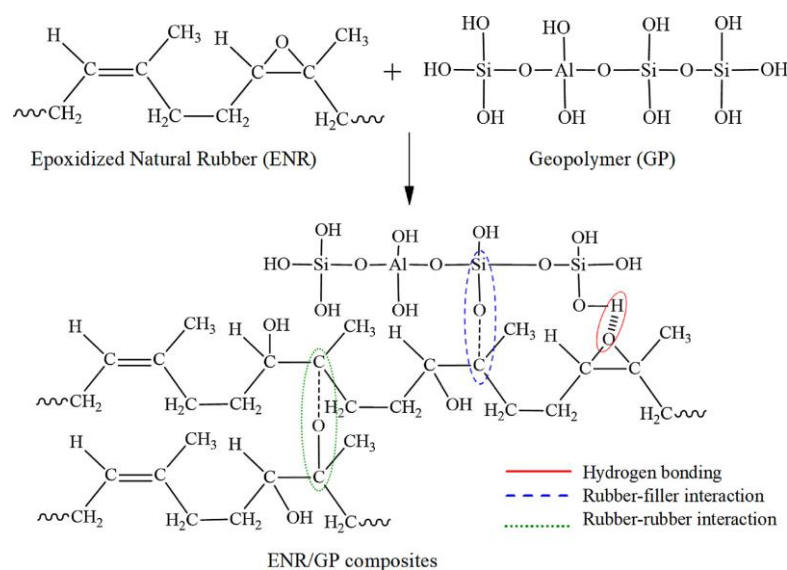
Figure 2. 7 The chemical reactions between ENR and GP

2.4.2 NR composites with rice husk ash

Natural fillers are biodegradable, environment friendly and easy to get because they are in abundant quantity. In addition, natural fillers are cheap and can reduce domestic wastes. Rice husk ash is a renewable resource of silica that obtained from burning agricultural waste rice husk. The major component of rice husk ash is silicon dioxide (SiO_2) and structure is similar to the conventional silica filler that used in the rubber industry [54]. Many studies of rice husk ash in NR compounds are shown below.

Ishak and Bakar (*in 1995*) studied two types of rice husk ash, namely white rice husk ash (WRHA) and black rice husk ash (BRHA) in epoxidized natural rubber (ENR). WRHA has about 96% silica content, while the BRHA has about 54% silica content and substantial carbon content about 44%. These ashes were mixed into ENR by two roll mixing mills. Two ashes were compared with two commercial fillers

(precipitated silica and carbon black). The results showed that overall vulcanized properties of WRHA were better than BRHA but it was inferior when compared with precipitated silica and carbon black. In addition, WRHA has high silica content but has vulcanized properties close to carbon black because of filler parameters such as surface area, surface reactivity, particle size, and metal oxide content. The addition of coupling agent of A-189 silane can improve the performance of WRHA and BRHA in ENR. Tensile and tear strengths of ENR vulcanizates increased with the addition of silane coupling agent because it helps to disperse and make chemical bonding of RHA fillers in the rubber matrix [6].

Ismail et al. (*in 1999*) studied white rice husk ash (WRHA) as filler in NR compounds by two roll mixing mills. Filler loading was 0, 10, 20, 30, 40 and 50 phr. The effect of multifunctional additive (MFA) was investigated. The results showed that the tensile and tear strengths increased with increasing WRHA loading until 10 phr after that there was the decrease in those properties because of agglomeration of filler particles. However, the tensile modulus and hardness increased with increasing filler loading. MFA loading at 3 phr was the optimal concentration for the maximum physical properties. At more than 3 phr, MFA produced weak boundary layer at interface between rubber and filler, so reducing physical properties [7].

Sae-Oui et al. (*in 2002*) studied two grades of rice husk ash (low- and high-carbon contents) as filler in NR and compared with other commercial fillers such as talcum, china clay, calcium carbonate, silica, and carbon black. Filler loading was 0, 15, 30, 45 and 60 phr. The results showed no significant difference in filler loading of both grades of rice husk ash and inert fillers (e.g., talcum, china clay and calcium carbonate). In addition, the mechanical properties (tensile strength, modulus, hardness, abrasion resistance, and tear strength) of two grades of rice husk ash were lower than those with silica and carbon black but were comparable to those with inert fillers. Surface area and surface activity of both rice husk were very low, which was the reasons for poor mechanical properties filled vulcanizates and their porous structure caused of failure at high loading. Silane-coupling agent slightly affected the properties of the ash-filled vulcanizates because of the lack of silanol groups on the ash surface [8].

Siti Salina Sarkawi and Yusof Aziz (*in 2003*) studied ground rice husk without burning as filler in rubber vulcanizates by two roll mixing mills. Rice husks were sieved to 300 µm and 180 µm. Filler loading was varied from 0 to 50 phr and was compared with carbon black and silica. The results showed that the tensile strength and elongation at break of both size rice husk increased up to 10 phr and then it tended to decrease as the concentration of rice husk increased. Rice husk had less significant effects on hardness property because the non-reinforcing nature of rice husk. However, the physical properties of rice husk-filled vulcanizates were lower than those of carbon black but were comparable to silica. The effect of particle size of fillers is shown in tensile strength, elongation at break and abrasion of NR composites. Under the study of effect of particle size of rice husk ash, it was indicated that rice husk ash with the particle size of 180 µm was better than that of 300 µm because the fillers with finer and smaller particle size were better dispersed in rubber compound [34].

Arayapranee et al. (*in 2005*) compared rice husk ash filled in NR with two commercial reinforcing fillers (silica and carbon black). Filler loading were varied from 0 to 40 phr. The results are showed that lower Mooney viscosity and shorter cure time could improve hardness but decreased tensile strength and tear strength. However, the NR composites reinforced with silica and carbon black were better mechanical properties than those with rice husk ash because silica and carbon black had highly surface area (small particle size) and surface activity. The dispersion of rice husk ash in the rubber matrix was investigated by scanning electron micrographs (SEM) and the result indicated that the dispersion of rice husk ash filler in the rubber matrix is discontinuous. Therefore, rice husk ash filled NR composites had a weak structure when compared to those with carbon black and silica [9].

Pongdong et al. (*in 2015*) used rice husk ash as reinforcing filler in epoxidized natural rubber (ENR) with various loading levels (0, 10, 20, and 30 phr) and compared with silica filler. The results indicated that rice husk ash caused faster curing reactions and increased Young's modulus and tensile strength of the composites relative to the unfilled composites. This might be attributed to the metal oxide impurities in rice husk ash that could enhance the crosslinking reactions, thus increasing the crosslink density. In addition, the mechanical properties and curing

behavior were improved by silanization with bis(triethoxysilylpropyl) tetrasulfide (Si69). The rubber-filler interactions reinforced the composites is suggested as shown in Figure 2.8 [54].
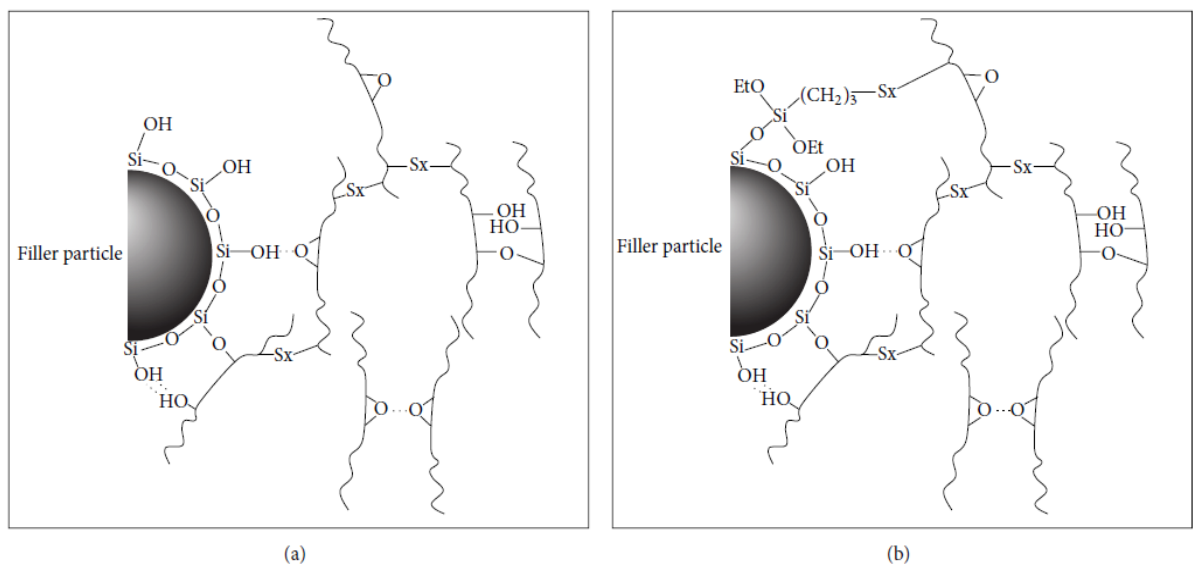
Figure 2. 8 The reaction models for rice husk ash or silica dispersed in ENR matrix (a) without silanization, (b) with silane coupling agent (Si69).

All the above studies focus on studying mechanical properties of NR composite with rice husk ash that preparing from solid NR. The limitations of their research are filler loading (not over 60 phr) and inferior dispersion of filler in NR composites.

2.5 Dielectric properties of composites with silica or rice husk ash

Dielectric materials can be used to store electrical energy in the form of charge separation when the electron distributions around constituent atoms or molecules are polarized by an external electric field. Dielectric analysis is important in case of batteries, sensors, fuel cells, super capacitors and in the development of microelectronic packaging materials for performance optimization of high frequency devices [14].

Measurement of dielectric properties involves measurements of the complex relative permittivity (ε), which consists of a real part and an imaginary part. The real

part of the complex permittivity, also known as **the dielectric constant** (ε') is a measure of the amount of energy from an external electrical field stored in the material. The imaginary part is zero for lossless materials and is also known as **loss factor or dielectric loss (ε'')**. It is a measure of the amount of energy loss from the material due to an external electric field. **The loss tangent** (tan δ) (dissipation factor or loss factor) represents the ratio of the imaginary part to the real part of the complex permittivity

$$tan\delta = \frac{\varepsilon''}{\varepsilon'}$$

Dielectric loss (loss tangent or tan δ) quantifies a dielectric material's inherent dissipation of electromagnetic energy (for example, as heat due to the charging and discharging of capacitor). Dielectric losses depend on frequency and the dielectric material. Heating through dielectric loss is widely employed industrially for heating thermosetting glues, for preheating plastics before molding, and for fast jelling and drying of foam rubber.

In communication systems, higher the dielectric loss means higher the attenuation and hence it is a limitation for long range transmission. At low frequencies, the overall conductivity can be made up of many different conduction mechanisms, but ionic conductivity is the most prevalent in moist materials. The ionic conductivity of materials will contribute to the dielectric loss [55, 56].

Previous studies about dielectric properties of composites with silica or rice husk ash are summarized as below:

Louis and Sudha (*in 2014*) investigated dielectric properties of LDPE composites with rice husk ash and hydrated silica at different filler concentrations. The results showed that dielectric constant depended both on amount of filler as well as the frequency. The composites showed higher dielectric constant at lower frequencies. In addition, the optimum hydrated silica filled composite (30 parts/100 parts of LDPE) exhibited good dielectric constant and increased dielectric loss, which leaded to the application as a good insulator. LDPE filled with rice husk ash can be used as high frequency dielectrics due to low dielectric loss because of the non-polar nature of rice husk ash [57].

Ahmed A. Al-Ghamdi et al. (*in 2016*) studied the electric, dielectric and microwave properties of NR-based composites comprising dual phase fillers prepared from furnace carbon black or conductive carbon black with a different amount of silica. The measurements were carried out at room temperature and incident power at the inlet of the coaxial measuring line varying from 800 µW up to 1300 µW within the frequency range of 1 GHz to 12 GHz. The results indicated that the carbon phase had a marked strong effect on properties mentioned above. The interpenetration of the two filler phases and the grade of isolation of the conductive carbon phase by the dielectric one depended on the ratio between them. With an increasing amount of the dielectric phase in the hybrid fillers, the electric conductivity and dielectric constant of the composites was lower, while their ability to absorb electromagnetic waves enhanced. The properties of composites make them suitable for several applications such as electromagnetic interference shielding materials, antennas for mobile devices, automobiles, sensors and military-related applications [58].

Khor et al. (*in 2016*) determined the dielectric properties of mixture of rice husk (RH), rice husk ash (RHA) with rice bran (RB) on different ratios in low frequency range (from 4 Hz to 1 MHz). The results indicated that the mixture of RHA and RB was a dipolar relaxation occurring between $10^3 - 10^5$ Hz and the peak was depressed and shifted to lower frequency as the RB content increased in the mixture. Moreover, AC conductivity decreased as the RB content increased. This might attribute to the production of natural oil content from RB. The conductivity was found to increase with the increase of RHA content. Silica is a major component in RHA that may react with the element calcium from RB, forming a compound with greater insulation properties. The result also indicated that amount of mobile carries was subjected to the RHA content [14].

The electrical properties (dielectric constant, dielectric loss and electrical conductivity) of NR composites filled with different types of filler are shown in Table 2.2.

Table 2. 2 Dielectric properties and electrical conductivity of NR composites with various fillers

Matrix	Filler	Frequency (Hz)	Dielectric constant	Dielectric loss	Electrical conductivity (1/Ω·m)	Ref.
NR	furnace carbon black	3×10^9	3.8	0.010	4.5×10^{-4}	[58]
NR	conductive carbon black	3×10^9	112	20	2.8×10^{-2}	
NR	graphite	10^3	4.500	3.5	2.2×10^{-2}	[59]
NR	carbon black	10^3	5	3.5	1.4	
NR	barium titanate	10^4	3.250	0.004	-	[60]
NR	oil palm fibers	10^4	9	0.2	4.0×10^{-7}	[61]
NR	carbon black	10^4	-	-	2.2×10^{-5}	[62]
NR	titanium dioxide	2.56×10^9	3.405	0.016	1.1×10^{-2}	[63]
NR	silicon dioxide	2.56×10^9	2.393	0.05	7.2×10^{-3}	
LDPE	RHA	10^2	3.6	0.36	-	[57]
LDPE	hydrated silica	10^2	17	238	-	
NR	short sisal/coir hybrid fiber	10^4	4.5	0.035	7.1×10^{-7}	[64]
NR	Keratin fibre from chicken feather	10^4	2.9	0.009	1.0×10^{-6}	[65]
NR	barium titanate/tannic acid-ferric ion/silver	10^3	3.7	0.018	1.0×10^{-10}	[66]
NR	Graphene Nanoplatelets /Carbon Black	10^4	3.3	12	-	[67]

CHAPTER III

EXPERIMENTS

3.1 Summary of scope and methodology

Experiments in this work can be described using the following diagram. Detail of each section was explained in this chapter.
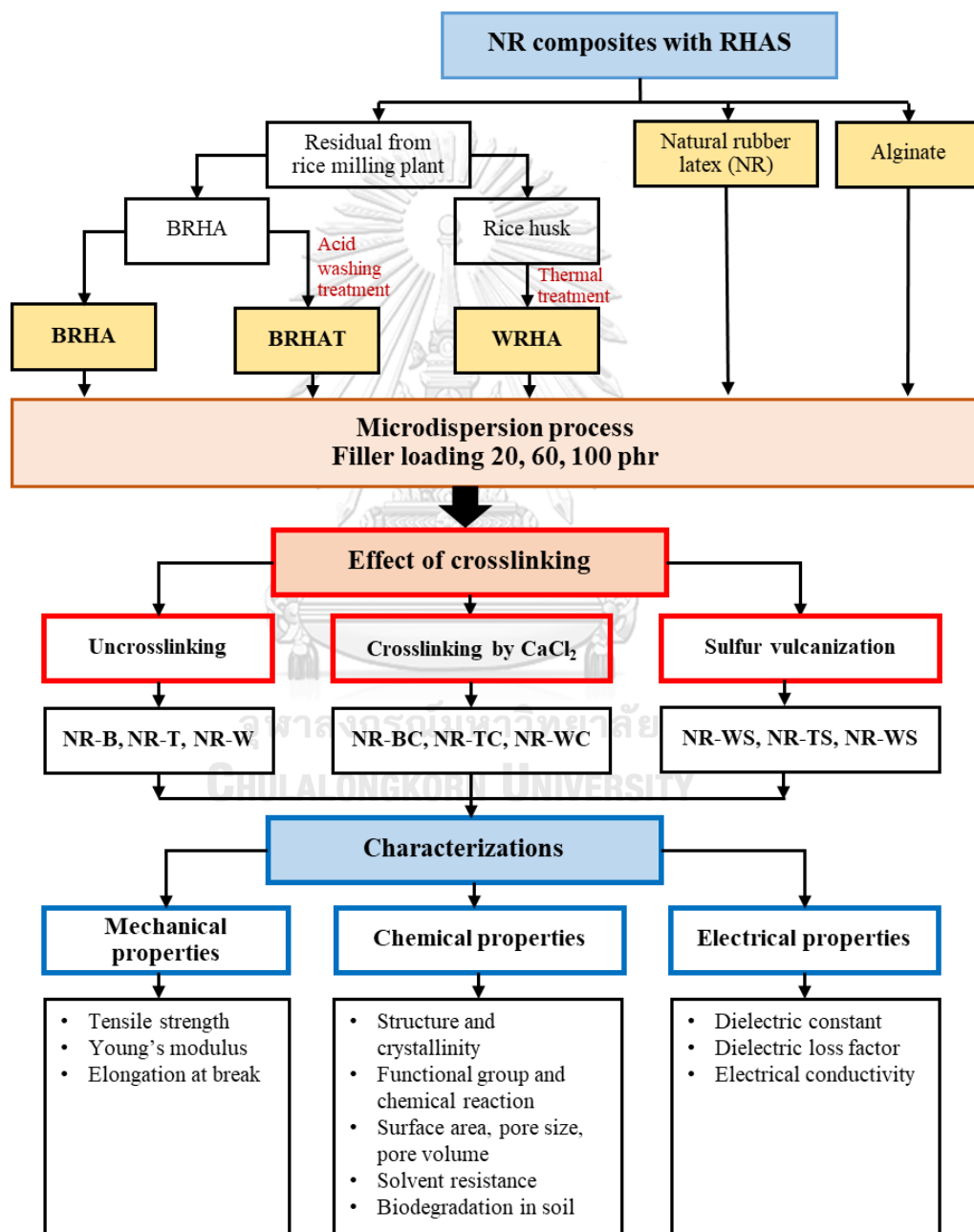
Figure 3. 1 Diagram of fabrication and characterizations of NR composites with RHAs

3.2 Materials

Rice husk and rice husk ash were obtained from a rice milling plant in Phra Nakhon si Ayutthaya province, Thailand that show in Figure 3.2. NR latex with a 60% dry rubber content was purchased from the Rubber Research Institute of Thailand, Bangkok, Thailand. Hydrochloric acid, sodium alginate and calcium chloride were purchased from Sigma-Aldrich (Thailand) Co Ltd., Bangkok, Thailand. Zinc oxide (ZnO), Potassium laurate (K-laurate), Potassium hydroxide (K), Zinc diethyldithiocarbamate (ZDEC), Wingstay-L (WSL) and Sulfur were purchased from the Rubber Research Institute of Thailand.

Figure 3. 2 Rice husk (**a**) and black rice husk ash (**b**) from rice milling plant

3.3 Methods

3.3.1 Preparation of rice husk ash

1) Black rice husk ash (BRHA) used in this study was provided by Nakhon Luang Rice Mill (Phra Nakhon Si Ayutthaya, Thailand), in which the combustion process was under oxygen depleted atmosphere due to the limited air supply. BRHA from a rice milling plant was dried in an electric oven at 105ºC for 12 h to remove water and stored in a glass bottle container at room temperature (~30ºC).

2) BRHA was further treated by acid-washing pretreatment in order to obtain purified BRHA ash, namely BRHAT.

The dried BRHA was pretreated by 20%w/w hydrochloric acid under L/S ratio of 20 ml Acid / g BRHA. The mixture was stirred at 80ºC for 2 hours to remove impurities. After that, the solid sample was filtered from the acid solution and rinsed

repeatedly with deionized (DI) water until the solution was neutral pH and then dried overnight at 105ºC. The product from the pretreatment of BRHA is referred as "BRHAT".

3) White rice husk ash (WRHA) was prepared in our laboratory (Chulalongkorn University, Bangkok, Thailand). Initially, rice husks were washed with distilled water to remove dirt and impurities and then were dried in an oven at 105ºC for 24 h. The dried rice husks were submitted to the heat treatment in ceramic crucibles, which was carried out in an atmosphere of air in an electric furnace at the temperature of 500ºC for 2 h [68].

The particle sizes of three types of rice husk ashes were reduced using ball milling (PM 100, Haan, Germany) at revolution speed 400 rpm for 15 min and sieved (Test sieve ASTM, 203x50 mm, 106 μm, 140 meshes) in order to obtain the powder with a size of less than 106 μm.

3.3.2 Preparation of natural rubber composite films

The NR composite films were reinforced by using BRHA, BRHAT and WRHA as filler. The filler loading used in this work was varied at 0, 20, 60 and 100 per hundred rubbers (phr). The microdispersion process [51] was applied for the preparation of composite films.

1) Initially, the filler was added into the aqueous solution of 1% w/v alginate (10 phr that the minimum amount of alginate for good dispersion of filler loading 20-100 phr, observation from smooth surface of composites after fabrication). Then, the slurry was thoroughly mixed under mechanical stirring at room temperature for 30 min.

2) Then, 5 g of 60 phr NR latex was slowly added into 30 mL of the slurry under continuous mixing by high-frequency mechanical stirring until the mixture was homogenous.

3) After that, the mixture was poured into a plastic tray and dried overnight (~12 h) in an oven at 40ºC to obtain NR composite films.

The composite films of NR combined with BRHA, BRHAT and WRHA are referred to as NR–B, NR-T and NR–W, respectively.

3.3.3 Crosslinking with CaCl$_2$

The aqueous solution of CaCl$_2$ at 1% w/v was used as crosslinking agent. The solution was prepared by dispersing CaCl$_2$ in distilled water and stirring at room temperature for 30 min. The NR composite films were soaked in 1% w/v CaCl$_2$ solution for crosslinking of alginate for ~1 h, and then the films were rinsed with distilled water to remove excess chloride. After that, the composite films were dried in an oven overnight at 40°C [69]. After crosslinking with Ca^{2+}, the crosslinked composite films of NR combined with BRHA and WRHA are referred to as NR–BC, NR-TC and NR–WC, respectively.

3.3.4 Sulfur vulcanization

Sulfur vulcanized NR composites prepared according to the following steps (the step #1 to the step #3) of micro-dispersion process. After step #1, the additives and crosslink agents were added to the slurry in proper amounts as shown in Table 3.1 and stirred at room temperature for 15 min. The NR composite films from the step #3 were cured in the oven at 110°C for 1 h. The filler loading used in this crosslinking process was at 100 phr that was RHA loading of the highest mechanical properties of uncrosslinking NR composites with RHA. The sulfur vulcanized composite films of NR combined with BRHA, BRHAT and WRHA are referred to as NR–BS, NR-TS and NR–WS, respectively.

Table 3. 1 Formula of composite materials of sulfur vulcanization

Ingredients	Function	Sulphur vulcanization (phr)
NR latex	Matrix	100
BRHA, BRHAT, WRHA	filler	100
Alginate	Dispersant	10
KOH	Stabilizer	0.2
K-laurate	Stabilizer	0.1
Zinc oxide	Activator	0.5
ZDEC(zinc diethyldithiocarbamate)	Accelerator	1.0
WSL (Wingstay-L)	Antioxidant	1.0
Sulphur	Crosslinker	1.5

3.4 Characterization

3.4.1 Morphology

Morphologies of rice husk ashes and composite films were observed by scanning electron microscope and energy dispersive X-ray spectrometer (SEM–EDS) (IT-500HR) using a JEOL, JSM-IT-500HR and JEOL, JED-2300 (JEOL, Tokyo, Japan). The specimens were frozen in liquid nitrogen and vacuum dried. After that, the specimens were sputtered with gold. The SEM–EDS performed at an accelerating voltage of 10 kV.3.5.2 Fourier Transform Infrared (FTIR) Spectroscopy

3.4.2 Particle size distribution

The overall components and particle size distribution of each dried sample were determined by X-ray fluorescence spectrometer analysis (Bruker model S8 Tiger, Karlsruhe, Germany) and laser particle size distribution analyzer (Mastersizer 3000, Malvern Panalytical, Malvern, UK), respectively.

3.4.3 Surface, pore size and pore volume analysis

The surface area, pore volume and average pore diameter of samples were determined by nitrogen (N_2) physisorption-desorption using a surface area and pore size analyzer (Autosorb-iQ-MP, Quantachrome, Boynton Beach, FL, USA).

3.4.4 Structural information crystallinity

The structural information and crystallinity of fillers and NR composite films were characterized using X-ray diffractometer (XRD, Bruker AXS Model D8 Discover, Karlsruhe, Germany) with Cu-K radiation in the 2θ range of 5–40. The operation conditions were at the accelerating voltage of 40 kV and electric current of 30 mA.

3.4.5 Functional groups and possible interaction

The functional groups and possible interaction between fillers were determined by Fourier transform infrared (FTIR) spectroscopy (PerkinElmer, Waltham, MA, USA) in the ranges of 4000–650 cm^{-1} with a resolution of 4 cm^{-1}.

3.4.6 Mechanical properties

For mechanical properties tests of dry film of NR, NR composites (Young's modulus, tensile strength and elongation at break) were performed using Universal Testing Machine (Instron, Norwood, MA, USA). The test conditions were according to ASTM D882. At least five specimens for each different blend composition were tested.

3.4.7 Water absorption capacity

The measurement of water absorption capacity (WAC) was performed by usingthe specimen films of 2 x 2 cm^2, with a thickness of 0.5–0.6 mm. The specimens were immersed in distilled water at room temperature for 0–18 days. The specimens were removed from water every 2 days, and excess water at the surface of the samples was blotted by Kimwipes® paper. The weight of wet sample was measured. All testing was carried out in triplicate. Water absorption capacity was calculated by using the formula:

$$WAC\ (\%) = \frac{W_h - W_d}{W_d} \times 100$$

Where, W_h and W_d are the weights of the specimen hydrated and dried, respectively.

3.4.8 Toluene uptake

For the test of toluene uptake, dried sample films (2 x 2 cm^2), with a thickness of 0.5–0.6 mm, were immersed in toluene at room temperature. The weight change was monitored at 1 h intervals for 8 h. All testing was carried out in triplicate. Toluene uptake was calculated by using the formula:

$$TU\ (\%) = \frac{W_t - W_d}{W_d} x100$$

Where, W_d and W_t are the weights of the specimen before swelling and after a time (t) of immersion, respectively.

3.4.9 Preliminary test of biodegradation in soil

For the preliminary test of biodegradation in soil, each test specimen, having 5x5 cm^2 and a thickness of 0.5–0.6 mm, was used for the measurement of biodegradation in soil. Potting soil purchased from a garden center (Bangkok, Thailand) was used for the experiment. The main composition of potting soil was loam soil, compost manure and coconut coir. The soil temperature was around 28–30°C. The moisture content of the soil was around 50–60%. The specimens were weighed and buried in soil at a depth of 10 cm for 3 months under ambient conditions, where the temperature range was 24 to 35°C as Figure 3.3. After 1, 2 and 3 months, the samples were removed from soil, washed with deionized water (DI) water, dried at 40°C for 12 h and recorded for their weights. The degradation was evaluated by measuring the weight loss by using the formula:

$$Biodegradation\ (\%) = \frac{W_0 - W_i}{W_i} \times 100$$

Where, W_o and W_i are the weights of the specimens before and after being buried in soil, respectively.

Figure 3. 3 Biodegradation in soil testing

3.4.10 Electrical properties analysis of natural rubber composite films

1) Dielectric properties [64]

The capacitance, resistance and dissipation factors were measured directly by using impedance analyzer with a precision impedance analyzer (4294A, Agilent, Santa Clara, California, USA) as Figure 3.4 at room temperature. The measurements were done at varying frequencies ranging from 10^3–10^6 Hz as per ASTM standard D-150-74. The samples were coated by silver paint as electrode on both sides before measurement.

Dielectric constant (ε')

The dielectric constant of a material is defined as the ratio of the capacitance of a condenser containing the material to that of the same condenser under vacuum. The capacitance of a condenser measures the extent to which it can store charges. Dielectric constant can determine by using the following equation:

$$\varepsilon' = \frac{Cd}{E_0 A}$$

Where ε' is dielectric constant, C is capacitance, A is surface area of sample, d is thickness of sample, and E_0 is dielectric permittivity (8.85x10^{-12} Farad.m^{-1}).

Dielectric loss (ε'')

The electrical loss or the amount of energy dissipated by the insulating material when the voltage is applied to the circuit can be represented by means of a dissipation factor. Most of the elastomers have lower dissipation factor at room temperature. The loss factor (dielectric loss, ε''), the dielectric constant (ε') and the dissipation factor (tan δ) are related by the following equation:

$$tan\delta = \frac{\varepsilon''}{\varepsilon'}$$

2) Electrical conductivity [70]

The electrical properties were measured and obtained using an impedance analyzer with an LCR meter. The measured electrical resistivity of the composite materials was converted into electrical conductivity by using the following equation:

$$\rho = \frac{RA}{L} = \frac{1}{\sigma}$$

Where ρ is the volume resistivity (Ωm), R is the resistance (Ω), A is the cross-section discs (m^2), L is the thickness (m), and σ is the electrical conductivity (Ωm)$^{-1}$.
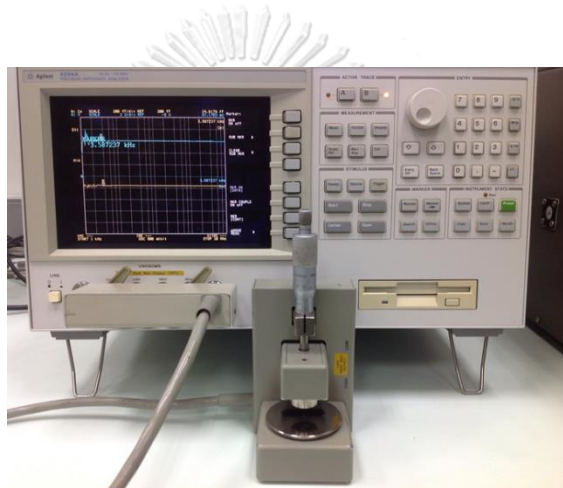
Figure 3. 4 Precision impedance analyzer

จุฬาลงกรณ์มหาวิทยาลัย

CHULALONGKORN UNIVERSITY

CHAPTER IV
RESULTS AND DISCUSSION

4.1 Characterization of BRHA, BRHAT and WRHA Particles

Rice husk ash is a major by-product of the combustion of rice husk to generate heat for boilers in rice milling plants, in which the burning temperature is usually above 800 °C. BRHA results from the pyrolysis of rice husk in poor oxygen atmosphere, whereas BRAHT treated by acid washing for elimination metal oxide impurities. WRHA is a byproduct from the combustion of rice husk in atmospheric air. The color of BRHA, BRHAT and WRHA are shown in Figure 4.1. The results of XRF analysis for chemical compositions of BRHA, BRHAT and WRHA are shown in Table 4.1. The main components of BRHA BRHAT and WRHA were found to be silica as silicon dioxide (SiO_2), at 87.0%, 90.90% and 95.3%, respectively. The minor components were alumina oxide (Al_2O_3) and potassium oxide (K_2O) and small amounts of CaO, P_2O_5, MgO, Fe_2O_3, SO_3, MnO, ZnO and Rb_2O. Moreover, the XRF data also demonstrate that small amount of the impurities in the BRHA were removed by acid washing. The BRHAT consisted only of SiO_2 as the primary component (90%) along with Al_2O_3 at lower levels and small amounts of K_2O, CaO P_2O_5, MgO, Fe_2O_3, SO_3 and MnO. These results agree with those of Chen et al.[71], who reported that metal impurities were eliminated from RHA under acidic conditions. In addition, the unburned carbon or loss of ignition value of BRHA, BRHAT and WRHA were found to be about 7.8%, 7.6% and 0.1%, respectively. The color of the rice husk depends on amount of unburned carbon in the ash [72]; the reported unburned carbon contents of gray-RHA and WRHA were 2.4% and 1.4%, respectively. The product of WRHA from combustion treatment contains higher silica content than BRHA and BRHAT, but the unburned carbon content of WRHA was lower than that of BRHA and BRHAT.

Figure 4. 1 BRHA, BRHAT and WRHA powder after grinding.

Table 4. 1 Chemical compositions of BRHA, BRHAT and WRHA

Chemical Compositions	BRHA (%wt)	BRHAT (%wt)	WRHA (%wt)
SiO_2	87.00	90.90	95.30
Al_2O_3	2.51	0.36	1.76
K_2O	1.07	0.54	0.89
CaO	0.52	0.15	0.71
P_2O_5	0.63	0.13	0.57
MgO	0.32	0.19	0.36
Fe_2O_3	0.16	0.10	0.13
SO_3	-	589 PPM	0.17
MnO	719 PPM	415 PPM	743 PPM
ZnO	64.1 PPM	-	113 PPM
Rb_2O	44.4 PPM	-	-
Loss on ignition	7.78	7.63	0.11

The SEM images of BRHA BRHAT and WRHA particles are shown in Figure 4.1a, b and c, respectively. BRHA and BRHAT formed black platelets of partially crystalline oxides of silicon and others, whereas WRHA was in roughly spherical form of aggregated white powders. Three types of RHA particles were produced in a wide range of sizes, from 1 to 10 μm. However, the average size of BRHA and BRHAT was relatively smaller, compared to WRHA.
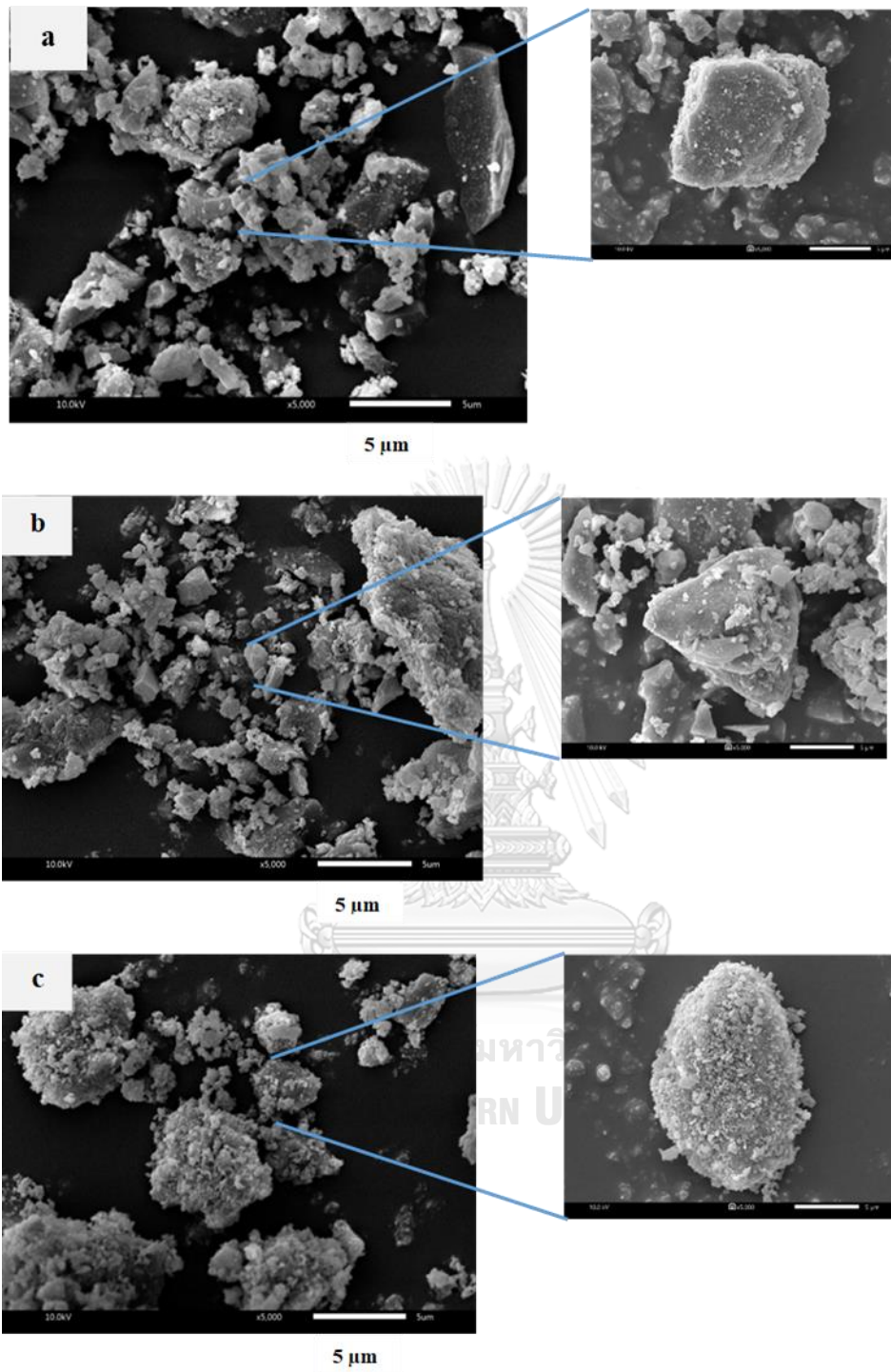
Figure 4. 2 Scanning electron microscope (SEM) images of BRHA (**a**), BRHAT (**b**) and WRHA (**c**) particles.

The XRD analysis was conducted on BRHA, BRHAT and WRHA particles, as shown in Figure 4.3a-c. According to the XRD pattern, BRHA and BRHAT were in the form of partially crystalline oxides of cristobalite, corundum and quartz alpha. The observation of cristobalite and quartz alpha in BRHA and BRHAT indicates that BRHA should be treated at temperatures greater than 900 °C during the combustion process [73]. On the other hand, the XRD pattern of WRHA exhibited a very small peak of quartz alpha and broadening of the cristobalite peak (at $2\theta = 22.5°$), which indicates the nature of amorphous silica [74]. The degrees of crystallinity of BRHA BRHAT and WRHA were 16.9%, 18.72% and 2.6%, respectively.

The SEM micrographs and XRD results confirm that BRHA and BRHAT are a partially crystalline silica oxide, whereas WRHA is an amorphous silica oxide. These results agree with those reported by Xu et al. and Osman et al. [75, 76], where WRHA with silica in a mainly amorphous form was produced at a con-trolled temperature below 800 °C, and BRHA with silica in partial crystalline phases was generated at temperatures above 800 °C.
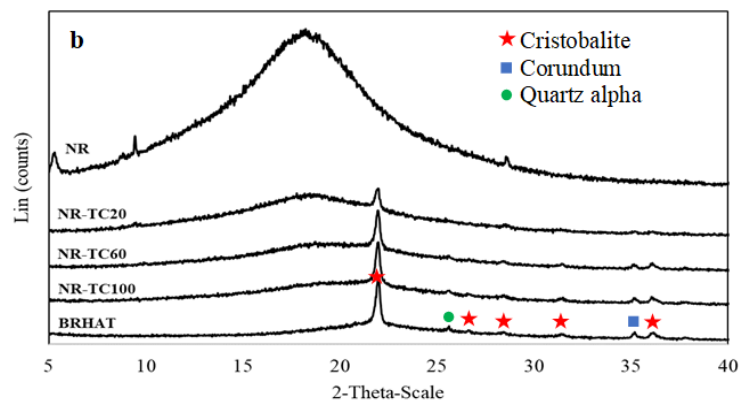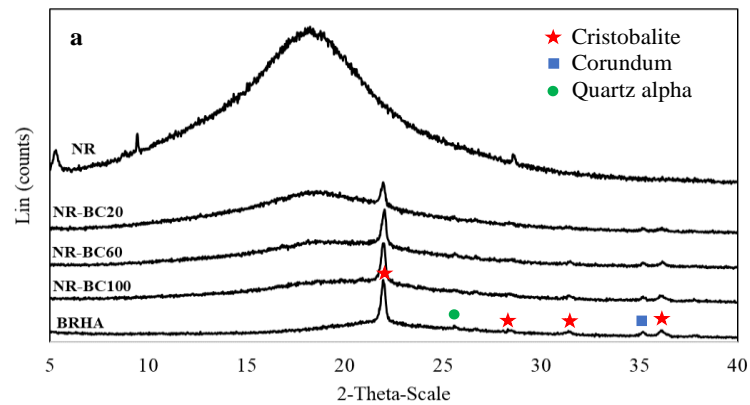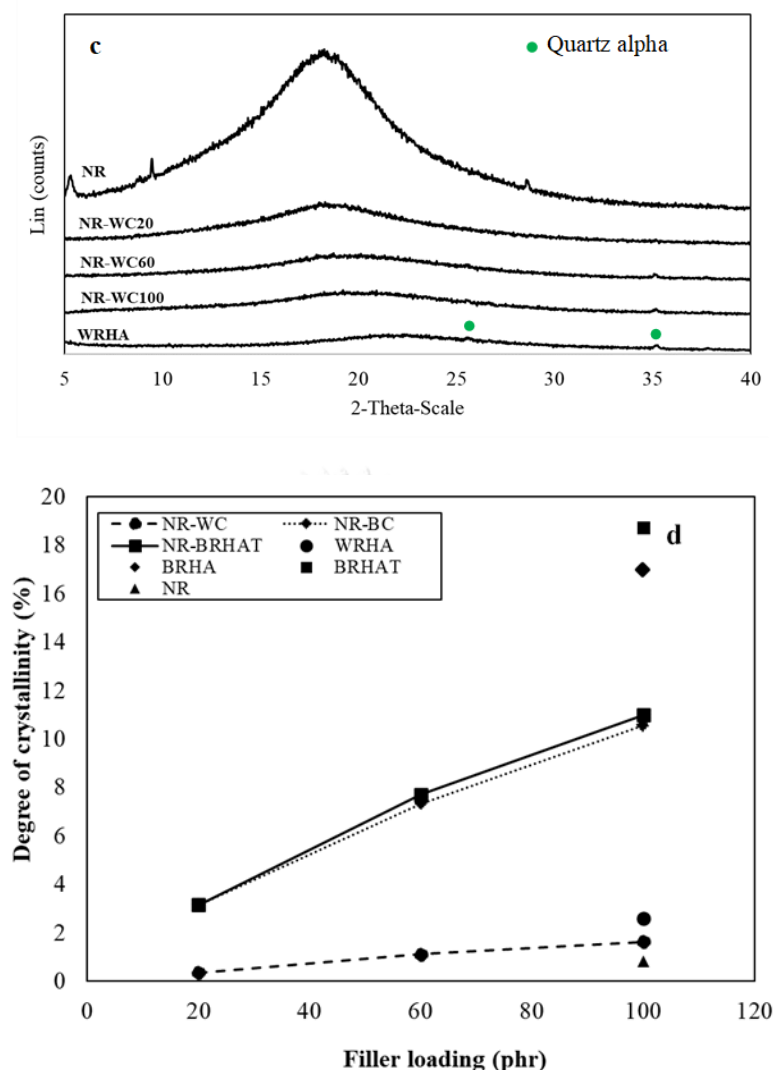
Figure 4. 3 X-ray diffraction of the composite films of crosslinked composite films of natural rubber (NR) combined with BRHA (NR–BC) (**a**), with BRHAT (NR-TC) (**b**) and with WRHA (NR–WC) (**c**) and degree of crystallinity (**d**) with loaded content of BRHA, BRHAT and WRHA at 0, 20, 60 and 100 per hundred rubbers (phr).

The particle size distributions of the BRHA, BRHAT and WRHA are shown in Figure 4.4. The BRHA particles ranged in size from 0.4 to ~100 μm, with an average size ≈ 6 μm. The d10, d50 and d90 values based on the volume distribution were 1.5, 6.2 and 28.5 μm, respectively. The BRHAT particles ranged in size from 0.4 to ~111 μm, with an average size ≈ 6 μm. The d10, d50 and d90 values based on the volume distribution were 1.5, 6.1 and 25.9 μm, respectively. The WRHA particles

ranged in size from 0.4 to 144 μm, with an average size ≈ 40 μm. The d10, d50 and d90 of WRHA were higher than those of BRHA and BRHAT (1.9, 17.8 and 70.4 μm, respectively). The results from the SEM observation (Figure 4.2) and the particle size distribution (Figure 4.4) indicated that an average particle size of WRHA was larger than that of BRHA and BRHAT. This result can be attributed to hydroxyl groups of silanol (Si-OH) on the surface of rice husk ash particles. The hydroxyl group had very strong intermolecular hydrogen bonds with another hydroxyl of adjacent silica particle. These hydrogen bonds could easily cause the formation of agglomeration of particles. WRHA particles have larger particle sizes, as compared to BRHA particles, due to the higher degree of agglomeration of the WRHA powders, because of their higher silica content.
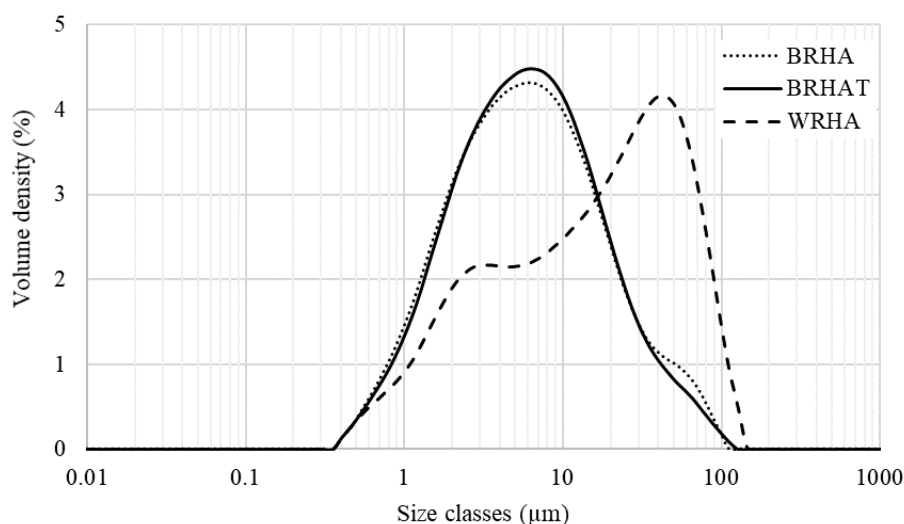
Figure 4. 4 Particle size distributions of BRHA, BRHAT and WRHA particles.

Pore size distributions of BRHA, BRHAT and WRHA are shown in Figure 4.5. Because WRHA formed agglomerated particles, WRHA presents bimodal pore structure of two groups of pores that are considerably different in size. The small pores inside of fine particle are less than 2.5 nm, and the pores between particles are 4–30 nm. On the other hand, BRHA and BRHAT shows a monodispersed mesoporous structure. Table 2 shows surface area, pore volume and pore size of BRHA, BRHAT and WRHA particles. Owing to the smaller particle size of BRHA, the specific surface area of BRHA (51.57 m^2/g) was greater than that of BRAHT

(44.36 m^2/g) and WRHA (40.06 m^2/g), as the decrease of particle size resulted in an increase in surface area. The average pore volume and average pore diameter of BRHAT were lower than those of BRHA and WRHA. The pore volumes of BRHA, BRHAT and WRHA were 0.24, 0.05 and 0.48 cm^3/g, respectively, with average pore diameter of 9.22, 4.89 and 23.92 nm, respectively. These results can be attributed to larger pore size in WRHA agglomerated particles.
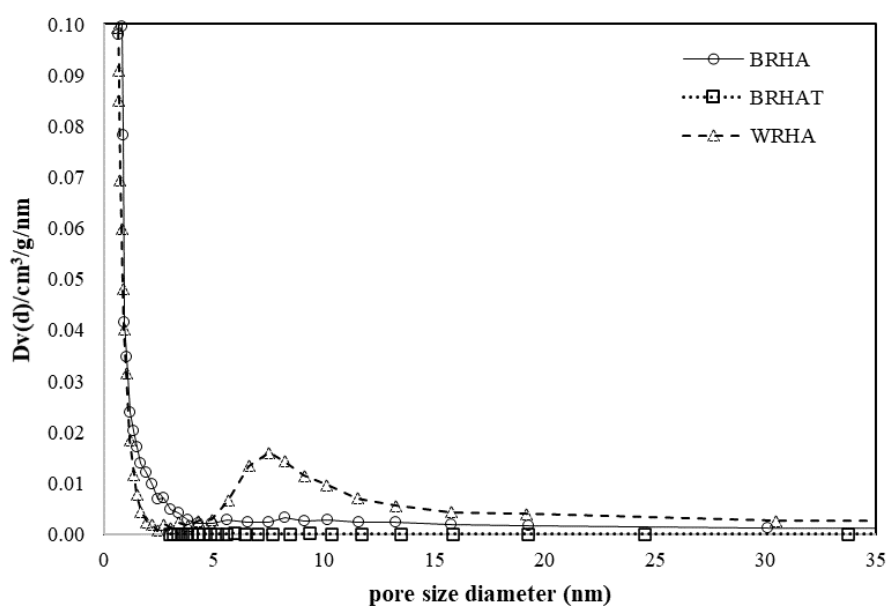
Figure 4. 5 Pore size distributions of BRHA (○), BRAHT (□) and WRHA (△).

Table 4. 2 The surface area, pore volume and average pore diameter of BRHA, BRHAT and WRHA.

Rice Husk Ash	BET Surface Area (m^2/g)	Pore Volume (cm^3/g)	Average Pore Diameter (nm)
BRHA	51.57	0.24	9.22
BRHAT	44.36	0.05	4.89
WRHA	40.06	0.48	23.92

4.2 Morphology of NR and NR Composite Films

The morphologies of the NR, NR–BC, NR-TC and NR–WC specimens are illustrated in Figure 4.6. From the outlook (Figure 4.6a), NR–BC, NR-TC and NR–WC composite films had a rather smooth surface. NR–BC and NR-TC films were black in color, whereas NR–WC films were light brown. The surface and cross-section areas of the neat NR film were smooth, whereas NR–BC and NR–WC had relatively rough surfaces. The degree of surface roughness increased with increases in BRHA, BRHAT and WRHA loading content. In addition, the cross-section area images show that BRHA, BRHAT and WRHA demonstrated homogenous dispersion in NR matrix without phase separation. SEM micrographs of surface and cross-section area of NR-W100 film without alginate are illustrated in Figure 4.7. Surface cracking presented on surface area of NR-W100 without alginate, whereas cross-section area presented the phase separation between NR and WRHA. The results reveal that alginate is a good dispersing agent for the dispersion of rice husk ashes in NR matrix up to 100 phr.

a)

b)

c)

	NR-BC	**TR-BC**	**WR-BC**

d)

NR-BC   NR-TC   NR-WC

20 phr

60 phr

100 phr
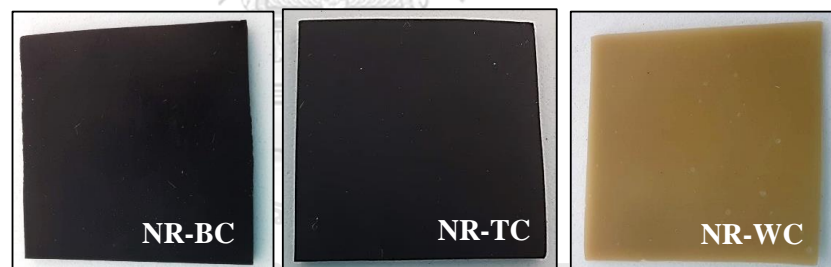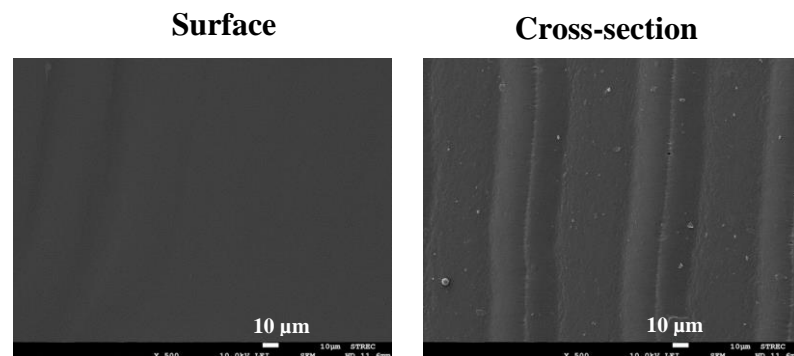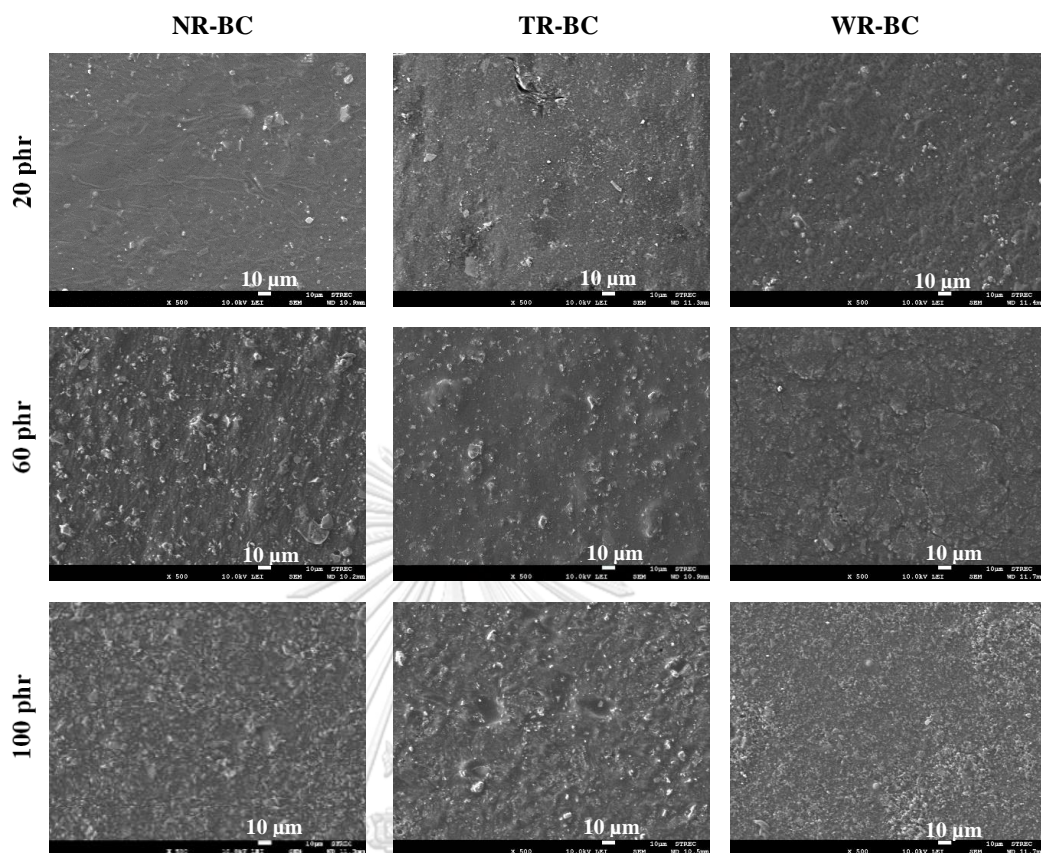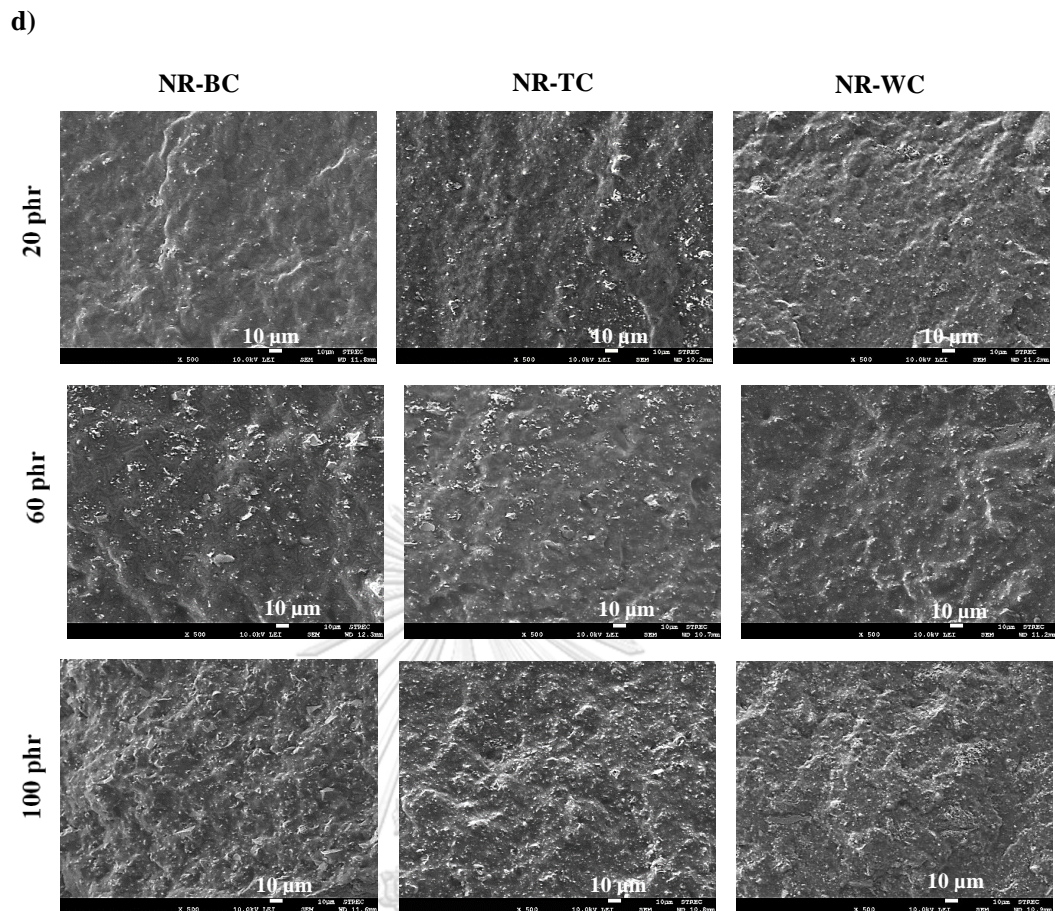
Figure 4. 6 The outlook (**a**) and SEM micrographs of surface morphologies and cross-section of pure NR (**b**), SEM micrographs of surface morphologies of NR-BC, NR-TC and NR-WC composite films (**c**) and micrographs of cross-section of NR-BC, NR-TC and NR-WC films (**d**) at different RHA loading.
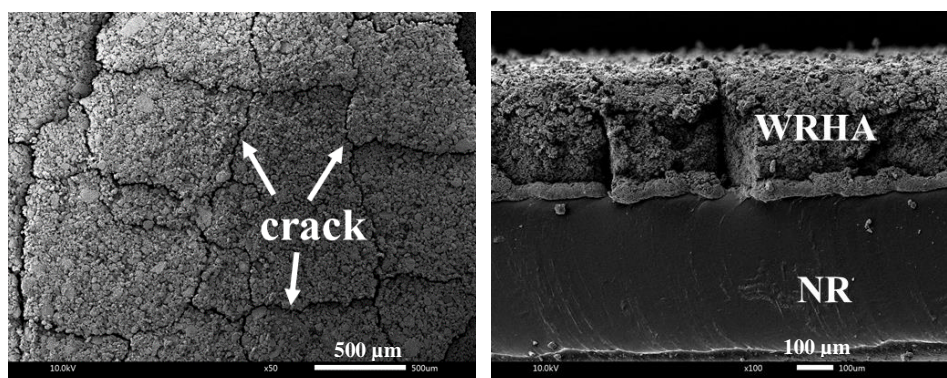
Figure 4. 7 SEM micrographs of surface morphologies (a) and cross-section (b) of NR-W100 without alginate

The distribution of RHA in NR composites was also investigated using energy-dispersive X-ray (EDX) spectroscopy, as shown in Figure 4.8. Silicon (Si) atom, the main component in three types of RHAs was used to indicate the distribution of RHAs in the composite films. From Si-mapping, the well-distributed RHA particles were found in the EDX mapping of NR-WC composites.
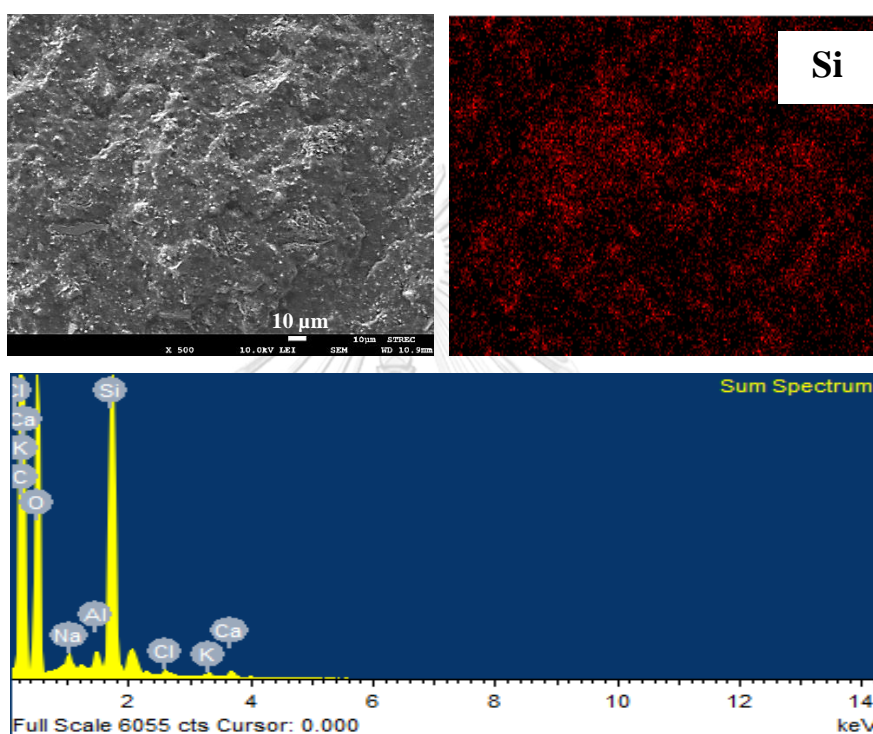
Figure 4. 8 SEM-EDX micrograph of NR-WC100 composite film

4.3 X-ray Diffraction (XRD) of NR and NR Composite Films

As shown in Figure 4.3, the XRD pattern of pure NR film demonstrates a broad peak with very low degree of crystallinity (0.8%), which indicates an amorphous structure for the polymer phase. NR–BC, NR-TC and NR–WC composite films revealed diffraction peaks corresponding to BRHA, BRHAT and WRHA structures, respectively. In addition, the diffraction peaks of three types of ash composites increased linearly with increasing filler loading content. The degree of crystallinity of composite films also linearly increased along with the filler loading content (Figure 4.3d).

4.4 Fourier Transform Infrared (FTIR) Spectroscopy

Figure 4.9 demonstrates the FTIR spectrum of NR, BRHA, BRHAT, WRHA, NR–B, NR–BC, NR-BS, NR-T, NT-TC, NR-TS, NR–W, NR–WC and NR-WS composites. Pure NR consists mainly of cis-polyisoprene. The functional groups for identifying cis-polyisoprene were the asymmetric stretching vibration of methyl groups ($-CH_3$) at 2960 cm−1 and C-H deformation at 1446 cm^{-1} [26]. The peaks observed at 2917 and 1663 cm^{-1} are assigned to symmetric stretching vibration of methylene ($-CH_2$) and C=C stretching [77]. The BRHA, BRHAT and WRHA have similar FTIR spectrum. The strong sharp peaks at 1080 and 1083 cm^{-1} are attributed to Si–O–Si asymmetric stretching, along with peaks at 796 and 800 cm^{-1}, which are due to symmetric Si-O-Si stretching and Si–O quartz [28, 78]. The main broad peak between 1000 and 1200 cm^{-1} of WRHA indicates characteristics of amorphous silica [72]. The FTIR spectrum clearly indicates that functional groups found on NR–B, NR-T, NR–W, NR–BC, NR-TC, NR–WC, NR-BS, NR-TS and NR-WS are the same as those found on NR, BRHA and WRHA. The spectra of the composites contain peaks at 2961, 2915, 1661 and 1067 cm^{-1}, which are assigned to ($-CH_3$), ($-CH_2$), C=C stretching and Si-O-Si asymmetric stretching, respectively. The composite films reveal a broad absorption band between 3400 and 3100 cm^{-1}, referring to the stretching of the O–H group. The hydroxyl regions of NR–BC, NR-TC and NR–WC are more dominant than those of the composite films without $CaCl_2$ crosslinking, which might indicate that the $CaCl_2$ crosslinking had an effect on the O-H interaction of sodium alginate (absorption band between 3500 and 3100 cm^{-1}) [79]. Daemi and Barikani had previously reported that the absorption regions of O-H group in calcium alginate were narrower than the normal peak of sodium alginate, because the calcium ion decreased in hydrogen bonding between hydroxyl functional groups, resulting in narrower bands of calcium alginate [80]. The position peaks of functional groups of NR–B, NR-T, NR–W, NR–BC, NR-TC and NR–WC composite films are slightly shifted, as compared to the original spectra of NR, BRHA, BRHAT and WRHA, which indicates the formation of interactions of BRHA, BRHAT and WRHA in the NR matrix without a chemical reaction [51, 69, 77]. In case of NR-BS, NR-TS and NR-WS that were crosslinked by sulfur vulcanization but not found position peak of

functional group of C- S linkages because these peak will present in fully vulcanized compound containing more than 12% sulfur [81].

a)
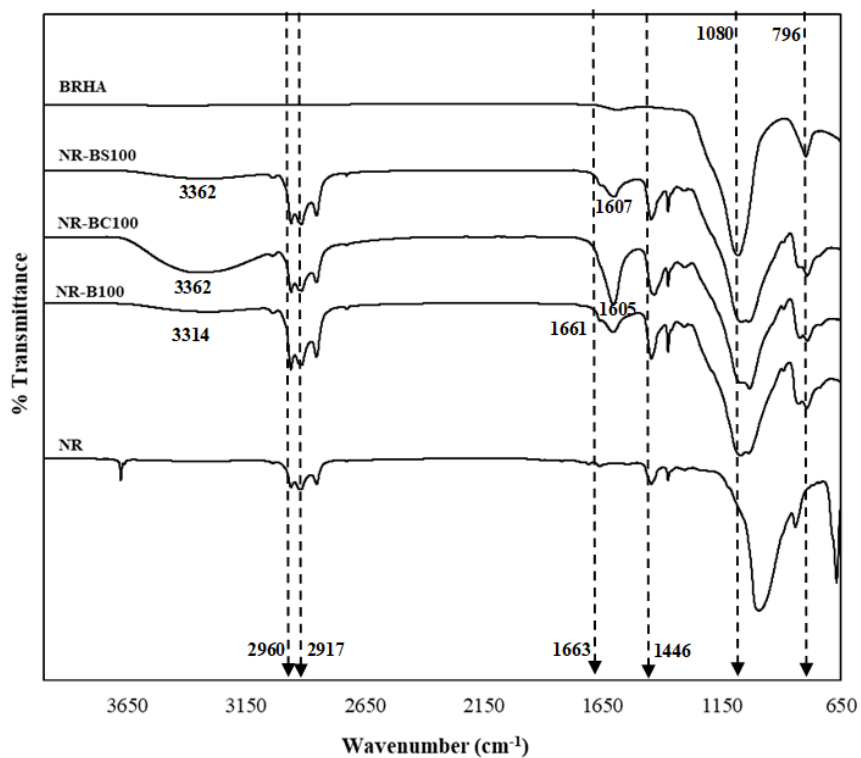
b)
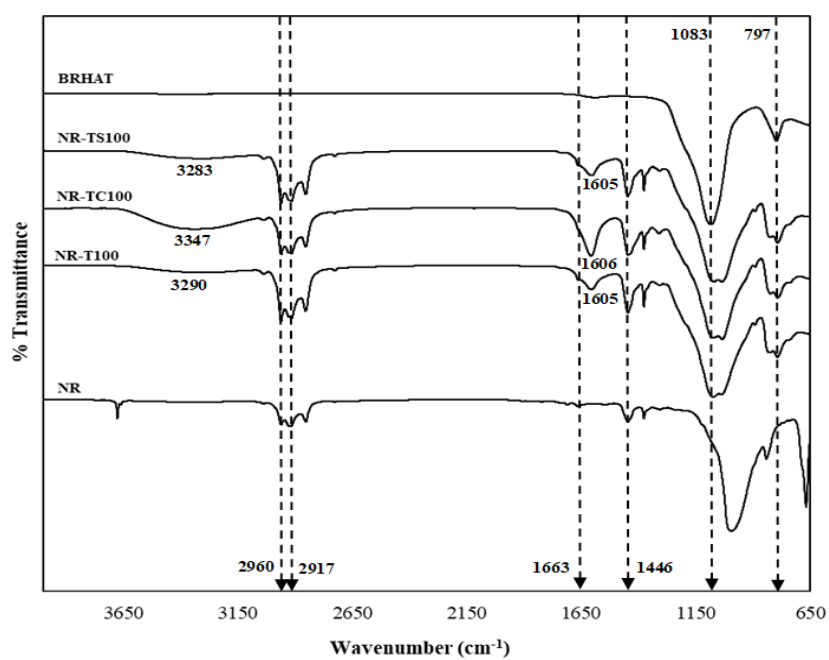
c)
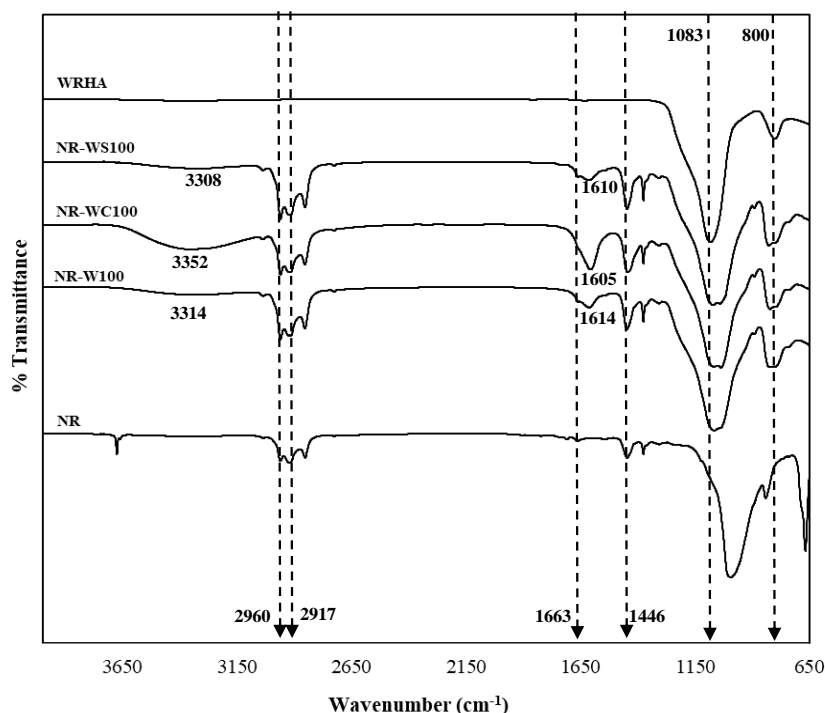
Figure 4. 9 Fourier transform infrared (FTIR) of the BRHA; NR; NR–B100; NR-BC100 and NR-BS100 composites (**a**), BRHAT; NR; NR–T100; NR-TC100 and NR-TS100 composites (**b**), WRHA; NR; NR–W100; NR-WC100 and NR-WS100 composites (**c**).

4.5 Mechanical Properties

The thickness NR composites with BRHA and WRHA at different filler loading are presented in Figure 4.10. The thickness of BRAH, BRHAT and WRHA composites increased with increasing filler content. Moreover, the thickness of composites after crosslinking slightly decreased in case of WRHA which may be due to some interaction between WRHA and NR matrix. The mechanical properties of BRHA, BRHAT and WRHA composites were examined in terms of tensile strength, Young's modulus and elongation at break, as shown in Figure 4.11. Uncured NR film was high elastic elongation, but it demonstrated low tensile strength. The tensile strength, Young's modulus and elongation at break of the uncured NR film were 1 MPa, 2 MPa and 113.3%, respectively. Figure 4.11a clearly shows that the addition of BRHA, BRHAT and WRHA to the NR matrix resulted in improvement among all

observed mechanical properties of the composite films. The tensile strength was relatively enhanced through the increase of BRHA and WRHA loading content in all cases. The maximum tensile strength values of the NR–B, NR–W, NR–BC and NR–WC were obtained by the filler loading at 100 phr, at 6.5, 10.4, 3.2 and 13.1 MPa, respectively. In NR-T and NR-TC composites, tensile strength increased with increasing filler content until a maximum level was reached (60 phr). The maximum tensile strength of NR-T and NR-TC were 6.7 and 5.5 MPa, respectively at 60 phr of BRHAT loading. The reduction of tensile strength may be attributed to agglomeration of BRHAT particles to form a domain that performed as a foreign particle, or result of physical contact between aggregates [82]. The results indicate that WRHA-filled NR films exhibit significantly higher tensile strength than those reinforced by BRHA and BRHAT, especially at filler loading content of 60 and 100 phr. The treatment of $CaCl_2$ crosslinking tended to improve tensile strength of the composite films reinforced with WRHA but reduced the strength of the films reinforced with BRHA and BRHAT.
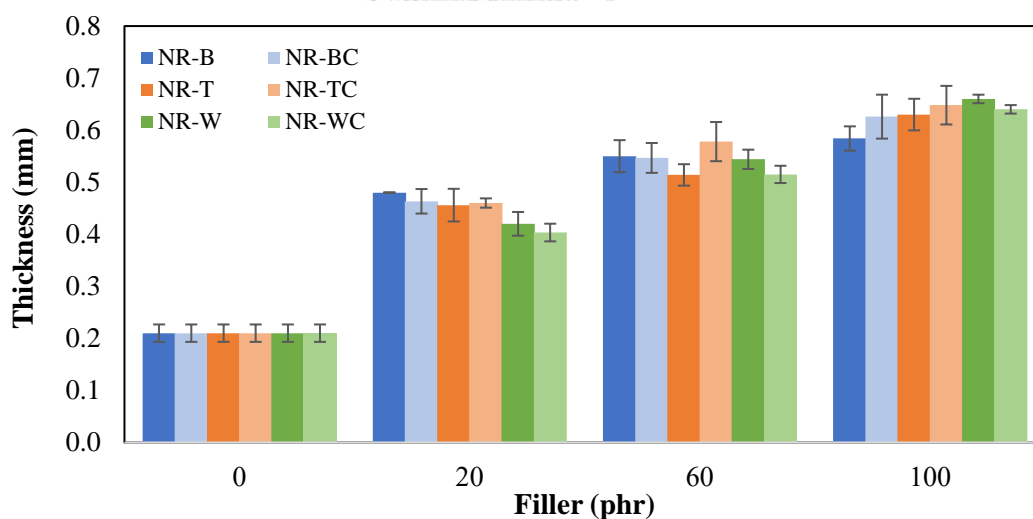
Figure 4. 10 The thickness of the pure NR film and the NR composite films
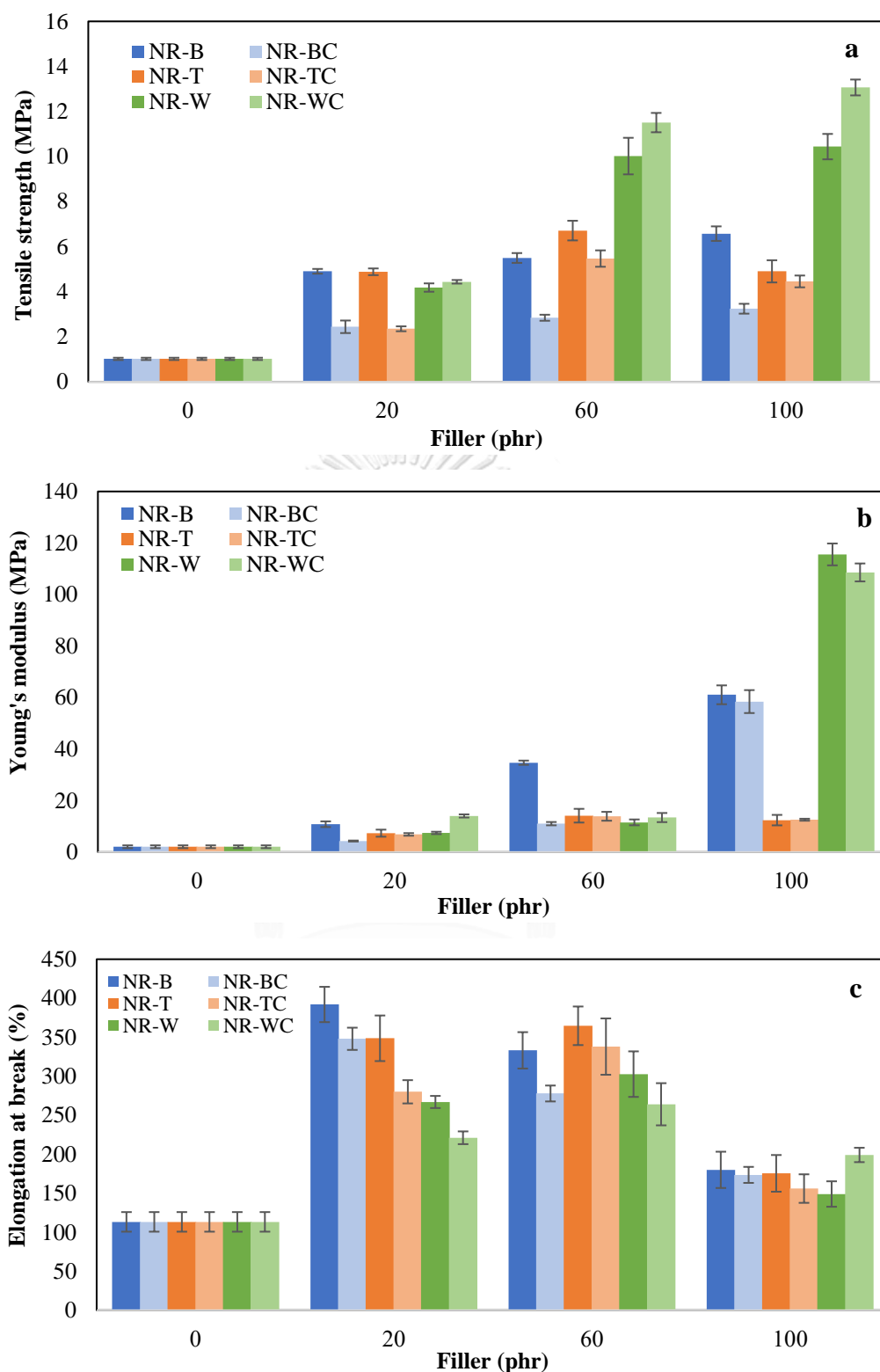
Figure 4. 11 Mechanical properties, tensile strength (**a**), Young's modulus (**b**) and elongation at break (**c**) of NR, NR–B, NR–BC, NR-T, NR-TC, NR–W and NR–WC composite with filler loading content at 0, 20, 60 and 100 phr.

The reinforcement effects on Young's modulus of composites filled with BRHA, BRHAT and WRHA were quite similar to those on tensile strength. The values of Young's modulus were improved significantly, as compared to that of pure NR film, and the values increased with increasing filler content, as shown in Figure 4.11b. The large modulus of NR composites with RHA could attribute to rubber molecule in rubber can return to their original position after being stretched. The maximum values of young's modulus of NR–B, NR–W, NR–BC and NR–WC films were obtained by BRHA and WRHA loadings at 100 phr, which were 61.1, 115.6, 58.4 and 108.6 MPa, respectively. Moreover, the maximum Young's modulus of NR-T and NR-TC films were 14.1 and 13.9 MPa that were obtained by BRHAT loadings at 60 phr. Young' s modulus of BRHAT composites were lower than BRHA composites could be attributed to metal impurities in BRAH and BRHAT particles. After acid treatment, silica content in BRHA increased but Al_2O_3, K_2O, CaO, P_2O_5, MgO and Fe_2O_3 contents decreased. These metal impurities might be important role to improve filler–filler and filler–rubber interactions, resulting in more improved mechanical properties of NR composites. These results agree with those of Panitchakarn et al.[51], who reported that the tensile strength and modulus of NR composite with coal fly ash that was treated by acid washing were lower than NR-composite with untreated coal fly ash.

As compared to the result of the NR film shown in Figure 4.11c, it is demonstrated that reinforcement with BRHA, BRHAT and WRHA can also improve elongation at break of the composite films. The maximum values of elongation at break of NR–B at 392.0% NR-T at 364% and NR–W at 302.7% were obtained at filler loading of 20 phr and 60 phr, which were 3.5-fold, 3.2-fold and 2.7-fold increases of that of the NR film, respectively. However, the values relatively decreased with further increases in filler loading beyond the optimal point, because the elasticity of the rubber chains was reduced when filler particles exceeded a certain amount in the rubber matrix [83, 84].

In the case of a small amount of filler in NR composite (20 phr), the tensile strength, Young's modulus and elongations at break of composites filled with BRHA and BRHAT were better than those filled with WRHA. These results might be attributable to the smaller particle size of BRHA and BRHAT, since the smaller

particle with higher specific surface area should facilitate a better filler—NR interaction [85]. However, when increasing filler loading in the NR composites to 60 and 100 phr, the tensile strength and Young's modulus of NR–WRHA were greater than those of NR–BRHA and NR-BRAHT. Thus, factors, such as surface activity, chemical composition of fillers, concentration, shape and interactions between fillers and NR matrix play important roles in the reinforcement of NR composites. As compared to BRHA and BRAHT, WRHA contains a higher concentration of silica but lower concentration of carbon. Higher concentration of silica and metal oxides in fillers could promote reinforcement in NR composites. Additionally, in this study, the solid dispersion of SiO_2 in NR matrix was successfully improved by the addition of alginate as dispersion agent, resulting in no phase separation at high filler loading in NR matrix. The results agree with those of previous works on vulcanized rubber composites [84, 86]; it was reported that the mechanical properties of rubber vulcanizates filled with WRHA were better than composites filled with BRHA.

Further crosslinking of the composites by $CaCl_2$ significantly improved the tensile strength of NR–WRHA, especially at high WRHA loading content. After the immersion of NR composites in $CaCl_2$ solution, calcium ion created gelation and ionic crosslinking with specific and strong interactions between Ca^{2+} with G blocks of alginate, forming the net structure [87]. This ionic crosslinking can improve the structural stability of the composite films and reinforce filler–filler and filler–rubber interactions, resulting in enhancement of the tensile strength of the composite film. After crosslinking sodium alginate/natural rubber/coconut composite by $CaCl_2$, the composites were highly stable [41]. However, it was found that the mechanical properties of NR–BC and NR–TC films were reduced by crosslinking the composites by $CaCl_2$. The different effects of $CaCl_2$ crosslinking on NR–BRHA, NR-BRHAT and NR–WRHA might be attributable to differences in the porous structure of those fillers. WRHA presents bimodal porous structure with higher porosity and higher pore sizes, resulting in better dispersion of $CaCl_2$ into the mixtures and more interactions of fillers–alginate–NR of NR–W films. Consequently, alginate crosslinking with Ca^{2+} could enhance the tensile strength of NR–WC. A similar observation was also noted by Costa et al. [86]. The efficiency and rate constant of vulcanization of NR–BRHA was found to be lower than that of NR–WRHA vulcanization, because the pores of

BRHA were too small for polymer chains to enter. Moreover, large internal surface areas might be a disadvantage, because a certain proportion of accelerator might become immobilized and inactivated. The adsorbed Ca^{2+} on surface might result in weakened filler–rubber interactions. Thus, mechanical properties of the NR–BC and NR–TC composite films were reduced by $CaCl_2$ crosslinking.

Table 4.3 shows the results of mechanical properties of BRHA, BRHAT and WRHA composites crosslinked with sulfur vulcanization with RHA loading at 100 phr in comparison to those of the films of neat NR and NR reinforced with RHA loading at 100 phr with/without $CaCl_2$ crosslinking. The results revealed that the mechanical properties of vulcanized NR composites were larger than neat NR film. Sulfur vulcanization generally changes the physical properties of natural rubbers. The hardness, modulus and tensile strength of vulcanized rubber increased, whereas elongation at break and solubility in solvents decreased when comparing to neat NR. All those changes could attribute to the degree of cross-linking in the rubber network [88]. In addition, tensile strength and elongation at break of sulfur vulcanized composites were relatively higher than tensile strength and elongation of NR-RHA composites with/without $CaCl_2$ crosslinking. However, Young's modulus of sulfur vulcanized composites was lower than that of the NR composite films with/without $CaCl_2$ crosslinking. In part of chemical mechanism of crosslinking by vulcanization process, the flexible NR molecular chains joined together by covalent bonding giving rise a three-dimensional network that resulted in enhance of tensile strength of vulcanized NR composites [89]. These results agree with those reported by Wahab et al. [90], who identified increment in tensile strength of thermoplastic elastomers from high-density polyethylene/NR/thermoplastic tapioca starch, indicating the increase in blend stiffness. In addition, the vulcanized NR process can prevent or reduce ability of polymer chains in NR to slip over each other result in a more rigid polymer blend. Interestingly, at the same RHA loading, tensile strength of NR-WC100 was only slightly less than that of NR-WS100. This result indicated ionic crosslinking alginate with $CaCl_2$ could effectively improve mechanical properties without using toxic chemical in crosslinking process.

Table 4. 3 Mechanical properties of NR, NR composites cross-linked with $CaCl_2$ and NR composites cross-linked with sulfur vulcanization.

NR composites	Young's modulus (MPa)	Tensile strength (MPa)	Elongation at break (%)
NR	2.07 ± 0.55	1.02 ± 0.05	113.30 ± 12.56
NR-B100	61.07 ± 3.66	6.58 ± 0.32	180.00 ± 23.25
NR-T100	12.41 ± 2.03	4.90 ± 0.49	175.50 ± 23.51
NR-W100	15.57 ± 4.25	10.44 ± 0.56	149.00 ± 16.31
NR-BC100	58.43 ± 4.45	3.24 ± 0.22	173.53 ± 10.28
NR-TC100	12.57 ± 0.39	4.46 ± 0.26	156.01 ± 18.29
NR-WC100	108.57 ± 3.48	13.07 ± 0.35	199.10 ± 9.20
NR-BS100	6.11 ± 0.96	11.67 ± 0.89	336.00 ± 15.75
NR-TS100	5.80 ± 0.64	11.37 ± 0.51	320.67 ± 17.91
NR-WS100	12.89 ± 0.95	13.19 ± 0.25	321.30 ± 29.45

The previous studies demonstrated the limitations of polar filler loading in NR composites. They found the tensile strength of the NR composite increased with increasing the filler content up to a maximum value (20–60 phr) and then decreased [6, 8, 83, 84, 91]. Higher filler loading in NR composite could lead to formation of filler agglomeration and undispersed filler in NR matrix, resulting in a weak filler–rubber interaction. RHA has high surface polarity and strong filler-filler interaction, which leads to filler agglomerates and poor RHA dispersion in NR matrix, resulting in low mechanical properties of NR composite. The present study demonstrates that the tensile strength of uncured NR composites increases with increasing BRHA and WRHA loading, and that the maximum tensile strength was obtained at BRHA/WRHA loading of 100 phr. The results indicate that the latex aqueous microdispersion process with dispersing agent is suitable for composite preparation to achieve homogeneous dispersion of RHA fillers in NR matrix. Sodium alginate is suitable for the use as a dispersing agent in this system, because it can improve RHA dispersion and reduce filler-filler interactions. Previously, sodium alginate as a dispersing agent was proven to improve the stability, filler dispersion and viscosity of

composites of NR–coal fly ash [51], NR–sago starch [92] and NR–microfibrillated cellulose [93].

4.6 Water Absorption Capacity

In the water sorption and toluene sorption tests, the length and width of the film specimen were 2 cm and 2 cm. The thickness was 0.5–0.6 mm. The film thickness slightly increased with increasing filler content but was not significantly changed by $CaCl_2$ cross-linking. The results of the water absorption capacity (WAC) tests of NR and NR composites filled with BRHA, BRHAT and WRHA are presented in Figure 4.12. The WAC of NR film was lower than NR–B, NR-T and NR–W films, due to the hydrophobic nature of NR. The water absorption of NR film was nonlinearly increased during a period of 0–6 days for water uptake of 0–31% and then was slightly increased during the immersion in water for 6–18 days. The water absorption behavior of filled polymer composites depended on the properties and nature of fillers such as functionality, polarity, specific surface area, filler loading and time in water [94]. The results demonstrate that the water absorption of NR–B, NR–BC, NR-T, NR-TC and NR–W increase with increasing filler loading content, due to the hydrophilic nature of silica and other metal oxides, which are the main components in three types of ashes. The water uptake rates of the composite NR films filled with BRHA, BRAHT and WRHA were higher, as compared to NR film, and the saturation point was reached after the immersion in water for 2 days. The fillers, BRHA, BRHAT and WRHA, are polar compounds and contain hydroxyl groups from silica and other metal oxides. The surface hydroxyl groups on metal oxides are sites for the absorption of water molecules by hydrogen bonding. Thus, the increased RHA loading content promoted WAC of the composite films. Metal content in BRHAT was lower than BRAH and WRHA resulted in higher WAC than NR-BRHA and NR-WRHA composites. NR composite filled with RHA was previously reported [95, 96]. Without the $CaCl_2$ crosslinking process, the composite film filled with WRHA demonstrated higher WAC than that filled with BRHA, which is likely due to the higher amount of SiO_2 in WRHA, as compared to BRHA. The maximum WAC at around 78% was obtained from NR–W films at WRHA loading content of 100 phr.
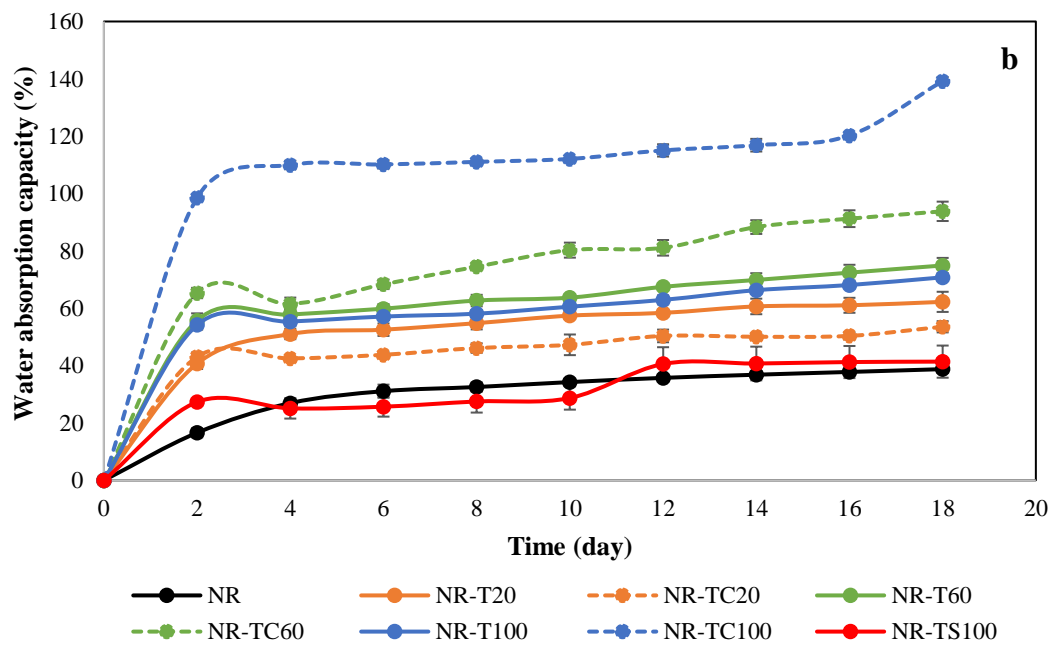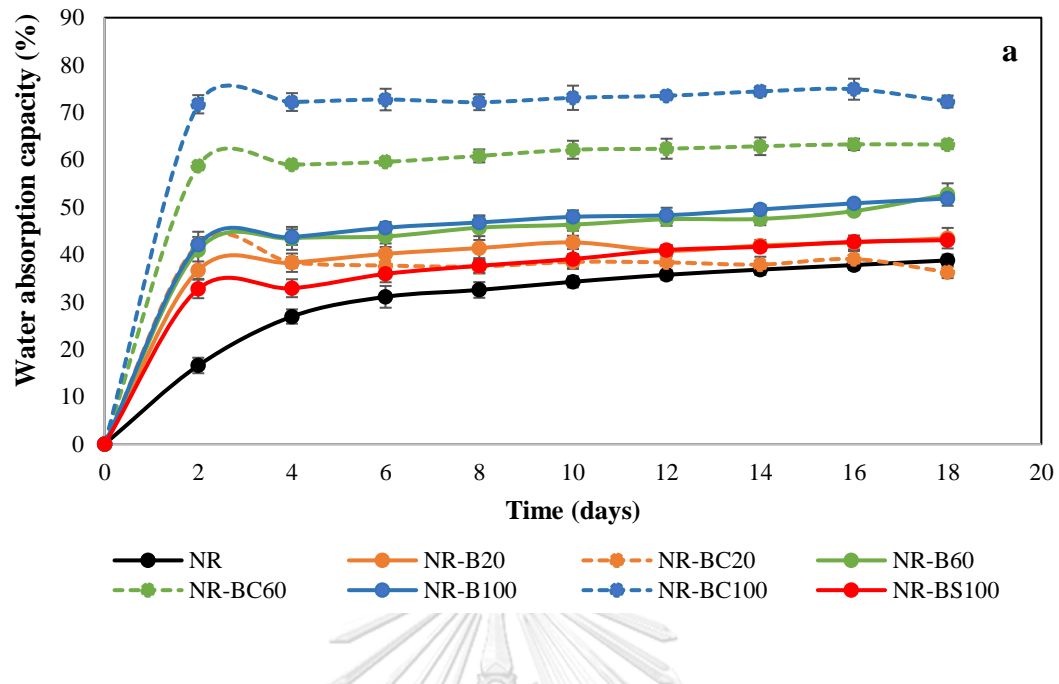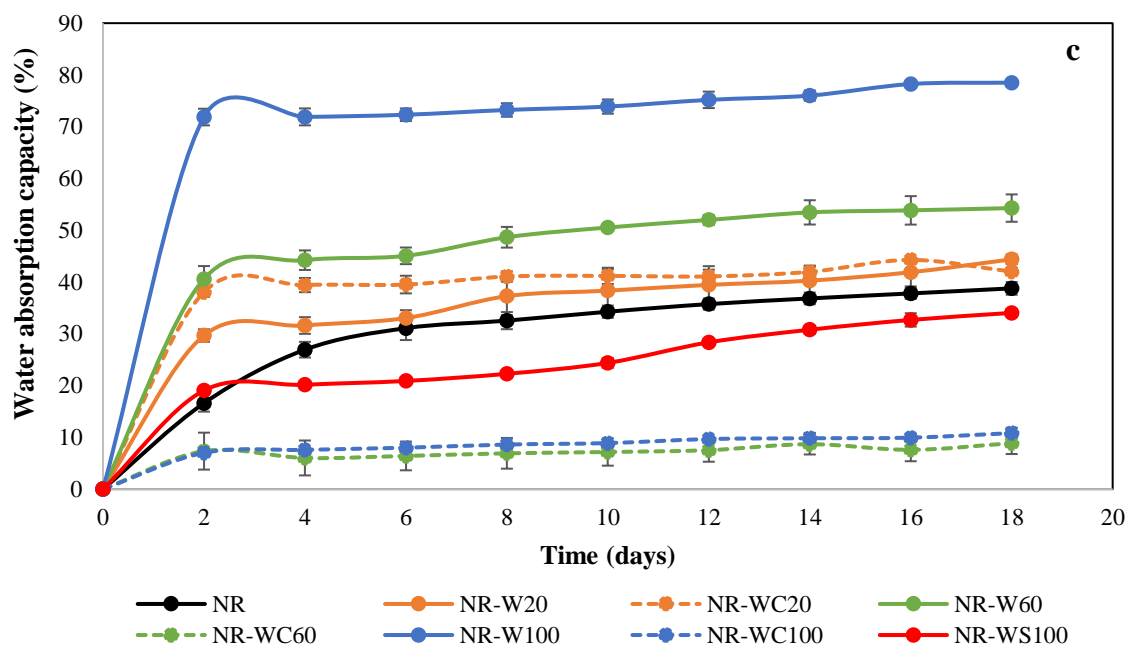
Figure 4. 12 Water absorption capacity of NR, NR–B, NR–BC (**a**), NR-T, NR-TC, NR-TS (**b**) and NR–W, NR–WC, NR-WS (**c**).

The treatment by $CaCl_2$ had different effects on the WAC of the NR composites filled with BRHA, BRHAT and WRHA. The $CaCl_2$ crosslinked NR–WC showed considerably enhanced resistance for water uptake, especially at high WRHA loading content of 60 and 100 phr (Figure 4.12c). The water uptake of NR–WC at WRHA loading 100 phr was reduced to 11%, which was only ≈1/7 that of NR–W100 and was only ≈1/4 that of NR film. Previously, a significant reduction in water solubility of crosslinked alginate-based films by 1% $CaCl_2$ was reported [87]. It was suggested that the crosslinking alginate by $CaCl_2$ generated an "egg box" network. The COO^- in the alginate binds to the $Ca^{2+,}$ resulting in reduced available alginate chains to bind with H_2O molecules. The crosslinking NR–W composites by $CaCl_2$ could also increase filler–rubber interactions and limited water diffusion into the NR–W composites. Accordingly, NR–WC presented lower WAC after crosslinking by $CaCl_2$. On the other hand, the WAC of NR composite films filled with BRHA and BRHAT were increased after crosslinking by $CaCl_2$ (Figure 4.12a, b). As previously discussed in the noneffective alginate crosslinking by Ca^{2+} of NR–BC and NR-TC composite films, in this case, the addition of $CaCl_2$ was found to reduce filler–rubber interaction in NR–BC and NR-TC composites. The available COO^- in alginate molecule and OH^-

in silica oxides could interact with water molecules, leading to higher water absorption of NR–BC and NR-TC. The addition of $CaCl_2$ might also increase hydrophilicity of the films and, therefore, increase the water diffusion into NR–BC and NR-TC films. The effect of different crosslinking agents, WAC of NR composites with sulfur vulcanized was the lowest comparing with WAC of NR composite with/without crosslinking by $CaCl_2$ at same filler loading. These results indicated sulfur vulcanized can reduce WAC of NR composites due to stiffer and stable structure of vulcanized NR films resulting in less penetrable by water molecules [97].

4.7 Toluene Uptake

The results of the toluene uptake of NR and NR composite films soaked in toluene for 8 h are shown in Figure 4.13. The maximum toluene uptake of NR film was 1746% at the immersion in toluene for 4 h; after that, the film was decomposed in toluene. Toluene and NR are nonpolar; thus, this solvent can be highly absorbed in NR film. The high uptake rate and poor chemical resistance to nonpolar solvents of uncured NR were previously reported [51, 77, 96]. Uncrosslinked NR chains can dissolve in toluene, and the decrease in the solvent uptake of NR composites may reveal good filler-rubber interaction [96]. The toluene uptake rate of NR–B, NR–T and NR–W composites at RHA loading of 20 phr was much less than that of NR film; however, after the immersion in toluene for 4 h, both NR–B, NR-T and NR–W were, to some extent, decomposed in toluene. Uncured NR composites might be dissolved in nonpolar solvents, such as toluene [98]. More resistance to toluene uptake was observed in the NR composites with higher BRHA, BRHAT and WRHA content. The toluene uptake of the composite films decreased with increased filler loading and was considerably lower, as compared to that of pure NR film [51, 93]. The low toluene uptake of NR–B, NR-T and NR–W films was exhibited at RHA loading of 60–100 phr, which represented about 260–300% (or 0.15–0.17 of that of the NR film), due to polar nature of silica oxides, the major constituent in three types of RHAs. The integration of polar fillers into NR matrix can reduce the toluene uptake rate and absorption capacity. In addition, the NR composites filled with BRHA/WRHA at 60–100 phr maintained their structural stability during immersion in toluene for 8 h. This observation indicates that the composite films had good dispersion of RHA in the NR

matrix. After crosslinking by CaCl₂, the NR composites filled with WRHA, BRHAT, BRHA demonstrated slightly improved resistance to toluene. The toluene uptakes of NR–BC, NR-TC and NR–WC were reduced to 170–180%. The crosslinked films had better stability in toluene, as no decomposition of the films was observed during immersion in toluene for 8 h. Thus, the CaCl₂ treatment seems to improve the solvent resistance of composite films. The addition of calcium ions into NR matrix possibly makes the surface more hydrophilic, resulting in lower diffusion of nonpolar solvent into NR matrix. The lowering of toluene uptake might also be attributable to the good interaction between filler and NR matrix [99]. Sulfur vulcanized NR composites present low toluene uptake that close to toluene uptake of NR composite with/without crosslinking by CaCl₂ at filler loading 100 phr. These results indicated sulfur vulcanized can improve resistance of nonpolar solvent uptake of NR composites. The structural stability of NR composites was improved because the rubber chain motions were restricted by sulfur vulcanized and addition of RHA.
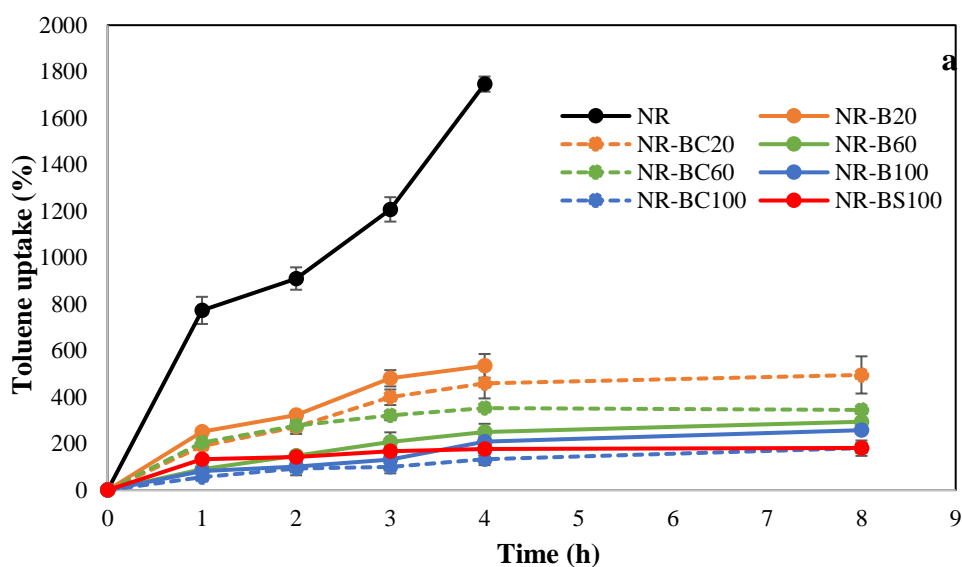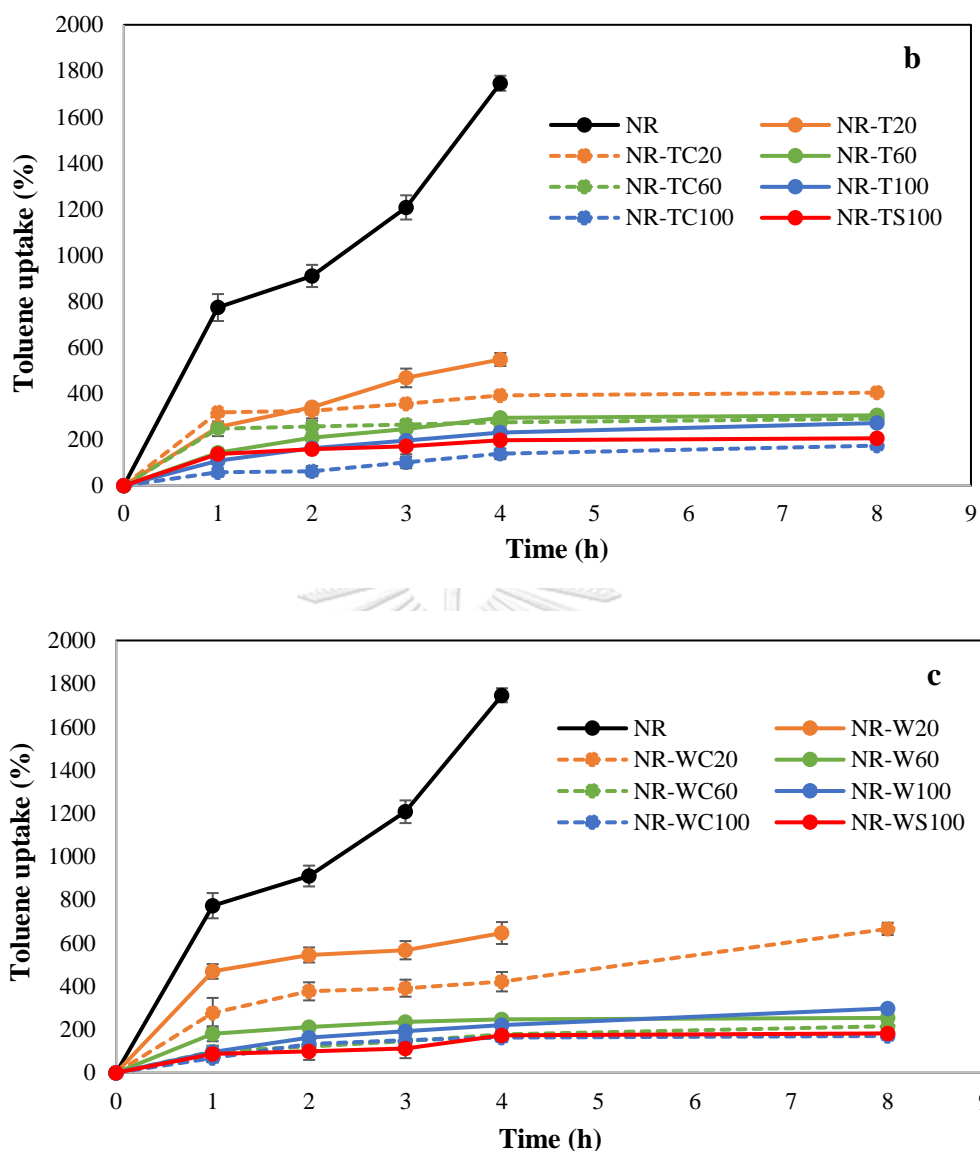
Figure 4. 13 Toluene uptake of NR, NR–B, NR–BC, NR-BS (**a**), NR-T, NR-TC, NR-TS (**b**) and NR–W, NR–WC, NR-WS (**c**).

4.8 Biodegradation in Soil

The preliminary study of biodegradation in soil of pure NR film and NR composite films filled with RHAs was determined in uncontrolled conditions (with an average temperature of ≈30 °C). The percentage weight loss and the visual analysis of the biodegraded samples after 1, 2 and 3 months are shown in Figures 4.14 and 4.15, respectively. The weight loss of the pure NR film was lower than all NR composite films at any degradation time, due to the slow degradation of NR in natural environments by microorganisms [100].

After 3 months, the weight loss of NR, NR–BRHA, NR-BRHAT and NR–WRHA were 5.3%, 7.6–13.0%, 5.3–14.5% and 7.6–18.4%, respectively. Overall, the NR–BRHA and NR–BRHAT composite presented comparable weight loss to NR–WRHA composites at similar RHA loading contents, except for the NR composites with 100 phr RHA loadings, of which, NR–W100 demonstrated relatively higher biodegradability in soil. The weight loss of composites increased with increased filler loading in all conditions. These results agree with those of Ramasamy et al. [101], who reported that the weight loss percentage of NRL foam increased with increased rice husk powder, because, at lower rice husk powder loading in foam composite, microbial activity was not high due to lack of microbial growth supports.
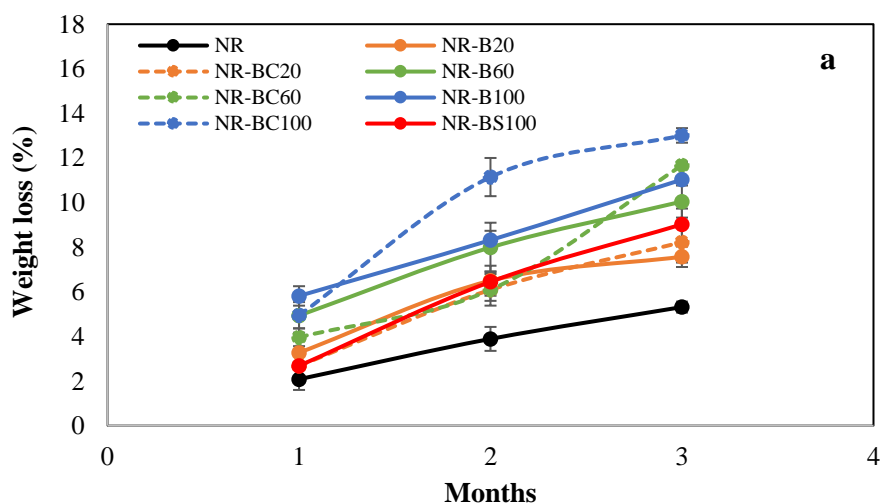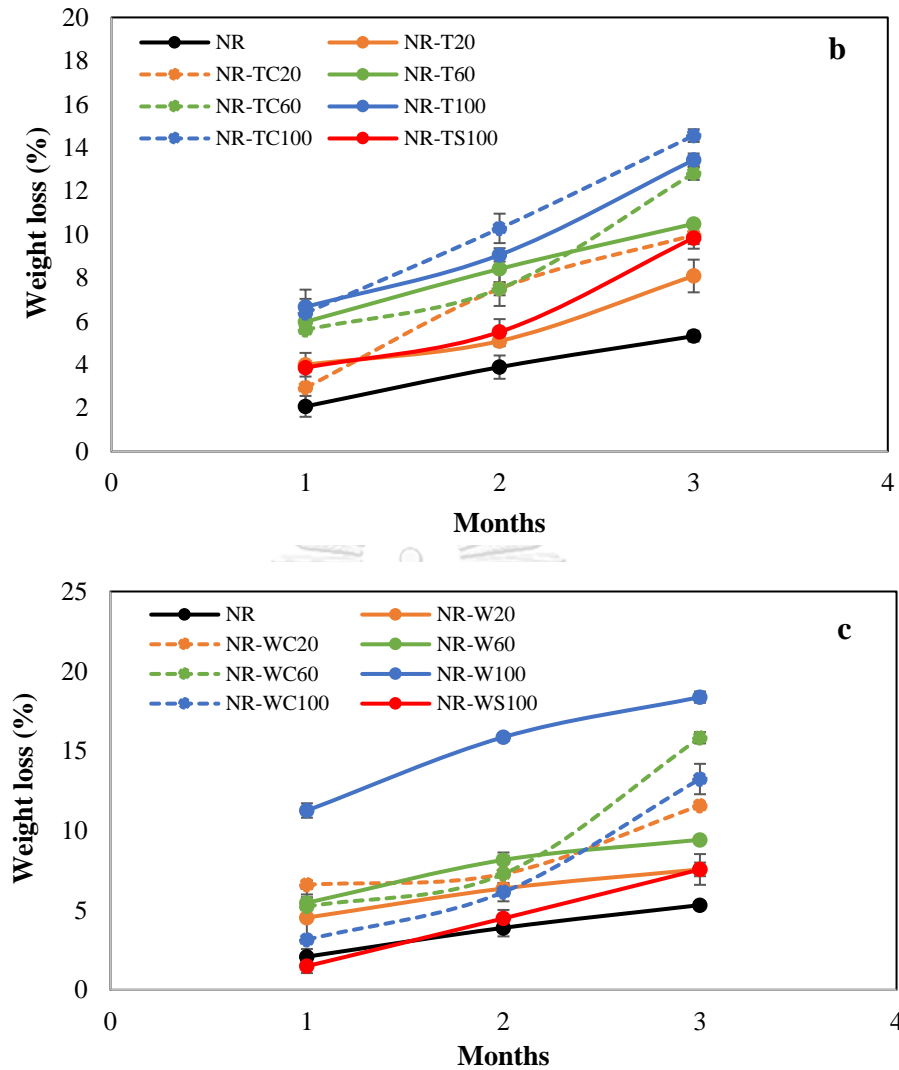
Figure 4. 14 Preliminary test for biodegradation in soil of NR, NR–B, NR–BC, NR-BS (**a**), NR-T, NR-TC, NR-TS (**b**) and NR–W, NR–WC (**c**).

Pure NR

1 month   2 months   3 months
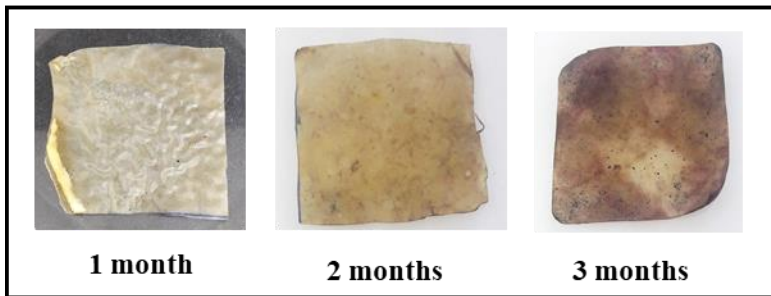
| NR-BC20 | NR-BC60 | NR-BC100 | NR-WC20 | NR-WC60 | NR-WC100 |

1 month
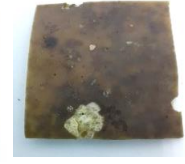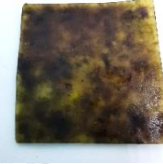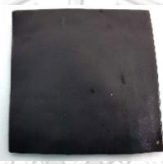
2 months
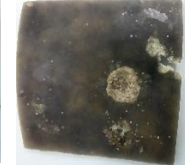
3 months
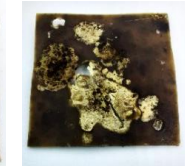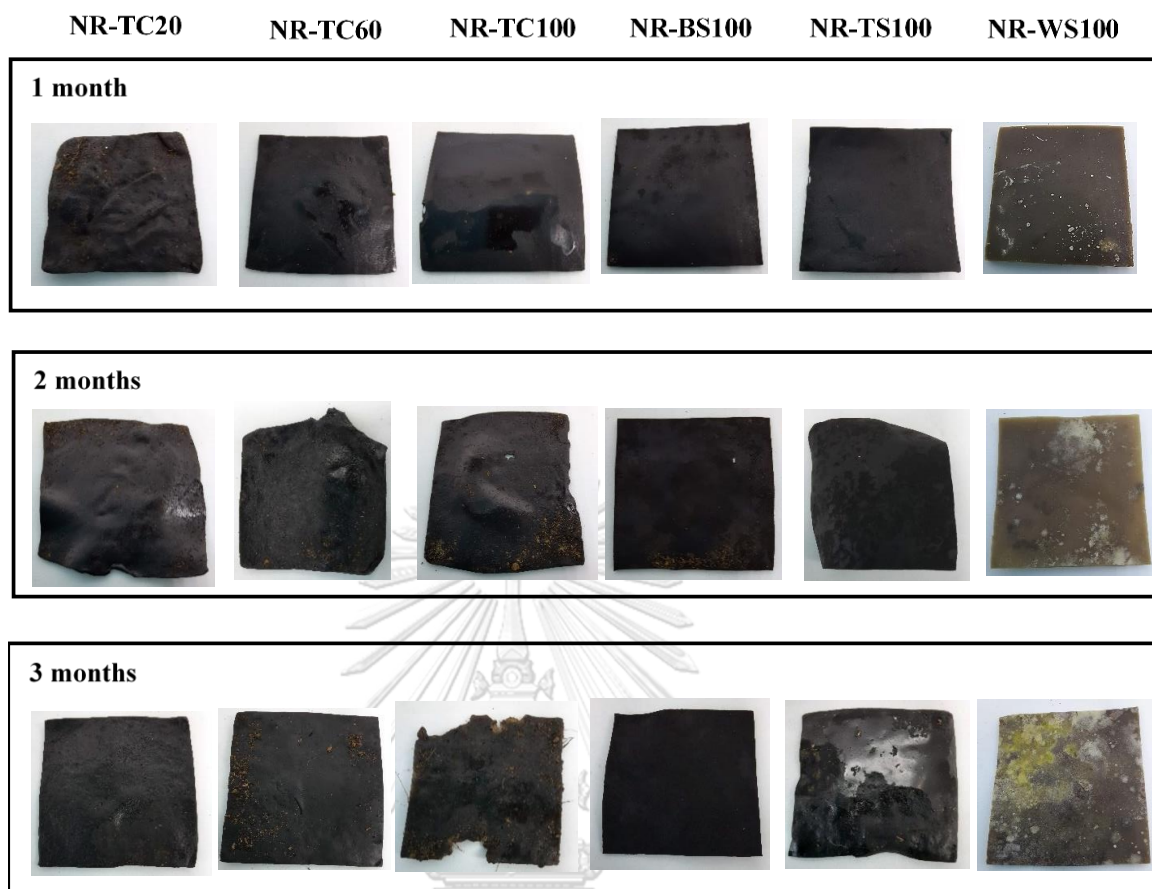
Figure 4. 15 The visual analysis of biodegradation in soil of pure NR, NR–BC, NR–WC, NR-TC, NR-BS100, NR-TS100 and NR-WS100 for 3 months.

The effect of the $CaCl_2$ treatment of the NR composites was observed from the composites at filler loading of 100 phr in both cases but in opposite directions. The weight loss of NR–BC100 and NR-TC100 were higher than that of NR–B100 and NR-TC100, respectively, whereas the weight loss of NR–WC100 was lower than NR–W100. These results are in accord with those on the water absorption capacity, which can be explained by the high number of fillers in NR matrix generating hydrophilic surfaces, resulting in enhanced water absorption of the composites. The higher water content in NR matrix could promote microbial activities that increase the rate of degradation [83, 102]. The weight loss of NR–WC100 was lower than NR–W100, because the $CaCl_2$ crosslinked film displayed a higher tensile strength with lower WAC, as compared to NR–W100. On the other hand, the weight loss of NR–BC 100 was higher than NR–B100 and the weight loss of NR–TC100 was

higher than NR–T100, due to the higher WAC of the composite after $CaCl_2$ crosslinking, as discussed earlier. It was also suggested that the use of sodium alginate as a dispersing agent in NR composites could increase the rate of biodegradation of the composites [92]. In addition, the weight loss of sulfur vulcanized NR composites was the lowest when comparing to composites with/without crosslinking by $CaCl_2$ that could attribute to high tensile strength, stable structure and low WAC properties of vulcanized NR composites with RHA.

Figure 4.15 presents visual analysis of the biodegradation of NR and NR composite films during a period of 1–3 months. The enhanced degradation of NR composite films filled with higher RHA loading was clearly observed, especially at 3 months of biodegradation in soil. Black spots were found in the composite films reinforced with WRHA, while white spots, as well as fogging on film surfaces, were observed after 1 month in soil, indicating soil microflora activities in the composites, which is a good indicator of biodegradation [103]. Moreover, after 3 months in soil, some parts of the composite films disappeared. The results revealed that NR–BRHA, NR–BRHAT and NR–WRHA could be biodegradable in soil.

4.9 Electrical Properties

4.9.1 Dielectric properties

Dielectric properties of materials are important characteristics for predicting behavior with respect to application in electronic materials, such as print circuit boards, power transformers, microelectronics, radio propagation, remote sensing and actuator applications [9]. The dielectric properties of polymers depend on cations, dipole moment and space charge polarizations [104]. On the other hand, dielectric behavior of composite materials depends on dielectric properties of the matrix and filler, chemical composition, structure, shape and morphology of particles and filler dispersion in the composite [105]. The dielectric constant is the amount of energy from an external electrical field stored in materials. The dielectric constant of NR–BRHA, NR–BRHAT and NR–WRHA composites at different filler loadings are presented in Figure 4.16. The frequency dependence of the dielectric constant at ambient temperature was analyzed. The NR film had a low dielectric constant, in the range of 1.8–2, attributable to the nonpolar nature of NR, which has only

instantaneous electronic and atomic polarization [70]. It was demonstrated that the dielectric constant of the NR composite films filled with RHAs increased with increased BRHA, BRHAT and WRHA loading at all frequencies. BRHA, BRHAT and WRHA contained 87, 90 and 95% silica oxides with polar hydroxyl groups of silanol (Si–OH) on surface. Silica as a dielectric metal oxide semiconductor has a dielectric constant of about 3–9, and it has been used in micro- and nano-electronic industries [13]. Thus, the increase of RHA in NR composites resulted in higher dipole or orientation polarization; thus, the dielectric constant was enhanced [70]. In addition, the increase in RHA loading resulted in an increased space charge, leading to polarization in the composite matrix [57]. It was shown that the NR composite films presented a higher dielectric constant at lower frequencies. At high frequency, molecular movements arrested or decreased orientation polarization that leads to the decreased value of the dielectric constant [57, 106]. The dielectric constants of NR–BRHA were relatively higher than those of NR-BRHAT and NR–WRHA, which should be due to the higher degree of crystallinity of BHRA, as compared to that of WRHA. Correlations between crystal structure and dielectric properties of metal oxides were reported [107]. Dielectric constant of NR-BRHAT composites was lower than NR-BRHA and NR-WRHA could attribute to lower metal impurities content in BRHAT after treatment by acid washing. Metal and carbon-based filler could be acting as charge centers and increasing segmental mobility in the polymer matrix, which would enhance the dielectric constant of composites [108, 109]. Oxides are suggested as promising materials in high dielectric materials, as they possess both high dielectric constants and large band gaps [107].
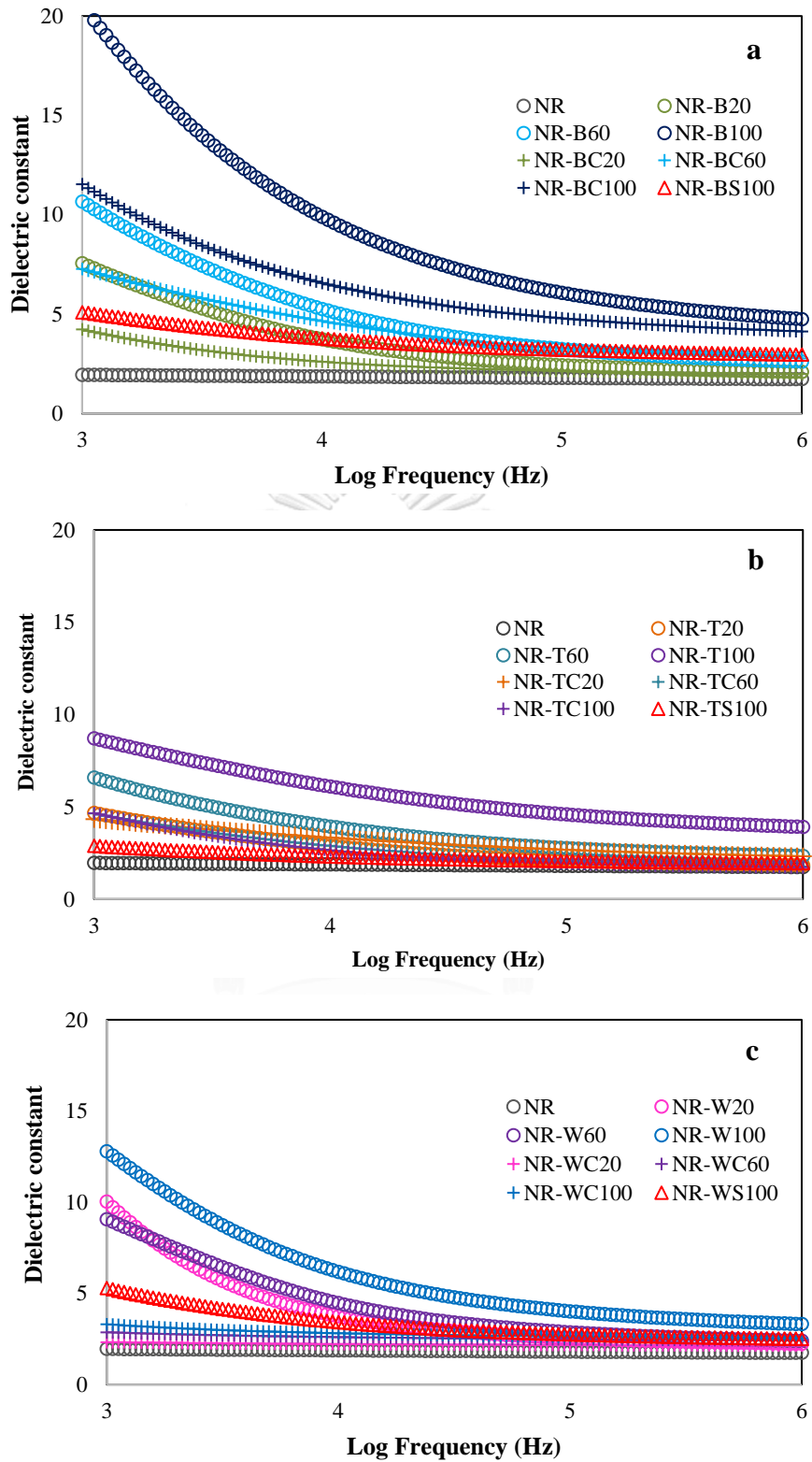
Figure 4. 16 Dielectric constant of NR, NR–B, NR–BC, NR-BS (**a**), NR, NR-T, NR-TC, NR-TS (**b**) and NR, NR–W, NR–WC, NR-WS (**c**)

The crosslinking of the composite films by CaCl$_2$ caused a considerable drop in dielectric properties in all cases. The addition of CaCl$_2$ might reduce the amount of electron charges, including COO$^-$ (from alginate) and OH$^-$ (from silica), in the composite films. The higher number of free protons suggests more localization of charge carriers along with mobile ions, resulting in higher dipole polarization and a higher dielectric constant [106]. For this reason, the value of the dielectric constant of composite film after crosslinking alginate was much lower than that of films without CaCl$_2$ treatment. The obtained values for the dielectric constants of the films from the lowest value to the highest value were NR < NR-TC < NR–WC < NR–BC < NR-T < NR–W < NR–B. These results could also imply that low metal impurities content in BRHAT resulted in reducing segmental mobility in the polymer matrix. Moreover, the stronger interactions between WRHA filler and NR matrix could lower the hydrophilicity and polarity of the composite films. In case of sulfur vulcanized crosslinking, dielectric constant of NR-WS, NR-BS and NR-TS was lower than dielectric constant of uncrosslinking NR composites with RHA. These results indicated that high tensile strength of vulcanized NR film resulted in low dielectric constant of NR composites with RHAs. A similar effect from the reinforcement that caused the reduction of orientation polarization and the dielectric constant was previously reported [70].
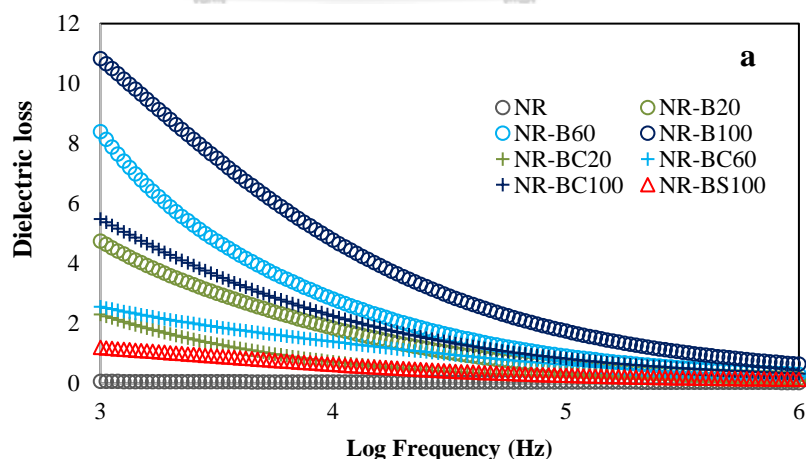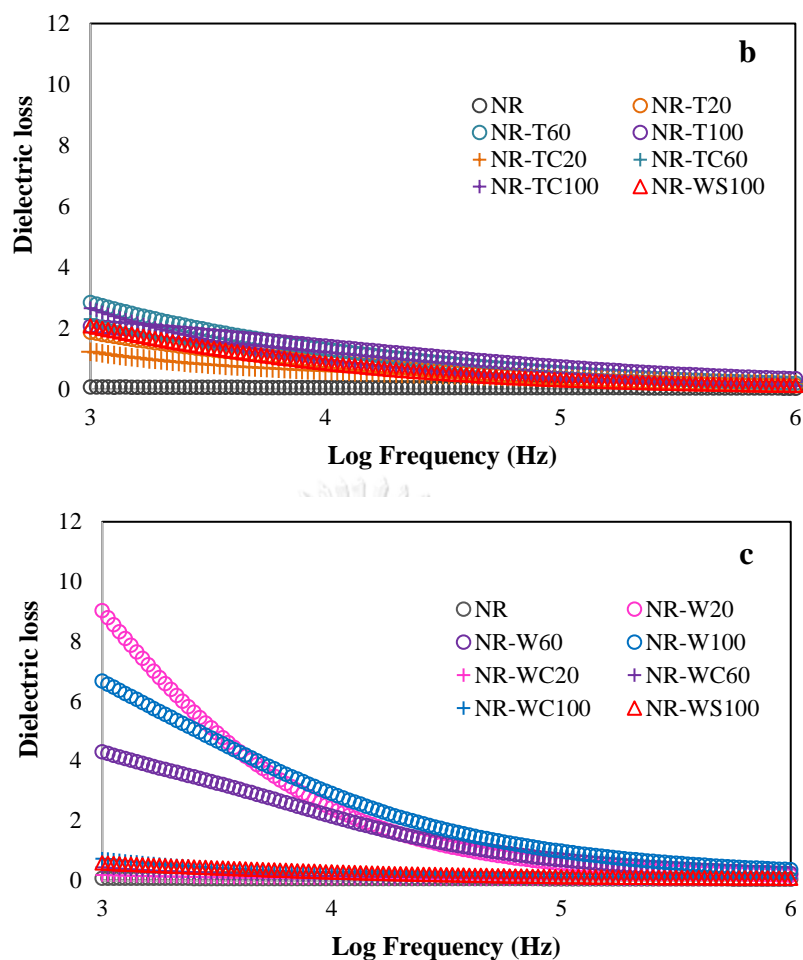
Figure 4. 17 Dielectric loss of of NR, NR–B, NR–BC, NR-BS (**a**), NR, NR-T, NR-TC, NR-TS (**b**) and NR, NR–W, NR–WC, NR-WS (**c**)

The dielectric loss factor presents the amount of energy loss from a material due to an external electric field [14]. The frequency dependence of dielectric loss of composites is shown in Figure 4.17. The values of dielectric loss demonstrate similar trends as those of the dielectric constant, which increased with increased filler loading and declined with increases in frequency. The increase of RHA loading enhanced the polar groups in the composite films, which led to enlargement of orientation polarization and relaxation in composite, resulting in relatively high energy loss [57]. In addition, increasing amorphous phase to the composite enhanced the flow of current through the amorphous region and generated amorphous phase relaxation, resulting in higher dielectric loss [70, 110]. At low frequency, dielectric loss was high, because of interfacial polarization enhanced by the difference between the

conductivity of various phases [57]. This result agrees with the previous work by Jamal et al. [109], in which the dielectric loss of nickel–rubber nanocomposites was high at frequency lower than 10^5 Hz, due to relaxation time of pure rubber enhanced when nickel nanoparticles were incorporated into the matrix. Moreover, the results indicate dielectric loss factor of NR–WC composites was lower than that of other composites at all WRHA loadings (~0.7–2.1 at frequency 10^3 Hz). The effect of crosslinking composite by CaCl$_2$ and sulfur vulcanized on the reduction of the dielectric loss factor was the same as that on the dielectric constant for similar reasons. Less free space in the matrix resulted in a low dielectric loss factor [106].

4.9.2 Electrical conductivity

The improved electrical conductivity by adding fillers in nonconductive biopolymeric matrixes is a simple and efficient method to produce electrically conductive multifunctional biopolymer composites, while maintaining the low cost, biocompatibility, biodegradation and processability of the initial material. Figure 4.18 illustrates electrical conductivity of NR, NR–BRHA, NR–BRHAT and NR-WRHA composites with different crosslinking agent and filler loading. Neat NR film exhibited low electrical conductivity about 2.1×10^{-15} 1/Ω.cm. Generally, electrical conductivity of elastomers was less than 10^{-12} 1/Ω.cm [111]. The results from Figure 4.18 indicated that electrical conductivity of NR-composites with three types of RHAs loading had a similar trend as observed from that of dielectric constant and dielectric loss. Electrical conductivity of NR-W was larger than NR-B and NR-T at RHA loading at 20 and 60 phr, whereas at filler loading at 100 phr, the electrical conductivity of NR-B was higher than NR-W and NR-T composites, respectively. These results could attribute to different compositions in three types of RHAs. BRHA composed of larger amount of metal and carbon than BRHAT and WRHA. Metal and carbon-based filler could create conductive path in NR matrix for electron transport [62]. It was demonstrated that the electrical conductivity of the NR composite filled with BRHA increased with increased BRHA loading. Electrical conductivity of NR-WRHA increased with increasing WRHA loading until the filler loading at 60 phr. However, it was found that the further loading of WRHA up to 100 phr caused the decrease in electrical conductivity of NR-W and NR-WC composite films. The main

composition of WRHA is silica, which is a poor conductor of electrons (electrical conductivity of silica was of about 5×10^{-14} $1/\Omega.cm$ at 300 °C [112]); thus, at WRHA loading of 100 phr, large amount loading of silica was integrated in NR matrix. The high silica content in the film did not increase conductive path for electrons, but resulted in the reduction of electrical conductivity. The maximum electrical conductivity of NR-B was 4.9×10^{-9} $1/\Omega.cm$ at BRHA loading 100 phr and maximum electrical conductivity of NR-W and NR-T were 4.0×10^{-9} and 7.8×10^{-10} $1/\Omega.cm$, respectively.

Effect of crosslinking of the composites indicted similar trend as that observed from the dielectric properties. The crosslinking of the composite films by $CaCl_2$ and sulfur vulcanize caused a reduction in electrical conductivity in all cases. The addition of $CaCl_2$ might reduce the amount of electron charges, including COO^- (from alginate) and OH^- (from silica), in the composite films. Ionic groups such as COO^- that could help in the movement of the electrons throughout the polymer chain resulted in higher electrical conductivity of uncrosslinking NR composites with RHAs [113]. The electrical conductivity of sulfur vulcanized NR-BS was almost the same as that of NR-WS, which were 6.0×10^{-11} and 6.9×10^{-11} $1/\Omega.cm$, respectively; whereas the electrical conductivity of vulcanized NR-TS was about 2.7×10^{-11} $1/\Omega.cm$. Reduction of electrical conductivity of vulcanized NR-composites reinforced with RHAs could be owing to sulfur crosslinking in NR matrix. The double bonds in carbon-based polymers allow electric flow or transport that could increase electrically conductive in polymer matrix [114, 115]. Sulphur atoms in vulcanization process catch rubber molecules chain at the carbon-carbon double bonds and form C-S-S-C crosslink between the rubber molecules. After vulcanization, double bond in rubber molecules was replaced by sulfur atom that might be caused of decreasing of electrical conductivity in vulcanized NR composites with RHAs.
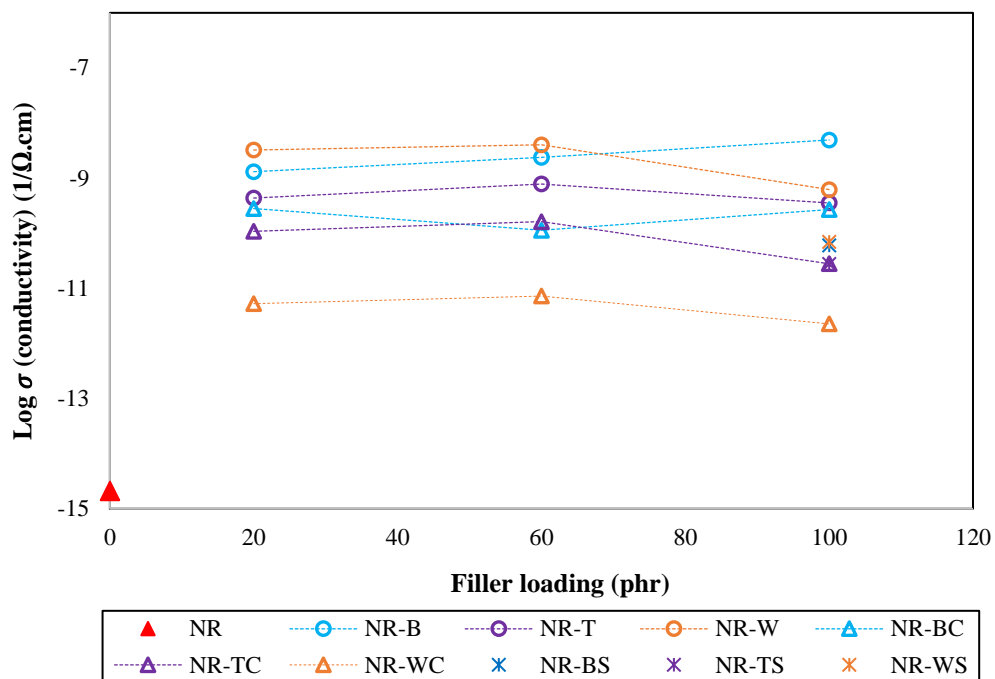
Figure 4. 18 Electrical conductivity of NR, NR–B, NR–T and NR-W composites with different crosslinking agent and filler loading

จุฬาลงกรณ์มหาวิทยาลัย

CHULALONGKORN UNIVERSITY
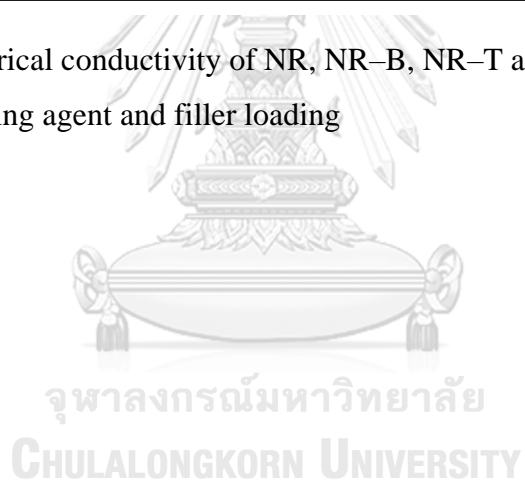
CHAPTER V

Bacterial cellulose reinforced with skim/fresh natural rubber latex for improved mechanical, chemical and dielectric properties

5.1 Introduction

Globally, the level of plastic waste pollution from fossil resources and non-biodegradable polymers has been increasing in recent years; as a result, biopolymers have attracted considerable attention in reducing plastic pollution. Natural biopolymers, produced by plants and several microorganisms, tend to be biodegradable, meaning that they can degrade from exposure to bacteria in soil, compost, or marine sediment [116]. The most widely used biomaterials from natural biopolymers include natural rubber, starch-based materials, cellulose-derived polymers and bacterial cellulose composites. However, biopolymers generally present poor mechanical properties, low chemical resistance, short fatigue life and limited processing capability in comparison to synthetic polymers [117]. Multiple studies interested in improving biopolymers have tested their reinforcement with filler, blending with other polymers and improvements in their production method. Biodegradable polymers can be used in many electronic applications such as flexible displays, sensors, actuators, optics, fuel cells, dielectrics, electromagnetic shielding, piezoelectrics, insulators, (semi) conductors and microwave absorbers [118].

Bacterial cellulose (BC) is an organic compound produced by several bacterial strains in the form of a gelatinous and translucent membrane [119]. BC possesses an interesting 3D nanofiber network structure and displays outstanding physical and chemical properties, including high crystallinities and hydrophilicity, high tensile strength, high water holding capacity, non-toxicity, high purity (absence of lignin and hemicellulose), biodegradability and liquid and gas permeability [120]. BC can be used for applications in the pharmaceutical industry, food packaging, battery separators, adsorbents, cosmetics, biomaterials, electrical conductors or magnetic materials, biomedical materials and scaffolding for tissue engineering [121, 122].

Natural rubber (NR) is one of the most important polymers produced by plants and is widely utilized as raw material for many products due to its excellent flexibility. NR has been used for applications such as vehicle tires, condoms, gloves,

health equipment and accessories, coatings, shoe soles and medical products. Natural rubber latex (NRL) is extracted from a tree called *Hevea brasiliensis* in the form of a colloidal latex of cis-1,4-polyisoprene. Generally, fresh natural rubber latex (FNRL) is composed of about 30-40 wt% dry rubber content (DRC), 1.5-2 wt% protein, 1.5 wt% carbohydrate and 1.3 wt% lipid. FNRL is commonly preserved by adding ammonia and then being centrifuged to obtain concentrated natural rubber latex (CNRL) with about 60 wt% DRC. Skim natural rubber latex (SNRL) is the leftover suspension obtained from the centrifugation process as a low-cost by-product or as waste in some small factories. SNRL is composed of a small amount of rubber particles of about 4-6 wt% DRC with a large amount of non-rubber components. The non-rubber components in SNRL contain mostly water and approximately 3.2 wt% proteins, 0.4 wt% lipid and 3.1 wt% carbohydrates/sugars [123-125]. Typically, SNRL is used to produce skim blocks, skim crepe and lower grade products such as car mats, bicycle wheels, push cars and castors.

Hevea latex shows a bimodal particle size distribution, which can be classified into small rubber particles (SRP: particle size between 10 and 250 nm) and large rubber particles (LRP: particle size between 250 nm and 3 μm) [17, 18, 126]. SNRL contains 81 wt% of SRP and 19 wt% of LRP, whereas FNRL is composed of 24 wt% of SRP and 76 wt% of LRP. SRP and LRP have different particle sizes and branch point structures, leading to the different characteristics and properties of SNR and FNR films [17, 20].

Recent research has focused on the dielectric properties of biopolymer composites, which are a key parameter in predicting the behavior of electronic materials. Natural fibers have also been of growing interest in electrically conductive polymer composites due to their inherent polar and hydrophilic nature [127, 128]. Previous research has studied the dielectric properties of natural fibers with polymers. The dielectric constant of polycarbonate-coated natural fabric *Grewia tilifolia* was 7.3×10^{-6} at 100 Hz and 30°C [128]. For polyaniline-coated nano-cellulose fiber/polyvinyl alcohol composites, the dielectric constant was 1.3×10^{8} at 40 Hz and room temperature [129]. From the previous data, BC appears to exhibit potential for usage in multiple applications, but one disadvantage is its low breaking elongation. NR possesses excellent elastic properties. However, to date, there have been very few

reports of a composite film of NR incorporated into BC matrices. In addition, no reports on composite films of cellulose filled with SNR and FNR have been documented so far. In our previous work, suitable conditions for the incorporation of concentrated natural rubber (CNR) to BC matrices was at 2.5% DRC of CNR concentration at an immersion temperature of 50°C. CNR-BC film from this condition exhibited high structural and thermal stability and favorable mechanical properties [130].

In Chapter IV, rice husk ash (RHA), which was a byproduct from burning rice husk (a cellulose-based fibrous material), was successfully used as filler in NR composite films. The NR-RHA composite films offer many advantageous properties, such as high mechanical properties, high chemical stability, significantly improved dielectric properties and biodegradability. According to the obtained properties, the composites offer potential for further development as stretchable conductive substrate or semiconducting polymer films for electronic applications. On the other hand, the study in Chapter V aims to use different types of NRL (SNRL and FNRL) as a filler to improve the mechanical, chemical and dielectric properties of cellulose matrix in form of BC. The effects of SNR and FNR concentrations and immersion temperature on the chemical, mechanical, biodegradation and dielectric properties of the composite films were investigated. The obtained results could be useful for the development of BC composite films filled with NR as a potential substitute for the existing substrate materials used in electrical insulators, electronic packaging and flexible electronic devices

5.2 Experimental

5.2.1 Materials

The stock culture of *Acetobacter xylinum* bacterial strain AGR 60 was supplied by Pramote Tammarat, the Institute of Food Research and Product Development, Kasetsart University, Bangkok, Thailand. Skim natural rubber latex (SNRL) and fresh natural rubber latex (FNRL) were supplied by Rubber Technology Research Centre (RTEC), Faculty of Science, Mahidol University, Nakhon Pathom, Thailand. SNRL and FNRL contained about 5% and 30% dry rubber content (DRC), respectively. Sucrose and ammonium sulfate were purchased from Ajax Finechem Pty Ltd (New South Wales, Australia). Acetic acid was purchased from Mallinckrodt Chemicals (Paris, KY, USA).

5.2.2 Film preparation

Bacterial cellulose (BC) pellicle was prepared by biosynthesis using coconut water as a based substance. The coconut water medium was mixed with 0.5% (w/v) ammonium sulfate, 5.0% (w/v) sucrose, and 1.0% acetic acid solution (30%, v/v) and sterilized at 110°C for 5 min. Precultures were prepared by a transfer of 15 mL stock culture to 300 mL in 500 mL Erlenmeyer flask and incubated statically at 30°C for 7 days. The sterile medium (60 mL) was added by A. xylinum stock culture (3 mL) in a sterile petri dish and statically incubated at 30°C for 7 days. The BC pellicles were purified by washing with deionized water (DI) for 30 min and, then treated with 1% (w/v) sodium hydroxide solution at room temperature for 24 h remove bacterial cells, washed with running water for 30 min and then rinsed with deionized (DI) water until the pH reached 7.

The procedure for the preparation of BC reinforced with SNR–BC and FNR-BC films were developed from Potivara and Phisalaphong (2019) [130] as follows. SNRL and FNRL were diluted with DI water to form 50 ml SNRL and FNRL suspensions of 1%, 2.5% and 5% w/v. BC pellicle was then immersed in SNRL and FNRL suspension for 48 h as the immersion temperature varied between 50 and 60°C. Then, they were washed with DI water, air-dried at 30°C for 48 h, and stored in plastic film at room temperature. BC was defined as the unmodified BC and SNR–BC and FNR-BC were defined as the modified BC by immersing in SNRL and FNRL

suspension, respectively. The xSNR–BCy or xFNR–BCy films were defined as the modified BC by immersing in SNRL and FNRL suspension at x% DRC and at an immersion temperature of y $^{\circ}$C. For example, 1SNR–BC50 was the BC film modified by immersing in an SNR suspension at 1% DRC and at a temperature of 50 $^{\circ}$C.

5.2.3 Characterizations

Morphologies of composites

Morphologies of neat BC, SNR, FNR, SNR-BC and FNR-BC composite films were observed by Scanning Electron Microscope and Energy Dispersive X-ray Spectrometer SEM-EDS (IT-500HR) using a JEOL, JSM-IT-500HR and JEOL, JED-2300 (Tokyo, Japan). The specimens were frozen in liquid nitrogen and vacuum dried. After that, the specimens were sputtered with gold. The SEM-EDS instrument was performed at an accelerating voltage of 10 kV. The average thickness of the dried BC, SNR, FNR films and BC composite films was measured using the Image J program.

Rubber and protein contents in NRL

The protein content of rubbers was determined by the analysis of nitrogen content using a LECO FP-258 nitrogen analyzer where the dried rubber sample (ca. 0.25 g) was accurately weighed and then subjected to combustion in an oxygen atmosphere. The measurement was repeated three times to obtain the average nitrogen content of each rubber sample. The nitrogen content estimate was multiplied by a factor of 6.25 to the equivalent amount of protein.

The functional groups and chemical structure

The functional groups and chemical structure of films were determined by Fourier Transform Infrared (FTIR) Spectroscopy (PerkinElmer, Waltham, MA, USA) in the ranges of 4000-650 cm^{-1} with a resolution of 4 cm^{-1}.

Mechanical properties

For mechanical properties tests of dry films of BC, SNR, FNR, SNR-BC and FNR-BC composites (Young's modulus, tensile strength, and elongation at break) were performed using Universal Testing Machine (Instron, Norwood, MA, USA). The tests were determined according to ASTM D882. At least five specimens for each different blend composition were tested and the average of the results has been taken.

Water absorption capacity

The measurement of water absorption capacity (WAC) was performed by using the specimen films with dimensions of $2{\times}2$ cm^2, with the thickness of 0.04-0.12 mm. The specimens were immersed in distilled water at room temperature for 0-16 days. The specimens were removed from water every 2 days and excess water at the surface of the samples was blotted by Kimwipes® paper. The weight of wet sample was measured. All testing was carried out in triplicate. Water absorption capacity was calculated by using the formula:

$$\text{Water absorption (\%)} = \frac{W_h - W_d}{W_d} \times 100$$

where, W_h and W_d are the weights of the hydrated and dried specimens, respectively.

Toluene uptake

For the test of toluene uptake, dried sample films of 2×2 cm^2, with the thickness of 0.04-0.12 mm were immersed in toluene at room temperature. The weight change was monitored at 1 h intervals for 8 h. All testing was carried out in triplicate. Toluene uptake was calculated by using the formula:

$$\text{Toluene uptake (\%)} = \frac{W_t - W_d}{W_d} \times 100$$

where, W_d and W_t are the weights of the specimens before and after immersion at a time (t), respectively.

Biodegradation in soil test

For the test of biodegradation in soil, each test specimen having 5x5 cm^2, with the thickness of 0.04-0.12 mm was used for the measurement of biodegradation in soil. Potting soil purchased from a garden center (Bangkok, Thailand) was used for the experiment, the main compositions of potting soil were loam soil, compost manure and coconut coir. The moisture content of the soil was around 50-60 wt%. The specimens were weighed and buried in soil for 6 weeks the depth of 10 cm for 6 weeks under ambient condition, where the temperature range was 24 to 35°C. After 2, 4 and 6 weeks, the samples were removed from soil, washed with DI water, dried at 40°C for 12 hours and recorded for their weights. The degradation was evaluated by measuring the weight loss by using the formula:

$$\text{Biodegradation (\%)} = \frac{W_0 - W_i}{W_0} \times 100$$

where, W_0 and W_t are the initial dry weight of the films (time = 0) and the residue dry weight of films after biodegradation in soil (time = t), respectively.

Dielectric properties

The dielectric constant and dielectric loss factors were measured directly by using impedance analyzer with a precision impedance analyzer (Agilent 4294A, USA) at room temperature. The measurements were done at varying frequencies ranging from 10^2-10^5 Hz. The samples were coated by silver paint as electrode on both sides before measurement.

Dielectric constant

The dielectric constant of a material is defined as the ratio of the capacitance of a condenser containing the material to that of the same condenser under vacuum. The capacitance of a condenser measures the extent to which it can store charges. Dielectric constant can determine by using the following equation:

$$\varepsilon' = \frac{Cd}{E_0 A}$$

Where ε' is dielectric constant, C is capacitance, A is surface area of sample, d is thickness of sample, and E_0 is dielectric permittivity (8.85x10^{-12} Farad.m^{-1}).

Dielectric loss (ε'')

The electrical loss or the amount of energy dissipated by the insulating material when the voltage is applied to the circuit can be represented by means of a dissipation factor. Most of the elastomers have lower dissipation factor at room temperature. The loss factor (dielectric loss, ε''), the dielectric constant (ε') and the dissipation factor (tan δ) are related by the following equation:

$$tan\delta = \frac{\varepsilon''}{\varepsilon'}$$

Electrical conductivity

The electrical properties were measured and obtained using an impedance analyzer with an LCR meter. The measured electrical resistivity of the composite materials was converted into electrical conductivity by using the following equation:

$$\rho = \frac{RA}{L} = \frac{1}{\sigma}$$

Where ρ is the volume resistivity (Ωm), R is the resistance (Ω), A is the cross-section discs (m^2), L is the thickness (m), and σ is the electrical conductivity (Ωm)$^{-1}$.

5.3 RESULTS AND DISCUSSION

5.3.1 Composition of SNRL and FNRL and morphology of BC, SNR, FNR and composite films

The SNRL was light brown in color, whereas FNRL appears as a milky white suspension (Figure 5.1a). NRL presents a bimodal particle size distribution of small rubber particles (SRP) (10 - 250 nm) and large rubber particles (LRP) (250 nm - 3 μm) [17, 130]. SNRL contains SRP: LRP in a ratio of ~ 4:1, while FNRL contains SRP: LRP in a ratio of ~ 1:3 [17]. The main components of natural rubber latex (NRL) are rubber hydrocarbon, water and proteins and other non-rubber components. Proteins associated with the rubber molecules and/or particles usually present in term of nitrogen content in a rubber sample. Nitrogen contents of LRP and SRP were about 0.127 and 0.661%wt, respectively [17]. The dry rubber and protein contents of SNRL and FNRL are shown in Table 5.1.

Table 5. 1 Dry rubber and nitrogen contents* of SNRL and FNRL.

Sample	Dry rubber content (DRC)	Protein content
	(% w/w)	(% w/w)
Skim natural rubber latex (SNRL)	8.01	18.50
Fresh natural rubber latex (FNRL)	36.68	4.75

*measured in the dry form of SNRL and FNRL
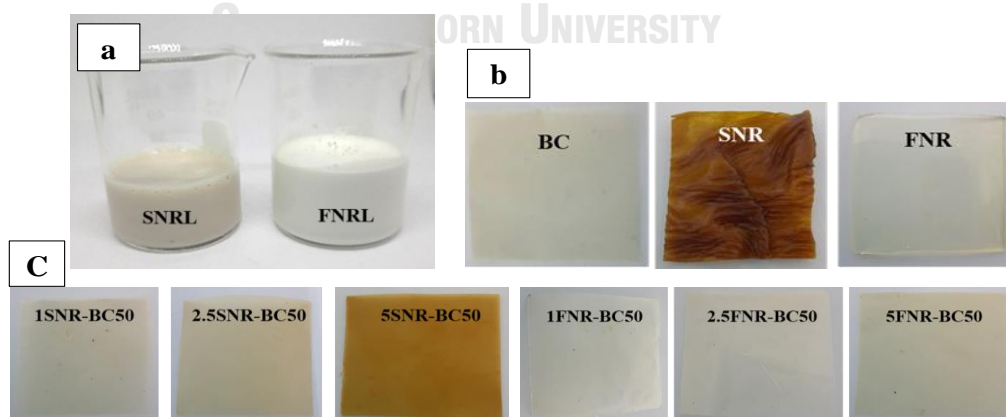
Figure 5. 1 Photographs of skim (SNRL) and fresh (FNRL) natural rubber latex (a) and dried BC, SNR and FNR films (b) and SNR-BC and FNR-BC composite films at different NRL concentrations (c)

The dried SNR film was dark brown in color with wrinkles on the film surface; on the other hand, the dried FNR film was white and transparent with a smooth surface. The dried film of BC was white with a smooth surface (Figure 5.1b). The photographs of the SNR-BC and FNR-BC composite films are shown in Figure 5.1c; the two different types of NR-BC composite film had a rather smooth surface, and the color of the films changed according to the concentration of SNRL/ FNRL. The SNR-BC and FNR-BC composites had a color and structure similar to BC at a low NR content. At a high concentration of SNRL and FNRL loading, the color of the composite films became more similar to the color of the dried SNR and FNR films, respectively.

The morphologies of the dried BC, SNR and FNR films are illustrated in Figure 5.2. The surface area of the never-dried BC film shows a coherent three-dimensional network of cellulose nanofibers of a highly porous system (Figure 5.2a). The diameter of BC nanofibers was about 40-100 nm and their pore size ranged between 0.2-2 µm. A similar diameter and pore structure of an unmodified BC hydrogel were reported in previous studies [130, 131]. The surface area of dried BC shows a dense nanocellulose fiber layer. The nanofibers also appeared as crossed and randomly oriented, as shown in Figure 5.2b. A cross section of the dried BC film presents multilayers of thin sheets (Figure 5.2c). The shrinkage and compact of the BC structure was attributed to evaporation of water in BC during the drying process.
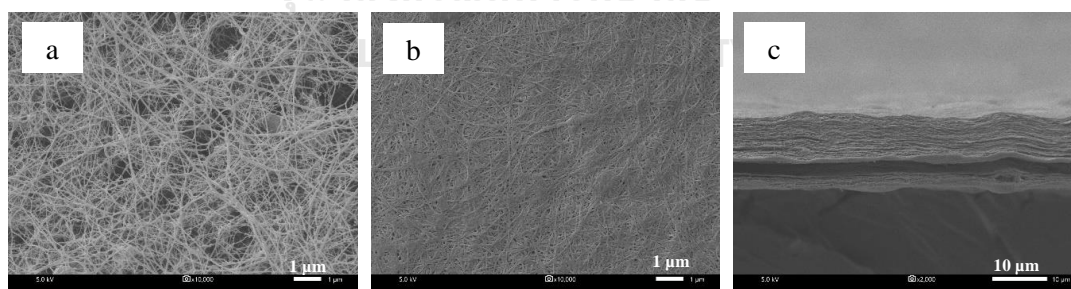
Figure 5. 2 Scanning electron microscopy (SEM) images of surface morphologies of never dried films of bacterial cellulose (BC) (a) dried BC films: surface (b) and cross-section (c)

The morphologies of SNR-BC and FNR-BC composite films are illustrated in Figure 5.3. The surface area of the SNR-BC and FNR-BC composites indicated that BC films were integrated with SNRL and FNRL, as can be seen clearly in 5SNR-BC50 and 5FNR-BC50. The incorporation of SNR and FNR into BC nanofibers led to the reduction of BC film porosity. The cross section of dried 5SNR-BC50 and 5FNR-BC50 films presented densely packed nanocellulose fibers combined with SNR and FNR, respectively. The thickness of the composite films increased with increased concentrations of SNR and FNR. Overall, the thicknesses of the SNR-BC films were greater than the FNR-BC films.
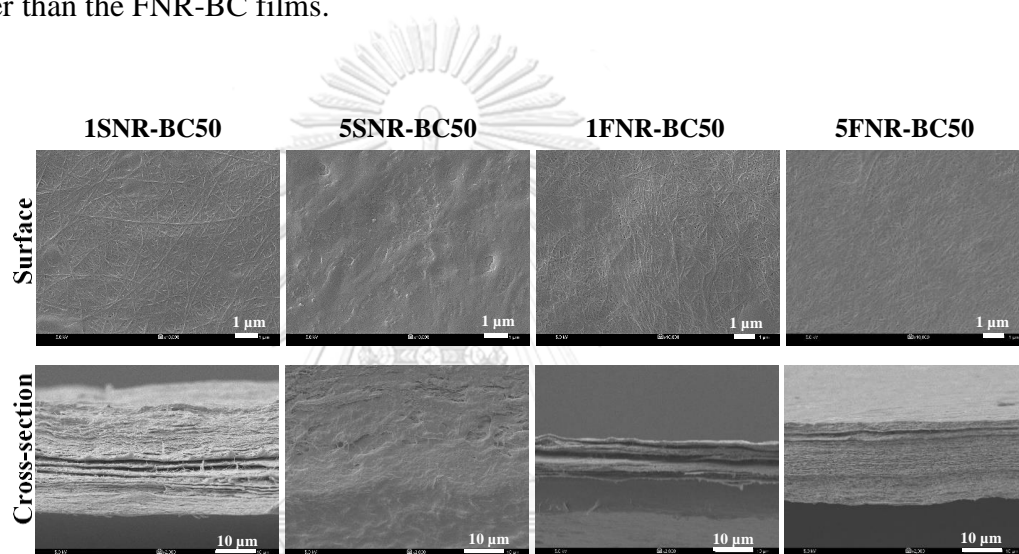
Figure 5. 3 SEM micrographs of surface morphologies (on the top) and cross-section (on the bottom) of dried films: 1SNR-BC50, 5SNR-BC50, 1FNR-BC50 and 5FNR-BC50.

The thickness and dry weight of BC composite films before and after the immersion in SNRL and FNRL suspensions are shown in Figure 5.4 and Figure 5.5, respectively. The thicknesses of both SNR-BC and FNR-BC composite films show a similar trend with a dry weight of composite films that relatively increase with an increased concentration of SNRL and FNRL loading, in the same way according to previous work [132] of BC films modified by loading of alginate gel. The highest thicknesses of SNR-BC and FNR-BC composites were obtained by the immersion in SNRL and FNRL suspension at 5% DRC (at 60 °C), which were a ~5.8-fold and ~3.1-fold increase over the unmodified BC film, respectively. The amount of

integration of SNR and FNR into BC was estimated from the change of the film's dried weight before and after immersion in SNRL and FNRL suspensions. The highest amount of SNR and FNR diffused and adsorbed into BC was observed at loadings of SNR and FNR at 5% DRC and 60 °C, where the amounts of SNR and FNR in the composite films were 86.7%, and 72.7%, respectively (the estimated ratios of SNR/BC and FNR/BC in the composite films were 6.5, and 2.7, respectively). Overall, the thickness and dry weight of SNR-BC films were higher than FNR-BC films in all conditions. The effect of immersion temperature on film thickness and dry weight showed a similar trend for both SNR-BC and FNR-BC composites. Increasing immersion temperature from 50°C to 60°C resulted in larger thickness and dry weight for SNR-BC and FNR-BC composites, which implied a larger amount of integration of SNR and FNR into BC. These results can be attributed to the fact that the increased immersion temperature increases SNR and FNR molecular motion and creates higher kinetic energy, resulting in a higher diffusion rate of SNR and FNR into the nanofiber network. Moreover, polymer chains become more flexible and free space between polymers increases at higher temperatures, which leads to enhanced diffusion [133]. Previously, modification of BC by immersion in concentrated natural rubber latex (CNRL) was studied, and the optimal conditions were reported at a concentration of 2.5%-5.0 % DRC and a temperature of 50°C to 60°C [130]. However, because CNRL contains mostly large NR particles, BC pellicles had to be immersed in a diluted CNRL suspension in the presence of a dilute aqueous solution of ethanol for enhanced diffusion [130].
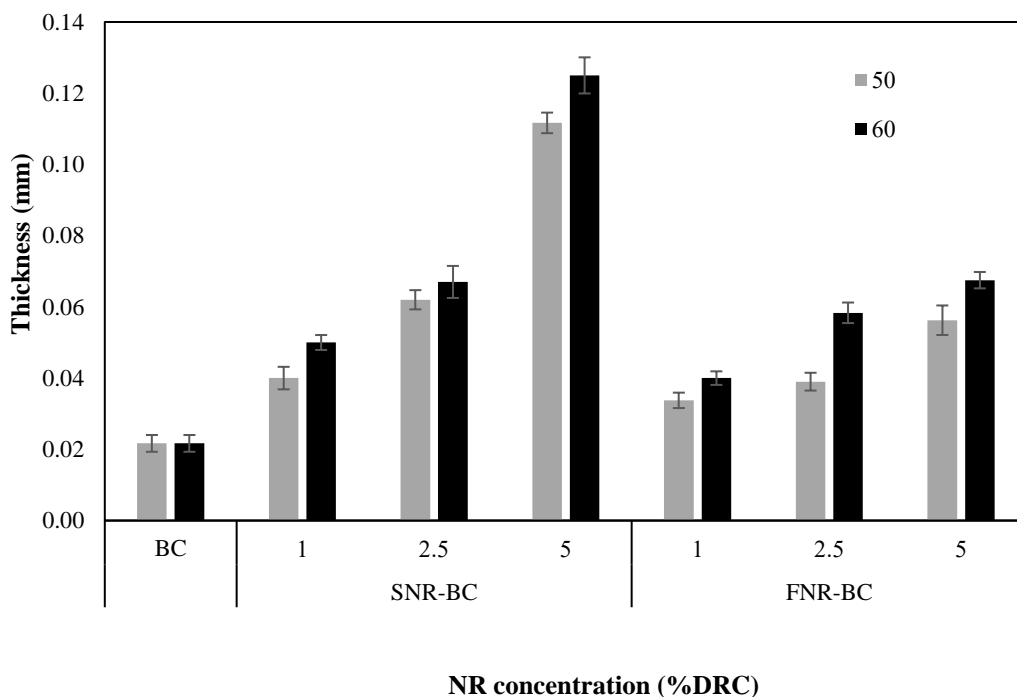
Figure 5. 4 Thickness of dried BC, SNR-BC and FNR-BC films modified by immersing in SNRL and FNRL suspension at various concentrations (0%-5% DRC) at temperature of 50 °C and 60 °C.

All results from SEM images and the thickness and dry weight of SNR-BC and FNR-BC composite films indicate that the diffusion and adsorption of SNRL into BC were greater than those of FNRL. These results can be attributed to the average particle size of SNRL and FNRL molecules. Previous studies reported that NRL from *Hevea brasiliensis* is typically comprised of a bimodal particle size distribution, with both small rubber particles (SRP, $\emptyset$ ~10 to 250 nm) and large rubber particles (LRP, $\emptyset$ ~250 nm to 3 μm) [126, 134]. SNRL consists of 81% wt. of SRP and 19% wt. of LRP, whereas FNRL consists of 76% wt. of LRP and 24% wt. of SRP [17]. Smaller rubber particles move more rapidly and easily diffuse through the pores of a BC network than larger rubber particles; therefore, the amount of SNR integrated into BC composites was larger than the amount of FNR integrated into BC composites.
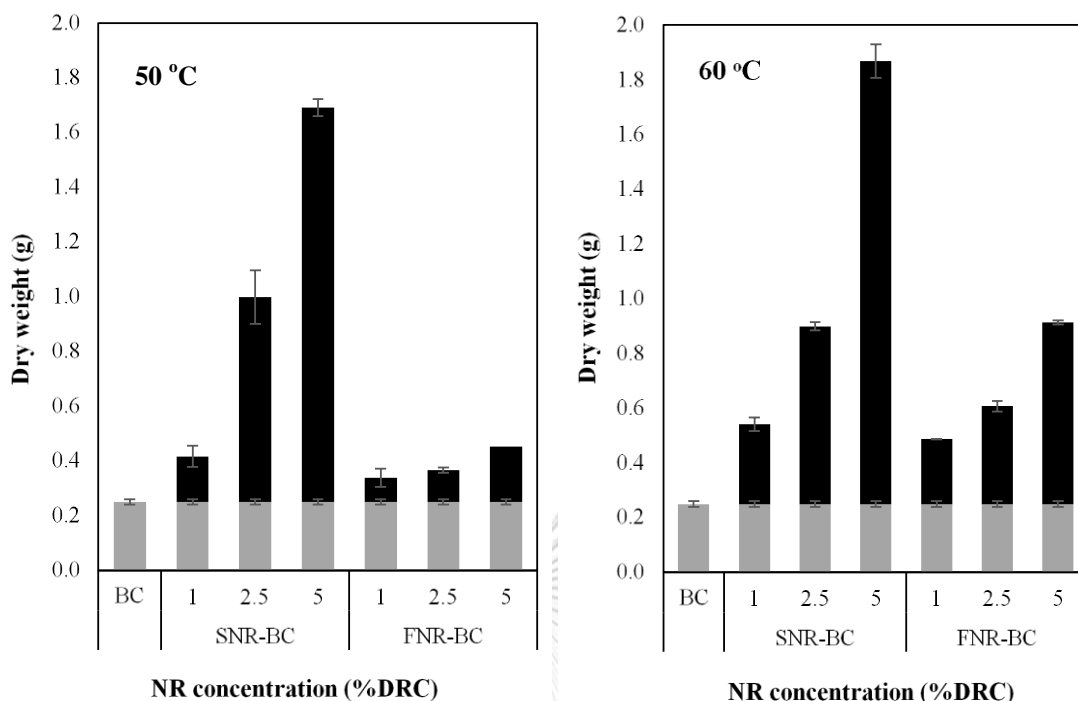
Figure 5. 5 Dry weight of BC composite films modified by immersing in SNRL and FNRL suspension at various concentrations (0%−5% DRC) at temperatures of 50 °C and 60 °C: the dry weight of BC (▪); the estimated dry weights of SNR and FNR (■).

5.3.2 Fourier Transform Infrared (FTIR) Spectroscopy

The FTIR spectra of BC, SNR, FNR, SNR-BC and FNR-BC composites are shown in Figure 5.6. The FTIR spectrum of pure BC shows a broad peak of O–H stretching of the hydroxyl group at 3340 cm^{-1} and at 2919 cm^{-1}, corresponding to C–H stretching. The absorption band located at 1107 cm^{-1} is attributed to C–O symmetric stretching [69, 77]. The SNR and FNR films show the principal peaks corresponding to cis-polyisoprene functional groups of NR. The asymmetric stretching vibration of methyl groups (─CH$_3$) occurs at 2960 cm^{-1} and C-H deformation occurs at 1447 cm^{-1}, while the peaks observed at 2927 cm^{-1} are assigned to the symmetric stretching vibration of methylene (–CH$_2$), and C=C stretching is observed at 1662 cm^{-1} [51, 130, 135]. The largest difference between the spectrum of the two NR types is that the principal peaks of proteins appear only within the spectrum of SNR. The broader peaks of around wavenumber 3280 cm^{-1} are assigned to the N–H stretching (amino acids or dipeptides) of protein molecules in SNR, while

the peaks are observed at 1567 and 1630 cm^{-1}, corresponding to N-H bending (amide II) and C=O stretching (amide I), respectively [125, 136, 137]. The FTIR results confirmed that the protein content in SNR was higher than FNR (18.50 wt% protein in SNRL and 4.75 wt% protein in FNRL as shown in Table 5.1). The intense broad band between 3200 and 3500 cm^{-1} could also correspond to hydroxyl groups. The broad band of the hydroxyl group is more apparent in SNR than FNR, which indicates a higher hydroxyl content in SNR. It was suggested that the hydroxyl groups in SNR are raised from the hydration of proteins and phospholipids, which were chemically bound and could not be removed after drying [20]. The FT-IR spectra of the SNR–BC and FNR-BC films indicate characteristic peaks of both BC and NR without new peaks. Moreover, SNR–BC and FNR-BC composites show a similar spectra trend at different SNR and FNR concentrations. At low SNR and FNR concentrations (1% and 2.5% DRC), SNR-BC and FNR-BC composites exhibit spectra more similar to BC. Whereas, at a high NR loading (5% DRC), SNR-BC and FNR-BC composites display spectra more similar to SNR and FNR.
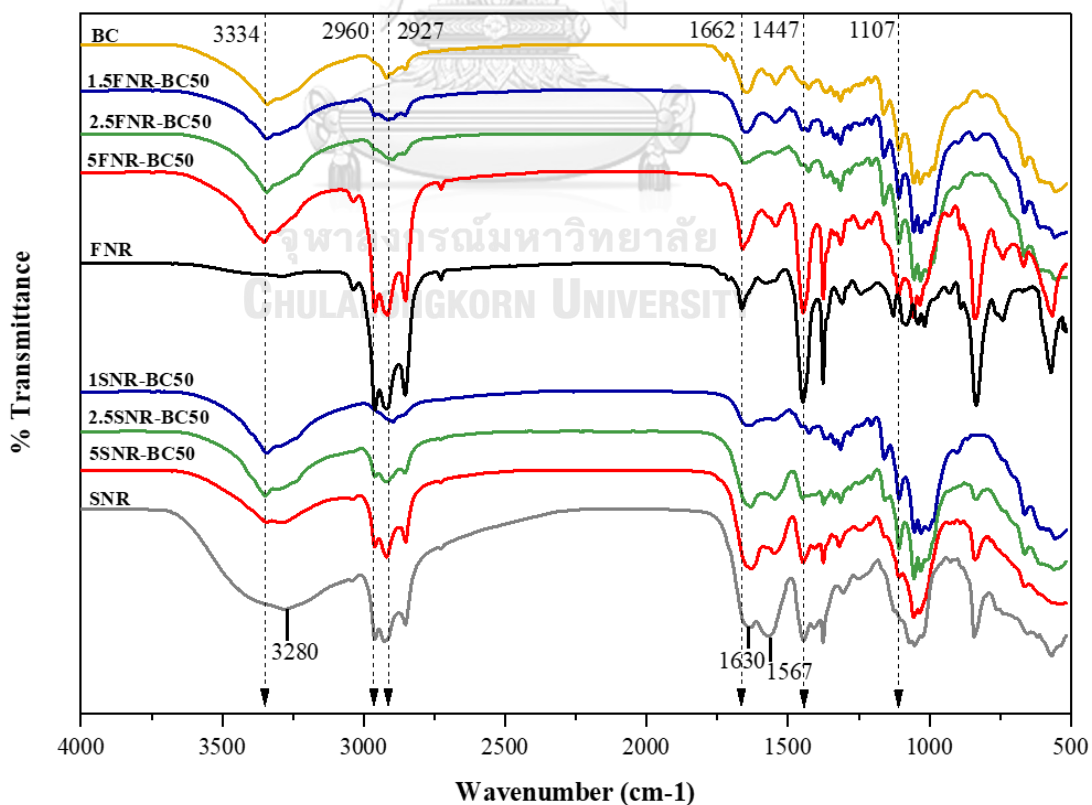
Figure 5. 6 FTIR spectra of BC, SNR, FNR, SNR-BC and FNR–BC composite films.

5.3.3 Mechanical properties

Mechanical properties of dried films of BC, SNR-BC and FNR-BC were presented in terms of elongation at break, tensile strength and Young' s modulus, as shown in Figure 5.7. SNR and FNR films used for mechanical testing were prepared from 50 mL of 5% DRC of SNRL and FNRL. The mechanical properties of pure SNR and FNR are shown in Table 5.2. It was revealed that the elongation at break and tensile strength of FNR were higher than those of SNR because the major component in the solid content of FNRL was polyisoprene (~30% DRC), with only a small amount of non-rubber components such as lipids, proteins and carbohydrates (~ 4.8 wt%). The solid content of SNR, on the other hand, was composed of a rubber content of about 3% DRC and 6.8 wt% of non-rubber components [124, 125, 137]. The large amount of LRP content in FNR resulted in high elongation at break and tensile strength. In addition, the Young's modulus of FNR was ~2.95 MPa, whereas the Young's modulus of SNR could not be determined due to the very low rubber content and the high concentration of non-rubber components in SNR films. BC has been reported as having a high tensile strength and Young's modulus, but low elongation at break. BC mechanical properties can vary depending on several factors such as culture processing conditions, bacterial strain used and drying processing conditions [130, 138-140]. As compared to SNR and FNR films, BC had lower elongation at break but revealed a considerably higher tensile strength and Young's modulus.

Table 5. 2 Mechanical properties of SNR, FNR and BC films.

NRL	Elongation at break (%)	Tensile strength (MPa)	Young's modulus (MPa)
SNR	28.32 ± 1.37	0.35 ± 0.02	n.d*
FNR	136.43 ± 3.12	0.75 ± 0.03	2.95 ± 0.46
BC	1.48 ± 0.15	107.03 ± 7.38	11201.33 ± 521.37

*n.d = cannot determine

Figure 5.7a clearly shows that the incorporation of SNR and FNR into BC resulted in improved elongation at break for both SNR-BC and FNR-BC composite films. The maximum elongation at break values of the SNR-BC and FNR-BC were 28.03% and 3.76%, respectively, from the immersion in 5% DRC of SNRL and FNRL at 60 °C. Compared with the unmodified BC film, the elongation at break was ~18.9-fold increase for SNR-BC and ~2.5-fold increase for FNR-BC. SNR-BC films exhibit significantly higher elongation at break than those of FNR-BC films. From the results of total dry weight (Figure 5.5), a higher amount of filler loading was obtained at the higher immersion temperature of 60 °C, especially at a high loading concentration at 5% DRC. Because NR possesses excellent elastic properties, this higher rubber content in composite films resulted in higher elongation at break for both SNR-BC and FNR-BC composite films. In addition, SNR and FNR coating on BC fibers could help fibers better absorb energy, prevent the fabric from breaking and help the fabric elongate longer before failure due to breaking [141]. It should be noted that the elongation at break of pure SNR film was lower than that of pure FNR film, but the elongation at break of SNR-BC was larger than FNR-BC films. This could be attributed to the larger amount of rubber loading into SNR-BC composite films (which could relate to the thickness or dry weight of composite films). In addition, the high protein content in SNRL might also have a positive effect on elongation at break. From the previous report, deproteinization of SNRL resulted in a decrease of elongation at break from 498.79% to 400.48% [125].

The tensile strength of SNR-BC and FNR-BC films are shown in Figure 5.7b. The composite SNR-BC film of 2.5SNR-BC50 presented the maximum tensile strength at 123.12 MPa, whereas the composite of 5FNR-BC50 presented the maximum tensile strength at 177.47 MPa. The tensile strength of FNR-BC increased with increasing FNR concentration; however, in the case of SNR-BC, tensile strength decreased with increased loading from 2.5 to 5%, which should be due to a high ratio of SRP particles in the composite film. The reinforcement effects on Young's modulus of BC composite integration with SNR and FNR were quite similar to those on tensile strength. The Young's modulus values of the composite films were significantly higher, as compared to those of pure SNR and FNR films, as shown in

Figure 5.7c. The maximum values of Young's modulus for SNR-BC and FNR-BC were obtained from 5SNR–BC50 (6.93 GPa) and 5FNR–BC50 (13.32 GPa). The neat BC film possessed excellent tensile strength and a high Young's modulus, whereas the SNR and FNR films have a low tensile strength and Young's modulus. By loading with SNR, the SNR diffused and combined with the BC network, resulting in a significantly higher elongation at break; however, the tensile strength changed slightly at a low SNR loading, but relatively decreased at a high SNR loading. Therefore, the Young's modulus of the SNR-BC composite films tended to decrease with the amount of SNR loading. These results agree with those reported by Urbina et al. [119], who presented the mechanical properties of BC/polyurethane nanocomposites prepared by immersing wet BC into waterborne polyurethane (WBPU) at different time intervals. It was reported that the amount of WBPU in the BC/WBPU nanocomposite increased with immersion time, and it was shown that while the Young' s modulus and the tensile strength of BC/WBPU decreased, elongation of the composite increased with increased immersion time. In the present study, only the composite film of 5FNR-BC50 presented a significantly improved tensile strength and Young's modulus compared to the unmodified BC film. This result could indicate that the loading of FNRL (which contains a high content of LRP) promotes a higher mechanical strength of the composite BC films, whereas the loading of SNRL (which contains a high content of SRP and protein particles) could promote greater flexibility in the composite BC films. Rubber coated on BC fiber could prevent the fiber from resisting external work load force [141]. In addition, NR has a high structural regularity and tends to crystallize spontaneously when it is stretched [142].

The particle size of the rubber molecules had a strong effect on the mechanical properties of SNR and FNR films. From previous work on the strength of LRP and SRP [17], it was reported that the strength of LRP (8.2 MPa) was much greater than that of SRP (3.2 MPa). This is due to strain-induced crystallization caused by phospholipids in NR during stretching. Moreover, the higher strength of LRP might be attributed to the branch-point network formed by the coordination of phospholipids in the LRP [143]. SRP are composed of a high protein content but a low rubber content. The mechanical strength of SRP films was very low, which could relate to the proteins in SRPL that had no direct effect on the strength [127]. The majority of

FNR particles are LRP, whereas the majority of SNR particles are SRP; therefore, the tensile strength and Young's modulus of FNR-BC composites tends to be higher than SNR-BC composites.

The tensile strength and Young's modulus of both SNR-BC and FNR-BC films tended to decrease with the increase of the immersion temperature from 50 $^{\circ}$C to 60 $^{\circ}$C. At a higher immersion temperature, a larger amount of SNR and FNR was integrated into BC matrices and a higher collision rate and particle agglomeration could occur. The agglomeration of NR particles might cause the poor distribution of NR in BC matrices [130]. Moreover, it was previously reported that a temperature range between 58 °C to 60 °C produced the decomposition of branch points generated by the interaction of proteins and phospholipids of NR molecules [144]. It was revealed in the present study that the tensile strength and Young's modulus of SNR-BC and FNR-BC composite films, especially at high SNRL or FNRL loadings, decreased with the increase of the immersion temperature from 50 °C to 60 °C.

The reinforcement of BC with SNR and FNR prepared via immersion of BC in SNRL and FNRL considerably enhanced the elongation at break of the SNR-BC composites; these are considered very high compared to the BC composite reinforced by concentrated natural rubber (CNR: 60 % DRC), which presented a maximum elongation at break of the CNR-BC film of only 3.0%–3.5% at 2.5%–5% CNRL loading [130]. Previous studies have also reported the maximum tensile strength of NR composites at 100 MPa when reinforced with BC fibers at a BC loading of 80 wt.% [77], 6 MPa at a BC loading of 7 phr [145] and 24 MPa at a BC loading of 10 phr [146]. It was revealed that the tensile strength of NR composites reinforced with BC were lower than the composite films of BC reinforced with NR (SNR, FNR and CNR).

The comparison of mechanical properties of BC composites filled with different types of NR is shown in Table 5.3. The reinforcement of BC with SNR and FNR prepared via immersion of BC in SNRL and FNRL considerably enhanced the elongation at break of the SNR-BC composites. These are considered to be very high compared with BC composites reinforced by CNR, which presented a maximum elongation at break of 3.2%–3.5% at a concentration of 5% DRC. On the other hand, the Young's modulus and tensile strength of CNR-BC were higher than those of

SNR-BC and FNR-BC. These results could be attributed to the amount of LRP in BC composites, as the major NR particles in CNR were LRP (82 wt%) [17]. The film fabricated from CNRL has higher mechanical strength, in terms of tensile strength, than the films fabricated from FNRL and SNRL. In addition, LRP particles were more difficult to transfer and diffuse into the BC network than SRP particles; therefore, the amount of CNR in CNR-BC composites was lower compared to the amount of SNR and FNR in SNR-BC and FNR-BC composites.
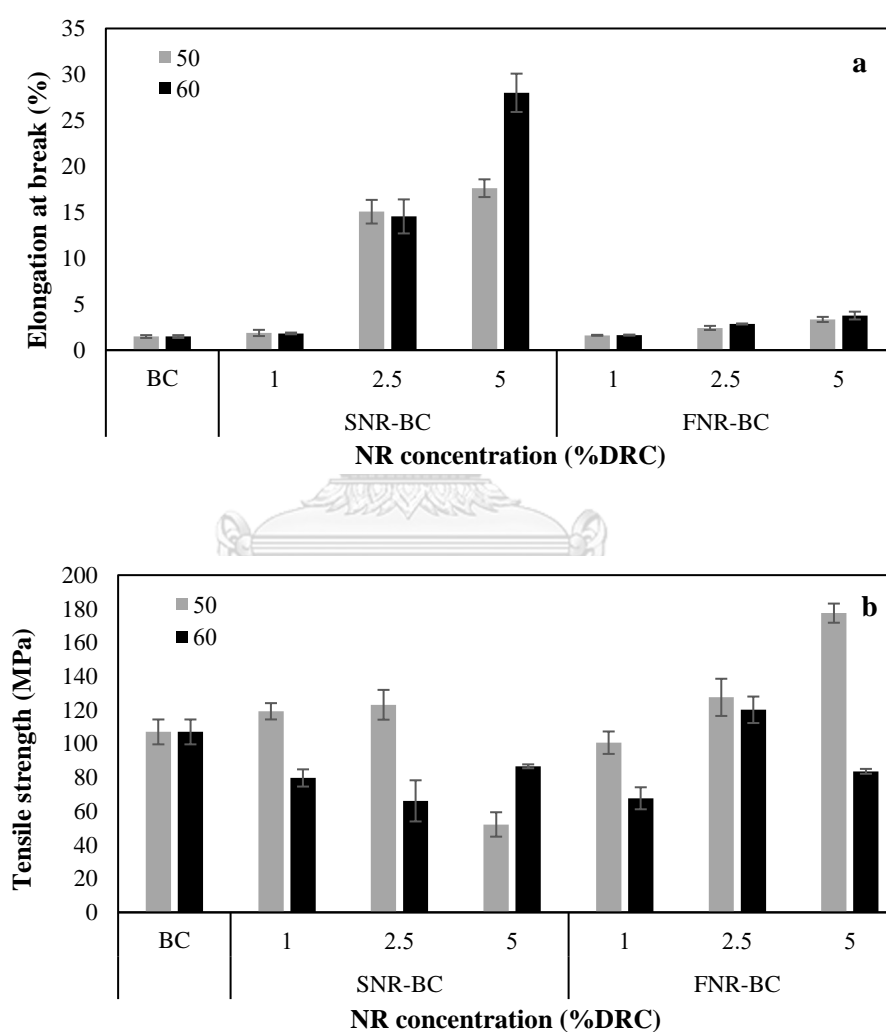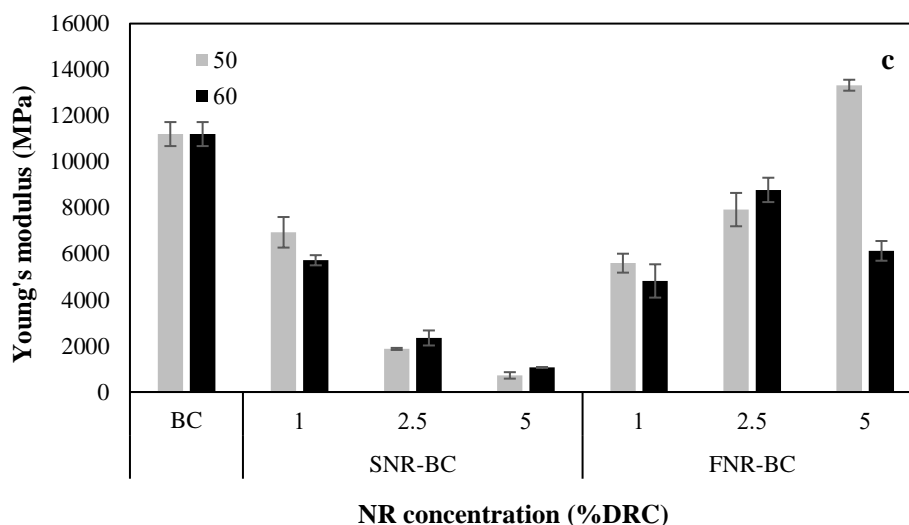
Figure 5. 7 Elongation at break (a), Tensile strength (b), and Young's modulus (c) of dried BC and NR-BC films modified by immersing in SNRL and FNRL suspension at various concentrations (0%–5% DRC) at temperatures of 50 °C and 60 °C.

Table 5. 3 Comparison of the mechanical properties of BC composites loading with different types of NR particles.

Types of NR	Composites	Mechanical properties			Amount of NR in BC composites (%)	Ref.
		Young's modulus (Mpa)	Tensile strength (Mpa)	Elongation at break (%)		
CNR	CNR	2.4	1.2	111.0	100.0	[130]
	5CNR-BC50	12000	250	3.2	30.0	
	5CNR-BC60	10000	240	3.5	41.3	
FNR	FNR	2.9	0.7	136.4	100.0	Our work
	5FNR-BC50	13323	177.5	3.3	44.9	
	5FNR-BC60	6129.5	83.7	3.8	72.7	
SNR	SNR	-	0.4	28.3	100.0	Our work
	5SNR-BC50	721.3	52.2	17.6	85.3	
	5SNR-BC60	1067.3	86.6	28.0	86.7	

5.3.4 Water Absorption Capacity

The results of the water absorption capacity (WAC) tests of BC, SNR, FNR, SNR-BC and FNR-BC composite films are presented in Figure 5.8. The WAC of BC was higher than the SNR, FNR and SNR-BC and FNR-BC composite films due to the hydrophilic nature of BC, which is composed of a high density of hydroxyl groups on its surface [147]. In addition, the hydrophilic nature of BC is attributed to the arrangement of BC fiber and the high surface area per unit of mass [138]. The water adsorption of BC film increased nonlinearly during a period of 0-4 days for a water uptake of 0–700%; afterwards, the water absorption slightly increased during immersion in water for 4-16 days. The maximum WAC of BC was about 809% at day 18. The WAC of SNR and FNR films was much lower than that of the BC, SNR-BC and FNR-BC composites due to the hydrophobic nature of NR. The WAC of SNR-BC and FNR-BC films decreased with increasing SNR and FNR concentrations due to the hydrophobic nature of rubber particles, which are the main components in NRL. The water uptake of 5SNR-BC50 and 5FNR-BC50 were reduced to ~187%, which was ≈ 1/4 that of neat BC film. At a low amount of SNR and FNR diffused into BC fiber, hydroxyl groups of cellulose were sites for the adsorption of water molecules via hydrogen bonding. At a larger amount of SNR and FNR integrated into BC fibers, small amounts of water could be adsorbed into SNR–BC and FNR-BC films. Thus, the water resistance of SNR-BC and FNR-BC films increased with SNR and FNR loading content in the films. Overall, the results demonstrated that the structural stability in water of the BC composite films was improved upon integrating SNR and FNR into BC matrices.

In addition, the WAC of the neat SNR film was slightly larger than the neat FNR film (the maximum WAC of SNR and FNR were 40% and 38%, respectively), and the WAC of SNR-BC films was slightly higher than FNR-BC composite films. Previous studies indicated that the core-shell of NR latex particles are made up of a hydrophobic core of polyisoprene surrounded by complex hydrophilic proteins and phospholipids [15, 148], and non-rubbers components in NRL can absorb water [149]. The major component of FNRL is rubber particles (polyisoprene), which have intrinsic hydrophobic properties, whereas proteins are one of the major components of SNRL. Therefore, the WAC of SNR and SNR-BC were relatively higher than that of

FNR and FNR-BC films. This agrees with a previous report by Danwanichakul and Than-ardna [150], which stated that SNR films were more hydrophilic than CNR films.
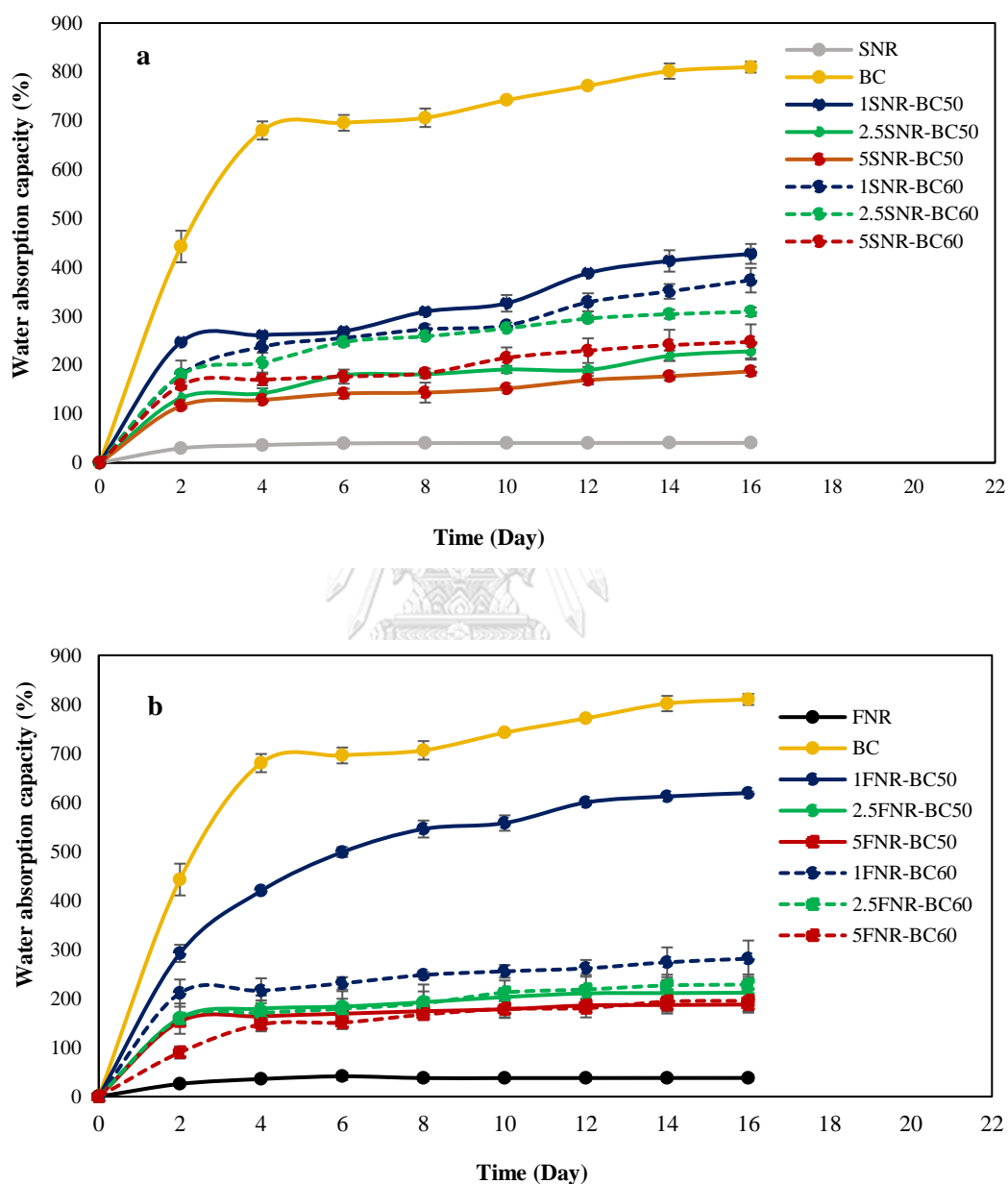
Figure 5. 8 Water absorption capacity (WAC %) of BC, SNR, SNR-BC films (a) and BC, FNR, FNR–BC films (b).

5.3.5 Toluene uptake

The toluene uptake of BC, SNR, FNR and BC composite films determined by soaking films in toluene for 8 hours are shown in Figure 5.9. Toluene uptake of BC was lowest when compared to SNR, FNR, SNR-BC and FNR-BC films due to hydrophilic nature of BC. The maximum toluene uptake of BC was 17% at an immersion time of 8 hours. The toluene uptake for both the SNR and FNR films is shown in the insert Figures of Figures 5.9a and 5.9b, respectively. At the initial absorption, the toluene uptake of the SNR and FNR films rapidly increased and reached a maximum value at 4934% and 5449%, respectively, within 2 hours. After that, the SNR and FNR films were gradually decomposed in toluene. The toluene uptake of SNR and FNR films was much higher than BC and BC composite films due to the nonpolar nature of NR, which can highly absorb nonpolar solvents. The high uptake rate of nonpolar solvents of uncured NR was previously reported in several studies [51, 151]. The toluene uptake of both SNR-BC and FNR-BC were higher than that of the neat BC film, but much less than those of the SNR and FNR films. The toluene uptake of BC composites increased with an increasing SNR and FNR content in BC composite films. A larger amount of rubber content in BC matrices resulted in a higher absorption of nonpolar solvent by the films. The lowest toluene uptake of SNR-BC and FNR-BC films was detected from the composite films of 1SNR-BC50 and 1FNR-BC50, respectively, which were about 0.0053 and 0.0070 that of the SNR and FNR film, respectively. In addition, the toluene uptake of the SNR film was lower than that of the FNR film, and the toluene uptake of the SNR-BC films was lower than those of the FNR-BC films due to the greater hydrophilic protein content in SNRL compared to FNRL. The SNR-BC and FNR-BC composite films demonstrated significant improvements in resistance to toluene when compared with SNR and FNR films.
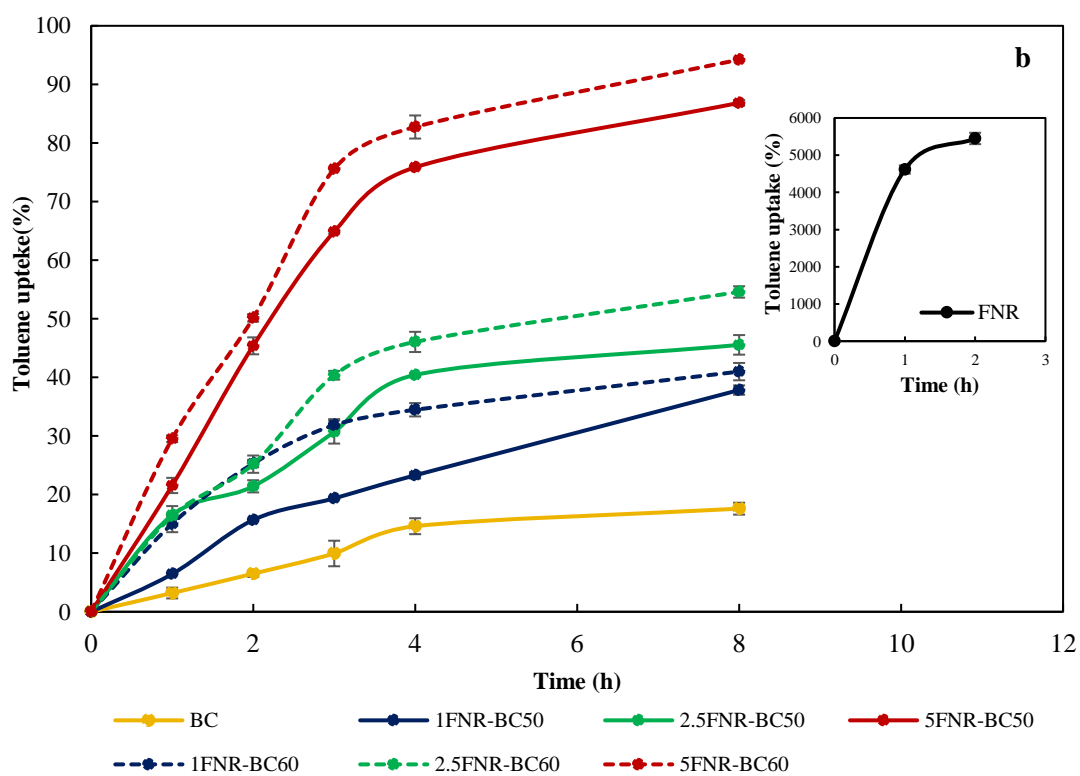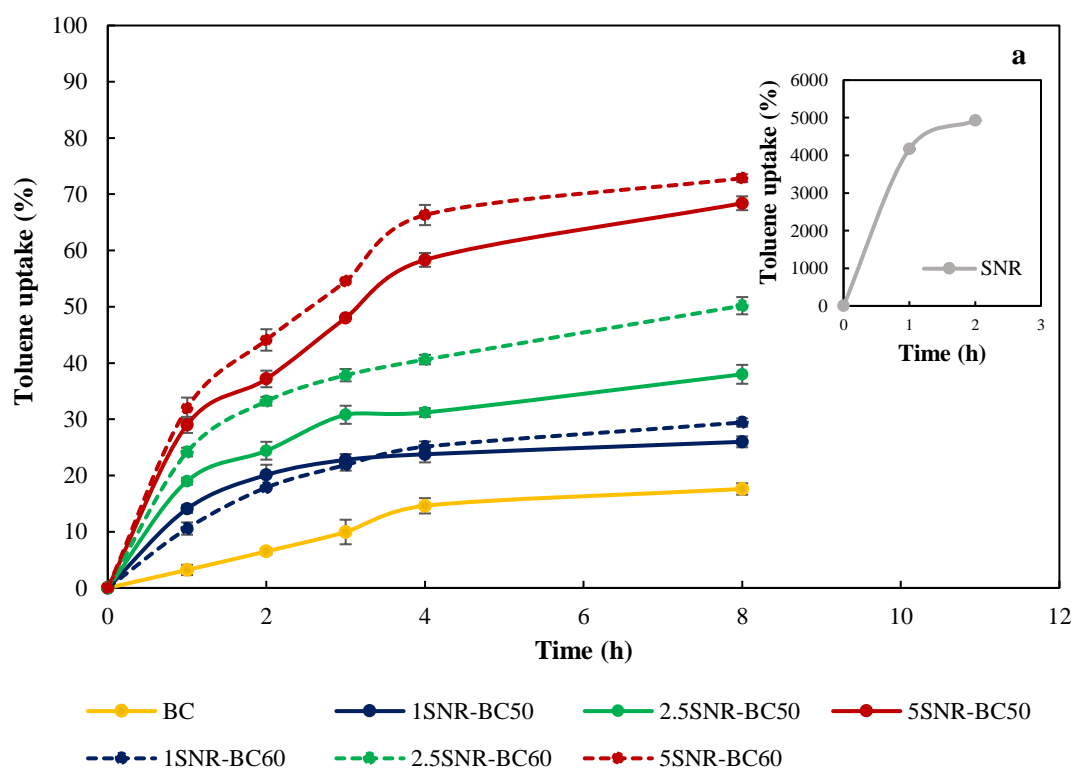
Figure 5. 9 Toluene uptake of BC, SNR, SNR-BC films (a) and BC, FNR, FNR–BC composite films (b).

5.3.6 Biodegradation in Soil

Biodegradation behavior is an important property for biocomposites. The study of biodegradation in soil of BC, SNR, FNR, SNR-BC and FNR-BC films was determined in uncontrolled conditions (with an average temperature of ≈ 30 °C). The percentage weight loss and the visual analysis of the biodegraded samples after 6 weeks are shown in Table 5.4 and Figure 5.10, respectively. Cellulose can be decomposed in soil by multiple microorganisms. The weight loss of neat BC film was larger than SNR, FNR film and BC composite films. The degradation of BC was 44.3% after 2 weeks, and it took about 4 weeks for BC to completely decompose in soil. BC structures are mainly composed of crystalline cellulose with a minor amount of amorphous cellulose chains. The amorphous regions were more easily degradable by cellulolytic microorganisms than the crystalline regions [152, 153]. Many previous studies have indicated that multiple microorganisms in the soil could completely degrade BC via enzymatic degradation [130, 154, 155]. The weight loss of the SNR and FNR films was relatively lower than BC and the BC composite films at any degradation time. The degradation of NR in natural environments by microorganisms was rather slow because the specific bacteria that can use rubber as carbon source grows slowly [100, 156]. After 6 weeks, the weight loss of SNR, FNR, SNR-BC and FNR-BC were 58.5%, 33.4%, 68.9-93.7% and 51.6-68.3% respectively. SNR-BC and FNR-BC films modified with 1% DRC of SNRL and FNRL were completely degraded in 6 weeks. BC in the composite films was degraded by soil microorganisms much more rapidly than SNR and FNR, and the decomposition of BC induced void formation in the composite films. Then the films were cracked and broken down into small pieces. The percentage weight loss of the SNR-BC and FNR-BC films decreased with increased NR concentration. The weight loss of SNR-BC films was higher than FNR-BC films, which should be attributed to the larger amount of non-rubber content (protein, lipids and carbohydrates) in SNR. Biodegradability could also relate to the water absorbability of BC composite films. The higher water content in films could promote the growth and activity of soil microorganisms that led to the hydrolysis of cellulose and NR, resulting in the increased degradation [83, 157]. Figure 6.10 presents a visual analysis of the biodegradation of BC, SNR, FNR, SNR-BC and FNR-BC films during a period of 2-6 weeks. The decreasing

degradation of BC composite films with higher SNR and FNR concentration was clearly observed, especially at 6 weeks of biodegradation in soil. Black spots were found in SNR, FNR and composite films after 2 weeks in soil, indicating blooms of soil microorganism activity in NR and SNR-BC films, which was a good indicator of biodegradation [83]. Moreover, after 4 weeks in soil, some parts of the composite films disappeared, and in some conditions, the films were degraded completely. Therefore, SNR-BC and FNR-BC films could be biodegradable in soil.

Table 5. 4 Weight losses of BC, SNR, FNR, SNR-BC and FNR-BC films in soil

Samples	Weight loss (%)			Samples	Weight loss (%)		
	2 weeks	4 weeks	6 weeks		2 weeks	4 weeks	6 weeks
BC	44.03	+++	+++	BC	44.03	+++	+++
SNR	11.15	22.10	58.45	FNR	13.82	21.52	33.44
1SNR-BC50	31.97	75.09	+++	1FNR-BC50	27.45	64.69	+++
2.5SNR-BC50	25.02	54.49	93.68	2.5FNR-BC50	6.89	51.3	68.32
5SNR-BC50	16.23	55.40	68.93	5FNR-BC50	9.86	38.42	51.61

+++ = complete degradation
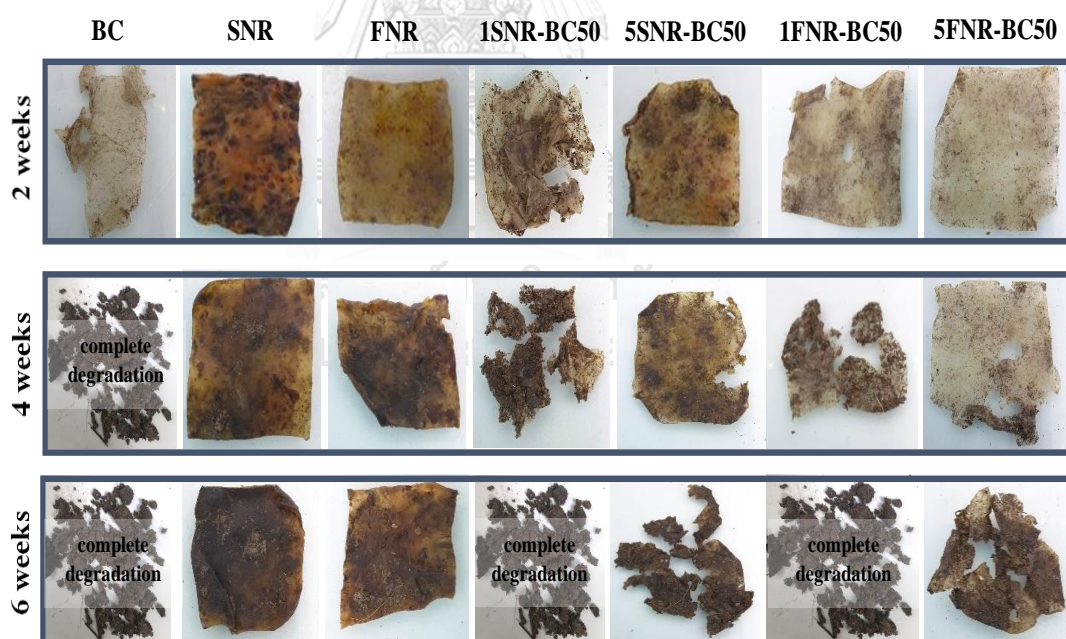
Figure 5. 10 The visual analysis of biodegradation in soil of BC, SNR, FNR, SNR-BC and FNR-BC films for 6 weeks.

5.3.7 Dielectric properties

The dielectric properties of materials are an important parameter for designing and predicting the behavior of electronic materials such as capacitors, semiconductor devices, radio propagation, remote sensors and insulating material. The dielectric properties of any polymer depend on its chemical composition, structure cations, dipole moment and space charge polarizations [104]. The dielectric constant is defined as the ability of a material to store energy from an external electrical field, and the dielectric constant of a material depends on the polarizability of the molecules. The polarizability of nonpolar molecules arises from electronic and atomic polarization, whereas the polarizability of polar molecules arises from orientation polarization [128]. The dielectric constant and dielectric loss of BC, SNR, FNR, SNR-BC and FNR-BC films are presented in Figure 5.11. The frequency dependence of the dielectric properties at ambient temperature was observed. In all cases, the dielectric constant and dielectric loss of neat BC, SNR, FNR and BC composites decreased with increasing frequency due to the attribution of relaxation behavior. The dielectric constant of the BC film was very low in the range of 0.48-3.12. The BC chain composed of a H-bond from the hydroxyl group resulted in greater polarity, which lead to polarization in the BC matrix [158]. The dielectric constants of SNR and FNR were in the ranges of 51.92 - 274.20 and 25.15 - 90.74, respectively, at 100 - 1,000 Hz, as shown in Figure 5.11c. The dielectric constants of SNR and FNR were very large when compared to that of CNR (the dielectric constant of CNR is in the range of 1.8–2 [151]), which could be attributed to the different amount of rubber and non-rubber content in SNR, FNR and CNR. The dielectric constants of the SNR-BC and FNR-BC films are shown in Figure 5.11a, b, respectively. The dielectric constant of neat SNR was larger than that of FNR, and the dielectric constant of the SNR-BC films was higher than the FNR-BC films at all filler content. The rubber content (polyisoprene) in SNR and FNR is a nonpolar component, but proteins and phospholipids in NR are polar components [159]. It was suggested that proteins in NR should have a strong effect on the dielectric constant of NRL and NR films. Previous research found that deproteinizing NRL resulted in a significant decrease in the dielectric constant and a dielectric loss of NRL [159, 160]. The protein content in SNRL (18.50 wt%) was higher than FNRL (4.75 wt%); therefore, SNR and SNR-BC

films were more polar than FNR and FNR-BC films. Moreover, the increase of SNR in BC matrices resulted in higher dipoles or orientation polarization; thus, the dielectric constant was enhanced. Previous work by Kosumphan et al. [161] reported the dielectric constant and dielectric loss of SNRL, which were both higher than those of CNRL. In addition, they found that the proportion of pure SNRL in a contaminated serum (cassava and calcium carbonate) decreased, resulting in a decreased dielectric constant. The dielectric constant of SNR-BC and FNR-BC films was found to increase with increasing SNR and FNR concentration. The high amount of SNR and FNR in BC matrices could result in high polar components with a large dielectric constant.

The dielectric loss factor presents the amount of energy loss from a material due to the movement or rotation of the atoms or molecules in an alternating electric field [128]. The frequency dependence of dielectric loss of BC composites is shown in Figure 5.11d-f. The values of dielectric loss exhibited a similar trend as those of the dielectric constant, which increased with increased filler content but declined with increases in frequency. The increase of SNR and FNR proportions in BC matrices enhanced the polar groups in the BC composite films, which led to the enlargement of orientation polarization, resulting in relatively high energy loss. Especially at low frequencies, natural proteins and phospholipids in NR could increase dielectric dissipation due to ionic conductivity, which facilitated the increase in dielectric loss [160].
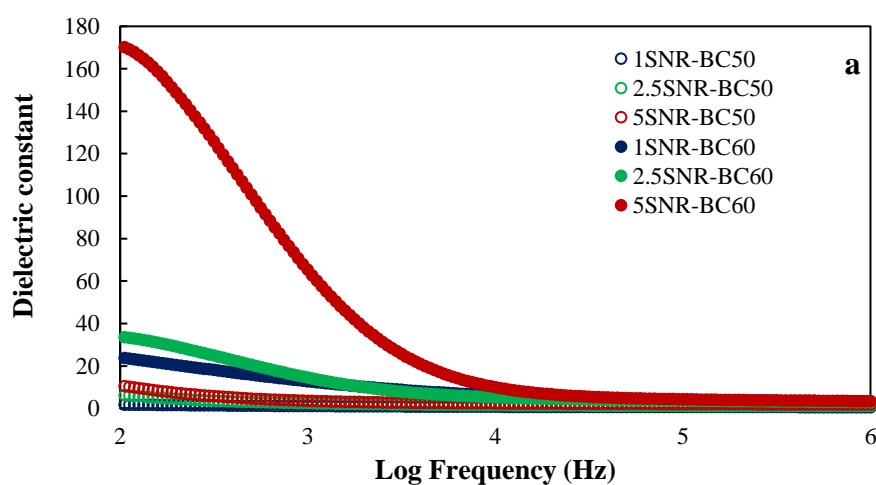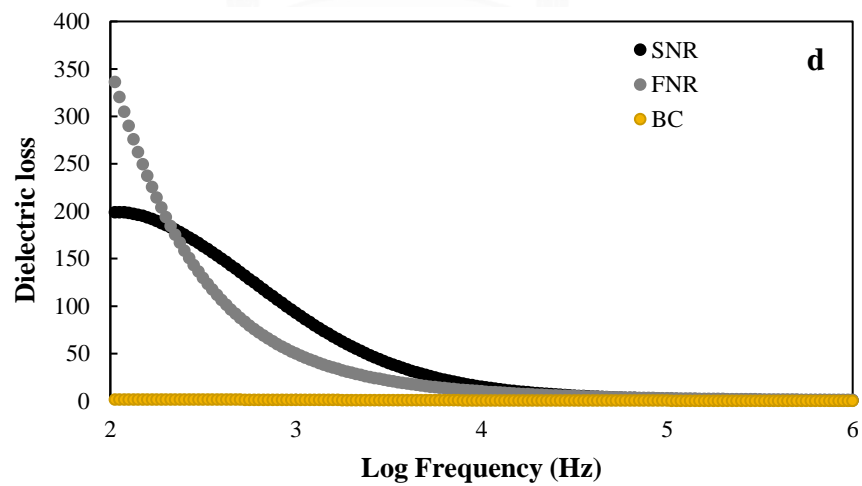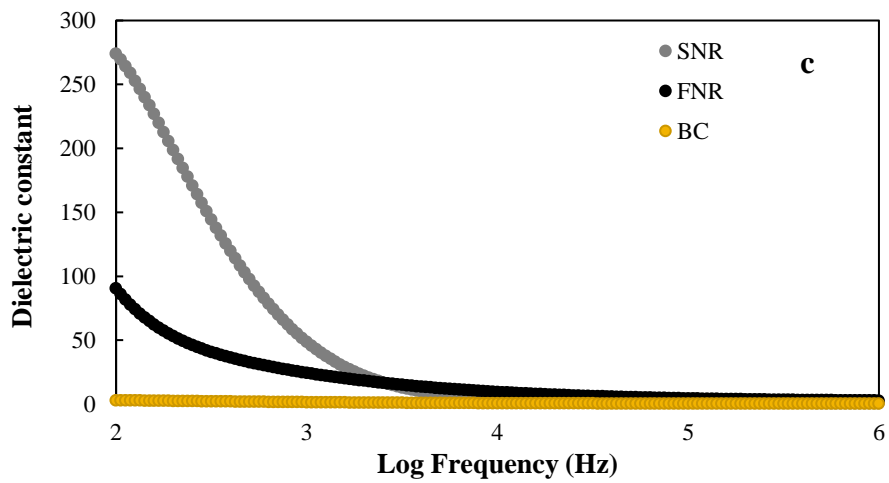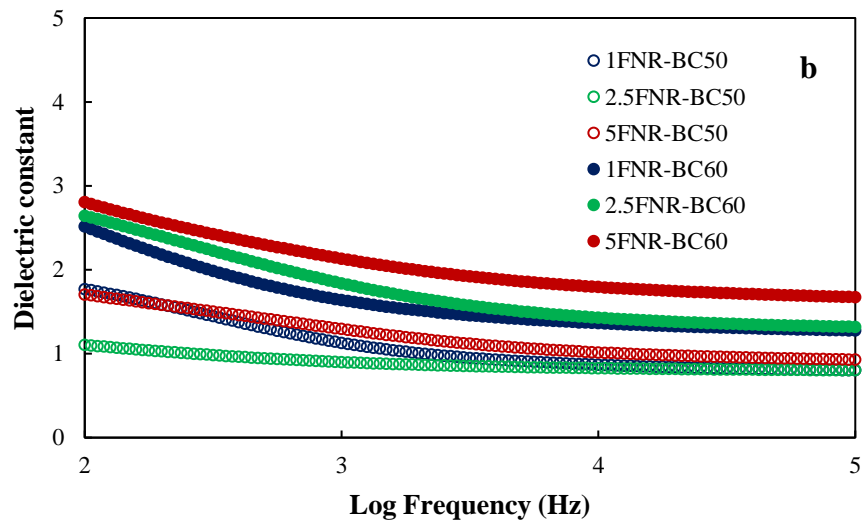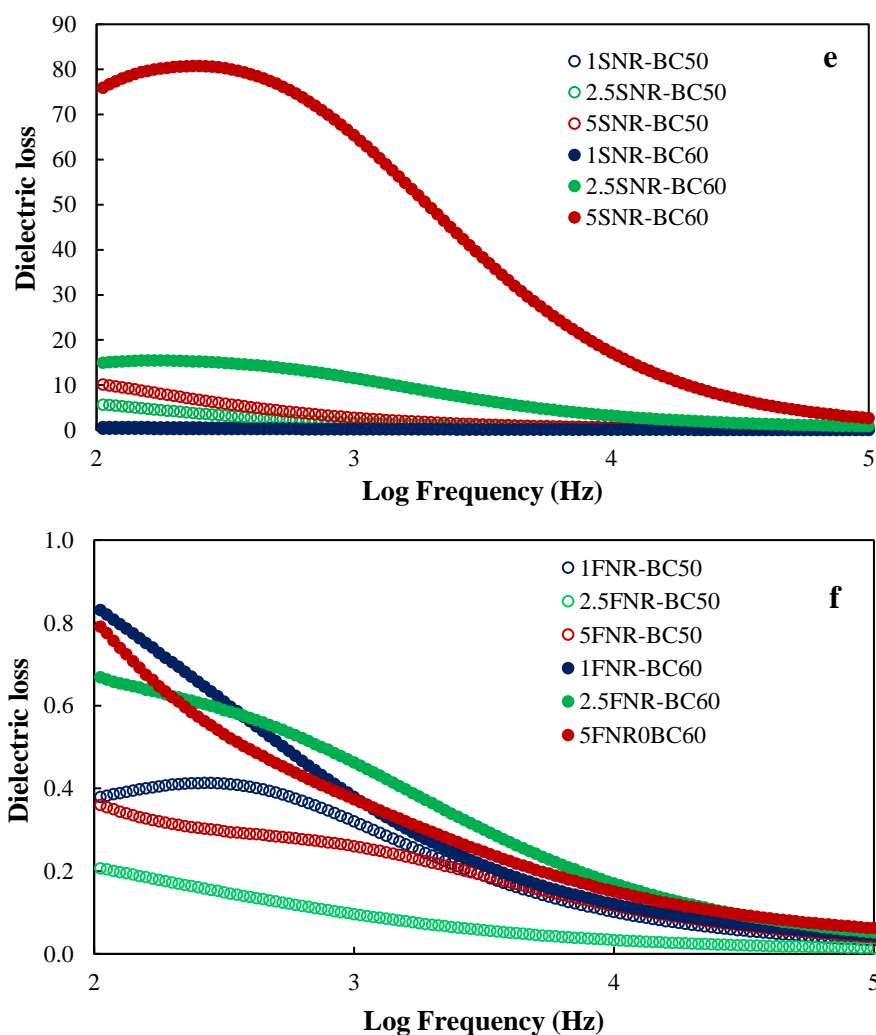
Figure 5. 11 Dielectric constant of SNR-BC (a) and FNR-BC (b) and pure SNR and FNR (c) and dielectric loss of pure SNR and FNR (d) and SNR-BC (e) and FNR-BC (f).

5.3.8 Electrical conductivity

The electrical conductivity of BC, SNR, FNR, SNR-BC and FNR-BC composites is shown in Figure 5.12. The neat BC film exhibited low electrical conductivity at ~ 6.1×10^{-13} 1/Ω.cm. The electrical conductivity of SNR and FNR were 1.9×10^{-10} and 4.4×10^{-9} 1/Ω.cm, respectively. Therefore, the electrical conductivity of FNR was slightly larger than that of SNR. The electrical conductivities of SNR and FNR were higher when compared to that of CNR (the electrical conductivity of CNR was 2.1×10^{-15} 1/Ω.cm), which could be attributed to the different amount of rubber and non-rubber content in SNR, FNR and CNR. Moreover, the electrical conductivity

of SNR-BC films was higher than that of FNR-BC films due to larger amount of SNR content in BC matrices. The electrical conductivities of SNR-BC and FNR-BC films increased with increasing NRL concentration and immersion temperature. The maximum values of electrical conductivity of SNR-BC and FNR-BC at 1.3×10^{-10} and 2.1×10^{-11} $1/\Omega.cm$, respectively were obtained at the immersion temperature of 60°C.
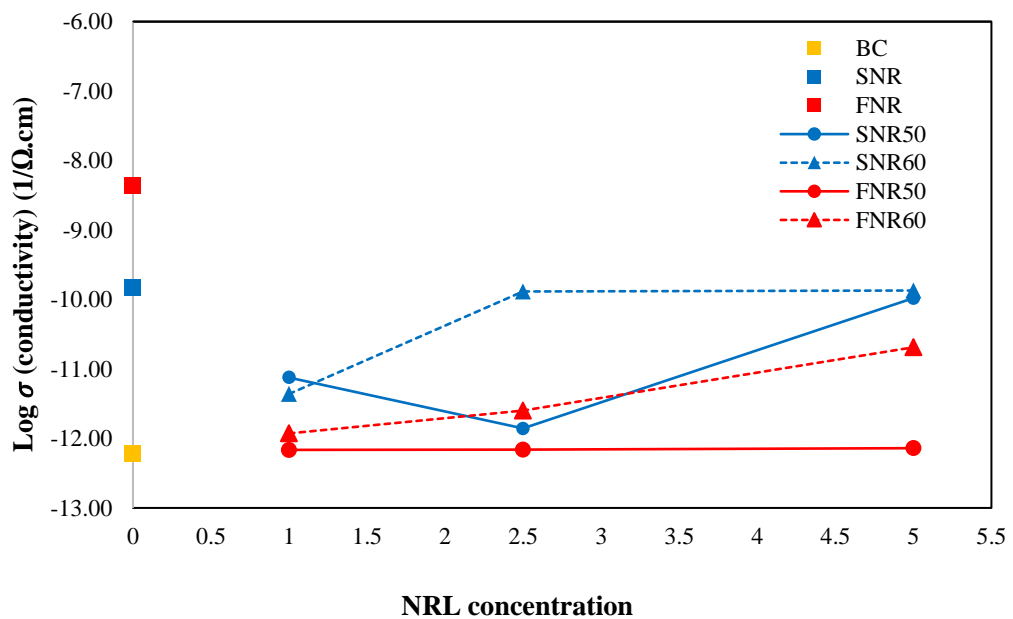
Figure 5. 12 Electrical conductivity of pure BC, SNR, FNR, SNR-BC and FNR-BC composites

CHAPTER VI
CONCLUSIONS AND RECOMMENDATIONS

6.1 Conclusions

6.1.1 NR composites filled with BRHA, BRHAT and WRHA were successfully prepared via a latex aqueous microdispersion process with the use of sodium alginate as a dispersing agent. SEM images presented good dispersion of RHAs in composite matrices and no phase separation with RHA loading in the range of 20–100 phr. The filler–rubber interactions of composites were observed via FTIR analysis. Types of RHAs and filler loading had strong effect on chemical and mechanical properties of NR-composites. NR-T composites exhibited lower chemical and mechanical properties than NR-B and NR-W due to the loss of some metal ions after acid washing pretreatment. The effective crosslinking of alginate in the composites by $CaCl_2$ was achieved on NR–WC films. The mechanical properties of NR composite films were improved by BRHA, BRHAT and WRHA reinforcement. NR–WC at filler loading of 100 phr presented the highest tensile strength and the lowest water and toluene uptake. The tensile strength of NR–WC was almost as large as that of NR-WS at same filler loading (100 phr). The results indicated that crosslinking NR–W composites by $CaCl_2$ could promote good filler–alginate–NR interaction, enhanced mechanical properties and structural stability of NR–WC films. The preliminary biodegradation in soil for 3 months revealed relatively improved biodegradability with RHA loading. The weight losses of NR–Bs, NR-Ts and NR–Ws after 3 months in soil were about 7.6–13.0%, 5.3–14.5% and 7.6–18.4%, respectively.

Moreover, the reinforcement considerably improved electrical properties of the composite films. Dielectric constant, dielectric loss factors and electrical conductivity of the composite films were enhanced with RHA loading. Dielectric properties had a trend similar to that of electrical conductivity of NR composites reinforced with RHA. NR-B composites showed higher dielectric properties and electrical conductivity than NR-W and NR-T composites due to the larger amount of metal oxides and carbon residues in BRHA. However, after crosslinking the composites by $CaCl_2$ or by sulfur vulcanization, the dielectric constant, dielectric loss

and electrical conductivity of composites significantly dropped due to the decrease in space polarization. Since the NR composites filled with RHAs exhibited improved properties in terms of mechanical properties, chemical resistance, biodegradability and electrical properties, they have potential for further development as stretchable conductive substrate or semiconducting polymer films for electronic applications.

6.1.2 BC reinforced with SRN and FRN were successfully prepared by immersing BC into diluted SNRL and FNRL suspensions at different immersion temperatures (50-60 $^{\circ}$C). It was found that SNR could more rapidly diffuse and be absorbed into BC matrices than FNR. At the higher immersion temperature of 60 $^{\circ}$C, a larger amount of SNR and FNR could be integrated into BC matrices compared to that at 50 $^{\circ}$C. FTIR analysis indicated no chemical interaction between SNR, FNR and BC. The tensile strength and elongation at break of BC composite films were improved by SNR and FNR reinforcement. The composite film of 5SNR-BC60 exhibited the highest elongation at break at 28 %, whereas the film of 5 FNR-BC50 exhibited the highest tensile strength at 177 MPa. The SNR-BC and FNR-BC films demonstrated good structural stability and high resistance to both water and toluene. From biodegradation tests in soil over 6 weeks, the biodegradability of SNR-BC and FNR-BC was 69-100% and 52-100%, respectively, at the end of 6 weeks in soil, depending on the NR content in the composite films. Moreover, the integration of SNR and FNR into BC demonstrated significantly enhanced dielectric properties of the BC composite films. The composite film of 5SNR-BC60 presented excellent dielectric properties in terms of dielectric constant (170 at 100 Hz) and dielectric loss (76 at 100 Hz). Therefore, the significant improvement of BC composite films in terms of mechanical strength, flexibility, structural stability, chemical resistance and electrical properties was achieved by using cheap natural products from NRL (SNR and FNR) as reinforcement agents. From these improved properties, the composite films display potential for further development as semiconducting polymer films and flexible electronic devices for electronic applications.

6.2 Recommendations

6.2.1 The study in Chapter IV demonstrated that the composites of NR-W100 and NR-WC100 exhibited good mechanical properties (excellent elongation at break), good chemical resistance and the films can be biodegraded in soil. The crosslinking NR-W composites by $CaCl_2$ under mild condition without toxic chemicals could effectively improve chemical and mechanical properties of the films. For future medical applications, the evaluation of film cytotoxicity should be carried out.

6.2.2 The dielectric properties of NR-RHA composites should be improved. For further developing NR-RHA composites as conductive or semiconductor materials, the NR-RHA composite should be added with some conductive filler, such as carbon black, graphite or metallic powders for reducing dielectric loss and increasing electrical conductivity.

6.2.3 The study in Chapter V demonstrated that BC reinforced with skim/fresh natural rubber latex (5SNR-BC60 and 5FNR-BC50) exhibited good chemical and mechanical properties (excellent tensile strength). The composite films can be biodegraded in soil with no toxic components. For the potential uses in medical applications, the evaluation of film cytotoxicity should be carried out.

6.2.4 Thermal stability and thermal degradation properties are importance for both biomedical material and electrical application. Therefore, in the further study, the NR composites and BC composites should be characterized in thermal stability and thermal degradation properties.

REFERENCES

1. Chuasuwan, Chetchuda. "Natural Rubber Processing." https://www.krungsri.com/bank/getmedia/5fc8fc4b-5f60-48ad-a306-5533ed9df767/IO_Rubber_2018_EN.aspx (accessed April).

2. Rippel, Márcia M, and Fernando Galembeck. "Nanostructures and Adhesion in Natural Rubber: New Era for a Classic." *Journal of the Brazilian Chemical Society* 20, no. 6 (2009): 1024-30.http://dx.doi.org/10.1590/S0103-50532009000600004

3. Khan, Imran, and A.H. Bhat. "Micro and Nano Calcium Carbonate Filled Natural Rubber Composites and Nanocomposites." In *Natural Rubber Materials, Volume 2: Composites and Nanocomposites*, edited by Hanna J. Maria Sabu Thomas, Jithin P. Joy, Chin Han Chan and Laly A. Pothen, 467-87: The Royal Society of Chemistry, 2013.

4. Santini, Raja. Effect of Natural Filler on the Characterization of Natural Rubber. Bachelor of Chemical Engineering, Universiti Malaysia Pahang, Malaysia, 2010.

5. Kumar, Ajay, Kalyani Mohanta, Devendra Kumar, and Om Parkash. "Properties and Industrial Applications of Rice Husk: A Review." (2012)

6. Ishak, ZA Mohd, and A Abu Bakar. "An Investigation on the Potential of Rice Husk Ash as Fillers for Epoxidized Natural Rubber (Enr)." *European Polymer Journal* 31, no. 3 (1995): 259-69.https://doi.org/10.1016/0014-3057(94)00156-1

7. Ismail, Hanafi, MN Nasaruddin, and US Ishiaku. "White Rice Husk Ash Filled Natural Rubber Compounds: The Effect of Multifunctional Additive and Silane Coupling Agents." *Polymer Testing* 18, no. 4 (1999): 287-98.https://doi.org/10.1016/S0142-9418(98)00030-0

8. Sae-Oui, P., C. Rakdee, and P. Thanmathorn. "Use of Rice Husk Ash as Filler in Natural Rubber Vulcanizates: In Comparison with Other Commercial Fillers." *Journal of Applied Polymer Science* 83, no. 11 (2002): 2485-93.https://doi.org/10.1002/app.10249

9. Arayapranee, Wanvimon, Nuchanat Na-Ranong, and Garry Rempel. "Application of Rice Husk Ash as Fillers in the Natural Rubber Industry." *Journal of Applied Polymer Science* 98, no. 1 (2005): 34-41. https://doi.org/10.1002/app.21004

10. Gui, Yan, Junchi Zheng, Xin Ye, Dongli Han, Meimei Xi, and Liqun Zhang. "Preparation and Performance of Silica/Sbr Masterbatches with High Silica Loading by Latex Compounding Method." 85 (2016): 130-39.https://doi.org/10.1016/j.compositesb.2015.07.001

11. Nagasawa, Naotsugu, Hiroshi Mitomo, Fumio Yoshii, and Tamikazu Kume. "Radiation-Induced Degradation of Sodium Alginate." 69, no. 3 (2000): 279-85

12. Lee, Kuen Yong, and David J Mooney. "Alginate: Properties and Biomedical Applications." 37, no. 1 (2012): 106-26

13. Qudratun, Iriani.Y , Kusumandari , Khoirum.S. "Effect of Sintering Temperature on Dielectric Constant of Silica Prepared from Rice Husk Ash." Paper presented at the Proceeding of The ASEAN Conference on Science and Technology 2014, Indonesia 2014.

14. Khor, S. F. "Dielectric Spectroscopy on Mixture of Rice Husk, Rice Husk Ash and Rice Bran from 4 Hz to 1 Mhz." *International Journal of Geomate* 11, no.

23 (2016): 2150-54.https://doi.org/10.21660/2016.23.1167

15. Yanchan Wei, Huifeng Zhang, Longmei Wu, Linhe Jin, and Shuangquan Liao. "A Review on Characterization of Molecular Structure of Natural Rubber." *MOJ Poly Sci* 1, no. 6 (2017): 197-99.DOI: 10.15406/mojps.2017.01.00032

16. Ho, CC. "The Production of Natural Rubber from Hevea Brasiliensis Latex: Colloidal Properties, Preservation, Purification and Processing." In *Natural Rubber Materials*, 73-106, 2013.

17. Sriring, Manus, Adun Nimpaiboon, Sirirat Kumarn, Chakrit Sirisinha, Jitladda Sakdapipanich, and Shigeyuki Toki. "Viscoelastic and Mechanical Properties of Large-and Small-Particle Natural Rubber before and after Vulcanization." *Polym Test* 70 (2018): 127-34.https://doi.org/10.1016/j.polymertesting.2018.06.026

18. Xiang, Qiulan, Kecan Xia, Longjun Dai, Guijuan Kang, Yu Li, Zhiyi Nie, Cuifang Duan, and Rizhong Zeng. "Proteome Analysis of the Large and the Small Rubber Particles of Hevea Brasiliensis Using 2d-Dige." *Plant Physiol Biochem* 60 (2012): 207-13.https://doi.org/10.1016/j.plaphy.2012.08.010

19. Yip, Esah, and Paul Cacioli. "The Manufacture of Gloves from Natural Rubber Latex." *Journal of allergy clinical immunology* 110, no. 2 (2002): S3-S14

20. Rippel, Márcia M, Lay-Theng Lee, Carlos AP Leite, and Fernando Galembeck. "Skim and Cream Natural Rubber Particles: Colloidal Properties, Coalescence and Film Formation." *J Colloid Interface Sci* 268, no. 2 (2003): 330-40.https://doi.org/10.1016/j.jcis.2003.07.046

21. Rippel, Márcia M, and Fernando Galembeck. "Nanostructures and Adhesion in Natural Rubber: New Era for a Classic." *Journal of the Brazilian Chemical Society* 20 (2009): 1024-30. https://doi.org/10.1590/S0103-50532009000600004

22. Coran, Aubert Y. "Vulcanization." In *Science and Technology of Rubber*, 339-85: Elsevier, 1994.

23. Mok, KL, and AH Eng. "Characterisation of Crosslinks in Vulcanised Rubbers: From Simple to Advanced Techniques." *Malays J Chem* 20 (2018): 118-27

24. Nasir, M, and GK Teh. "The Effects of Various Types of Crosslinks on the Physical Properties of Natural Rubber." *European Polymer Journal* 24, no. 8 (1988): 733-36.https://doi.org/10.1016/0014-3057(88)90007-9

25. Prasara-A, Jittima. Comparative Life Cycle Assessment of Rice Husk Utilization in Thailand. Doctor of Philosophy, RMIT University, Thailand, 2009.

26. Ismail, Muhammad Shoaib, and AM Waliuddin. "Effect of Rice Husk Ash on High Strength Concrete." *Construction building materials* 10, no. 7 (1996): 521-26.https://doi.org/10.1016/0950-0618(96)00010-4

27. Katsuki, Hiroaki, Sachiko Furuta, Takanori Watari, and Sridhar Komarneni. "Zsm-5 Zeolite/Porous Carbon Composite: Conventional-and Microwave-Hydrothermal Synthesis from Carbonized Rice Husk." *Microporous Mesoporous Materials* 86, no. 1-3 (2005): 145-51.https://doi.org/10.1016/j.micromeso.2005.07.010

28. Deshmukh, Pallavi, Dilip Peshwe, and Shailkumar Pathak. "Ftir and Tga Analysis in Relation with the % Crystallinity of the Sio2 Obtained by Burning Rice Husk at Various Temperatures." *Advanced Materials Research* 585 (2012): 77-81.https://doi.org/10.4028/www.scientific.net/AMR.585.77

29. Sankar, S, Sanjeev K Sharma, Narinder Kaur, Byoungho Lee, Deuk Young Kim, Sejoon Lee, and Hyun Jung. "Biogenerated Silica Nanoparticles Synthesized

from Sticky, Red, and Brown Rice Husk Ashes by a Chemical Method." *Ceramics International* 42, no. 4 (2016): 4875-85.https://doi.org/10.1016/j.ceramint.2015.11.172

30. Bakar, Rohani Abu, Rosiyah Yahya, and Seng Neon %J Procedia chemistry Gan. "Production of High Purity Amorphous Silica from Rice Husk." *Procedia chemistry* 19 (2016): 189-95.https://doi.org/10.1016/j.proche.2016.03.092

31. Yalcin, N, and V Sevinc. "Studies on Silica Obtained from Rice Husk." *Ceramics International* 27, no. 2 (2001): 219-24.https://doi.org/10.1016/S0272-8842(00)00068-7Get

32. Fernandes, Iara Janaína, Daiane Calheiro, Felipe AL Sánchez, Alini Luísa Diehl Camacho, Tatiana Louise Avila de Campos Rocha, Carlos Alberto Mendes Moraes, and Vânia Caldas de Sousa. "Characterization of Silica Produced from Rice Husk Ash: Comparison of Purification and Processing Methods." *Materials Research* 20 (2017): 512-18.https://doi.org/10.1590/1980-5373-MR-2016-1043

33. Shen, Yafei, Peitao Zhao, and Qinfu Shao. "Porous Silica and Carbon Derived Materials from Rice Husk Pyrolysis Char." *Microporous Mesoporous Materials* 188 (2014): 46-76.https://doi.org/10.1016/j.micromeso.2014.01.005

34. Sarkawi, Siti Salina, and Yusof Aziz. "Ground Rice Husk as Filler in Rubber Compounding." *Jurnal Teknologi* (2003): 135–48.https://journals.utm.my/jurnalteknologi/article/view/435

35. Hua, Shuibo, Haizhen Ma, Xun Li, Huixia Yang, and Aiqin Wang. "Ph-Sensitive Sodium Alginate/Poly (Vinyl Alcohol) Hydrogel Beads Prepared by Combined Ca2+ Crosslinking and Freeze-Thawing Cycles for Controlled Release of Diclofenac Sodium." *International journal of biological macromolecules* 46, no. 5 (2010): 517-23.https://doi.org/10.1016/j.ijbiomac.2010.03.004

36. Imeson, Alan P. *Thickening and Gelling Agents for Food*: Springer Science & Business Media, 2012.

37. Kalyani, Swayampakula, Biduru Smitha, Sundergopal Sridhar, and Abburi Krishnaiah. "Pervaporation Separation of Ethanol–Water Mixtures through Sodium Alginate Membranes." *Desalination* 229, no. 1-3 (2008): 68-81.https://doi.org/10.1016/j.desal.2007.07.027

38. Saarai, Amarjargal, V Kasparkova, T Sedlacek, and Petr Sáha. "A Comparative Study of Crosslinked Sodium Alginate/Gelatin Hydrogels for Wound Dressing." Paper presented at the Proceeding of the 4th WSEAS International Conference on Engineering Mechanics, Structures, Engineering Geology. WSEAS Press, Greece 2011.

39. Simpson, Nicholas E, Cheryl L Stabler, Chiab P Simpson, Athanassios Sambanis, and Ioannis Constantinidis. "The Role of the Cacl2–Guluronic Acid Interaction on Alginate Encapsulated Btc3 Cells." *Biomaterials* 25, no. 13 (2004): 2603-10.https://doi.org/10.1016/j.biomaterials.2003.09.046

40. Kuo, Catherine K, and Peter X Ma. "Maintaining Dimensions and Mechanical Properties of Ionically Crosslinked Alginate Hydrogel Scaffolds in Vitro." *Journal of Biomedical Materials Research Part A* 84, no. 4 (2008): 899-907. https://doi.org/10.1002/jbm.a.31375

41. Riyajan, Sa-Ad, and Pramuan Tangboriboonrat. "Novel Composite Biopolymers of Sodium Alginate/Natural Rubber/Coconut Waste for Adsorption of Pb(Ii) Ions." *Polymer Composites* 35, no. 5 (2014): 1013-21.

https://doi.org/10.1002/pc.22747

42. Riyajan, Sa-Ad "Physical Property Testing of a Novel Hybrid Natural Rubber-Graft-Cassava Starch/Sodium Alginate Bead for Encapsulating Herbicide." *Polymer Testing* 58 (2017): 300-07.https://doi.org/10.1016/j.polymertesting.2017.01.009

43. Waddell, Walter H, and Larry R Evans. "Use of Nonblack Fillers in Tire Compounds." *Rubber Chemistry Technology* 69, no. 3 (1996): 377-423.https://doi.org/10.5254/1.3538378

44. Katueangngan, Kavichat, Tulyapong Tulyapitak, Anuwat Saetung, Siriwat Soontaranon, and Nattapong Nithi-uthai. "Renewable Interfacial Modifier for Silica Filled Natural Rubber Compound." *Procedia chemistry* 19 (2016): 447-54.https://doi.org/10.1016/j.proche.2016.03.037

45. Jarnthong, Methakarn, Lusheng Liao, Fuquan Zhang, Yueqiong Wang, Puwang Li, Zheng Peng, Chutarat Malawet, and Punyanich Intharapat. "Characterization of Interaction between Natural Rubber and Silica by Ftir." Paper presented at the AIP Conference Proceedings 2017.

46. Sarkawi, SS, Wilma K Dierkes, and Jacobus WM Noordermeer. "Elucidation of Filler-to-Filler and Filler-to-Rubber Interactions in Silica-Reinforced Natural Rubber by Tem Network Visualization." *European Polymer Journal* 54 (2014): 118-27.https://doi.org/10.1016/j.eurpolymj.2014.02.015

47. Sarkawi, S SALINA, Wisut Kaewsakul, Kannika Sahakaro, Wilma K Dierkes, and Jacobus WM Noordermeer. "A Review on Reinforcement of Natural Rubber by Silica Fillers for Use in Low-Rolling Resistance Tires." *Journal of rubber research* 18, no. 4 (2015): 203-33

48. Al-Hartomy, Omar A, Ahmed A Al-Ghamdi, Said A Farha Al Said, Nikolay Dishovsky, Mihail Mihaylov, and Milcho %J Journal of Composite Materials Ivanov. "Influence of Carbon Black/Silica Ratio on the Physical and Mechanical Properties of Composites Based on Epoxidized Natural Rubber." 50, no. 3 (2016): 377-86

49. Savetlana, Shirley, I Sukmana, and FA Saputra. "The Effect of Carbon Black Loading and Structure on Tensile Property of Natural Rubber Composite." Paper presented at the IOP Conference Series: Materials Science and Engineering 2017.

50. Kardan, M "Carbon Black Reinforcement in Natural Rubber-Based Adhesives and Sealants." *International Polymer Science Technology* 31, no. 1 (2004): 7-10.https://doi.org/10.1177/0307174X0403100102

51. Panitchakarn, Panu, Jaygita Wikranvanich, and Muenduen Phisalaphong. "Synthesis and Characterization of Natural Rubber/Coal Fly Ash Composites Via Latex Aqueous Microdispersion." *Journal of Material Cycles and Waste Management* 21, no. 1 (2018): 134-44.https://doi.org/10.1007/s10163-018-0774-x

52. Maan, Arti, Utpal Kumar Niyogi, Anil Kumar Singh, Dayal Singh Mehra, and Sunita Rattan. "Development and Characterization of Fly Ash Reinforced Natural Rubber Composite." *Journal of Polymer Materials* 31, no. 4 (2014): 397-408

53. Yangthong, Hassarutai, Suwaluk Wisunthorn, Skulrat Pichaiyut, and Charoen Nakason. "Novel Epoxidized Natural Rubber Composites with Geopolymers

from Fly Ash Waste." *Waste Management* 87 (2019): 148-60.https://doi.org/10.1016/j.wasman.2019.02.013

54. Pongdong, Wiphawadee, Charoen Nakason, Claudia Kummerlöwe, and Norbert Vennemann. "Influence of Filler from a Renewable Resource and Silane Coupling Agent on the Properties of Epoxidized Natural Rubber Vulcanizates." *Journal of Chemistry* 2015 (2015).https://doi.org/10.1155/2015/796459

55. Brodie, Graham, Mohan V Jacob, and Peter Farrell. *Microwave and Radio-Frequency Technologies in Agriculture: An Introduction for Agriculturalists and Engineers*: Walter de Gruyter GmbH & Co KG, 2016.

56. Nasreen, Shamima, Gregory M Treich, Matthew L Baczkowski, Arun K Mannodi-Kanakkithodi, Yang Cao, Ramamurthy Ramprasad, and Gregory Sotzing. "Polymer Dielectrics for Capacitor Application." *Kirk-Othmer Encyclopedia of Chemical Technology* (2000): 1-29.https://doi.org/10.1002/0471238961.koe00036

57. Louis, N. Samson Maria, ArjumanBanu, and S. Sudha. "Effect of Rice Husk Ash and Hydrated Silica on the Dielectric Proper- Ties of Ldpe Composites." *Mater. Sci. An Indian J* 11 (2014): 0974-7486

58. Al-Ghamdi, Ahmed A, Omar A Al-Hartomy, Falleh R Al-Solamy, Nikolay Dishovsky, Mihail Mihaylov, Petrunka Malinova, and Nikolay Atanasov. "Natural Rubber Based Composites Comprising Different Types of Carbon-Silica Hybrid Fillers. Comparative Study on Their Electric, Dielectric and Microwave Properties, and Possible Applications." *Materials Sciences Applications* 7, no. 06 (2016): 295.http://dx.doi.org/10.4236/msa.2016.76027

59. Ravikumar, K, K Palanivelu, and K Ravichandran. "Dielectric Properties of Natural Rubber Composites Filled with Graphite." *Materials Today: Proceedings* 16 (2019): 1338-43

60. Rattanapan, Apaipan "Study of the Mechanical, Dynamic Mechanical and Dielectric Properties of Natural Rubber/Barium Titanate Composites." *SNRU Journal of Science Technology* 10, no. 1 (2018): 45-51

61. Marzinotto, M, C Santulli, and C Mazzetti. "Dielectric Properties of Oil Palm-Natural Rubber Biocomposites." Paper presented at the 2007 Annual Report-Conference on Electrical Insulation and Dielectric Phenomena 2007.

62. Thongruang, Wiriya, Churairat Ritthichaiwong, Pisanu Bunnaul, Pruittikorn Smithmaitrie, and Kanadit Chetpattananondh. "Electrical and Mechanical Properties of Ternary Composites from Natural Rubber and Conductive Fillers." *Songklanakarin Journal of Science Technology* 30, no. 3 (2008)

63. Al-Sehemi, Abdullah G, Ahmed A Al-Ghamdi, Nikolay T Dishovsky, P Malinova, Nikolay T Atanasov, and Gabriela L Atanasova. "Natural Rubber Composites Containing Low and High Dielectric Constant Fillers and Their Application as Substrates for Compact Flexible Antennas." *Polymers Polymer Composites* 29, no. 4 (2021): 233-45

64. Haseena, AP, G Unnikrishnan, and G Kalaprasad. "Dielectric Properties of Short Sisal/Coir Hybrid Fibre Reinforced Natural Rubber Composites." *Composite Interfaces* 14, no. 7-9 (2007): 763-86

65. Sreenivasan, Divia P, A Sujith, Avinash Nelson Asokan, and C Rajesh. "Dielectric Properties of Composites of Natural Rubber and Keratinfibre from Chicken Feather." *Fibers Polymers* (2021): 1-14

66.	Yang, Dan, Liyuan Yu, Yafei Liang, Qungui Wei, Yufeng Ni, and Liqun Zhang. "Enhanced Electromechanical Performance of Natural Rubber Composites Via Constructing Strawberry-Like Dielectric Nanoparticles." *ACS Applied Polymer Materials* 2, no. 12 (2020): 5621-29

67.	Al-Hartomy, Omar A, Ahmed A Al-Ghamdi, Falleh Al-Salamy, Nikolay Dishovsky, Rossitsa Shtarkova, Vladimir Iliev, and Farid El-Tantawy. "Dielectric and Microwave Properties of Graphene Nanoplatelets/Carbon Black Filled Natural Rubber Composites." *International Journal of Materials Chemistry* 2, no. 3 (2012): 116-22

68.	Muthadhi, A., and S. Kothandaraman. "Optimum Production Conditions for Reactive Rice Husk Ash." *Materials and Structures* 43, no. 9 (2010): 1303-15.https://doi.org/10.1617/s11527-010-9581-0

69.	Chiaoprakobkij, N., S. Seetabhawang, N. Sanchavanakit, and M. Phisalaphong. "Fabrication and Characterization of Novel Bacterial Cellulose/Alginate/Gelatin Biocomposite Film." *J Biomater Sci Polym Ed* 30, no. 11 (2019): 961-82.https://doi.org/10.1080/09205063.2019.1613292

70.	Jacob, Maya, K. T. Varughese, and Sabu Thomas. "Dielectric Characteristics of Sisal–Oil Palm Hybrid Biofibre Reinforced Natural Rubber Biocomposites." *Journal of Materials Science* 41, no. 17 (2006): 5538-47.https://doi.org/10.1007/s10853-006-0298-y

71.	Chen, Pei, Wenbo Gu, Wenxuan Fang, Xiaoyu Ji, and Rushan Bie. "Removal of Metal Impurities in Rice Husk and Characterization of Rice Husk Ash under Simplified Acid Pretreatment Process." *Environmental Progress Sustainable Energy* 36, no. 3 (2017): 830-37. https://doi.org/10.1002/ep.12513

72.	Jaya, Ramadhansyah Putra, Mohd Al Amin Muhamad Nor, Zainal Arifin Ahmad, and Zakaria Mohd Amin. "Properties of Mortar Containing Rice Husk Ash at Different Temperature and Exposed to Aggressive Environment." *Advanced Materials Research* 620 (2012): 87-93.https://doi.org/10.4028/www.scientific.net/AMR.620.87

73.	Venkatanarayanan, Harish Kizhakkumodom, and Prasada Rao Rangaraju. "Material Characterization Studies on Low- and High-Carbon Rice Husk Ash and Their Performance in Portland Cement Mixtures." *Advances in Civil Engineering Materials* 2, no. 1 (2013).https://doi.org/10.1520/ACEM20120056

74.	Madathil Sreekumar, V., R. Marimuthu Pillai, B. Chandrasekhara Pai, and M. Chakraborty. "Microstructural Development in Al/Mgal2o4in Situ Metal Matrix Composite Using Value-Added Silica Sources." *Sci Technol Adv Mater* 9, no. 1 (2008): 015004.https://doi.org/10.1088/1468-6996/9/1/015004

75.	Rosiah Osman, Nor Hapishah Abdullah, Khamirul Amin Matori, Mohd. Nizar Hamidon, Ismayadi Ismail, Syazwan Mustaffa. "Effect of Temperature Towards Rice Husk Silica Characterization with Different Preparation Methods." *International Journal of Basic & Applied Sciences* 17 (1) (2017): 15-20

76.	Xu, Weiting, Tommy Y. Lo, and Shazim Ali Memon. "Microstructure and Reactivity of Rich Husk Ash." *Construction and Building Materials* 29 (2012): 541-47.https://doi.org/10.1016/j.conbuildmat.2011.11.005

77.	Phomrak, Sirilak, and Muenduen Phisalaphong. "Reinforcement of Natural Rubber with Bacterial Cellulose Via a Latex Aqueous Microdispersion Process." *Journal of Nanomaterials* 2017 (2017): 1-

9.https://doi.org/10.1155/2017/4739793

78. Saikia, Bhaskar J., and Gopalakrishnarao Parthasarathy. "Fourier Transform Infrared Spectroscopic Characterization of Kaolinite from Assam and Meghalaya, Northeastern India." *Journal of Modern Physics* 01, no. 04 (2010): 206-10.https://doi.org/10.4236/jmp.2010.14031

79. Laia, Andreia Grossi Santos de, Ezequiel de Souza Costa Junior, and Hermes de Souza Costa. "A Study of Sodium Alginate and Calcium Chloride Interaction through Films for Intervertebral Disc Regeneration Uses." In *21 CBECIMAT: Brazilian congress of engineering and materials science*, 7341-48. Brazil, 2014.

80. Daemi, H., and M. Barikani. "Synthesis and Characterization of Calcium Alginate Nanoparticles, Sodium Homopolymannuronate Salt and Its Calcium Nanoparticles." *Scientia Iranica* 19, no. 6 (2012): 2023-28.https://doi.org/10.1016/j.scient.2012.10.005

81. Linnig, Frederic J, and James E Stewart. "Infrared Study of Some Structural Changes in Natural Rubber During Vulcanization." *Rubber Chemistry Technology* 31, no. 4 (1958): 719-36.https://doi.org/10.5254/1.3542330

82. Da Costa, HM, LLY Visconte, RCR Nunes, and CRG Furtado. "The Effect of Coupling Agent and Chemical Treatment on Rice Husk Ash-Filled Natural Rubber Composites." *Journal of Applied Polymer Science* 76, no. 7 (2000): 1019-27.https://doi.org/10.1002/(SICI)1097-4628(20000516)76:7

83. Jayathilaka, Lokuvithana P. I., Thilini U. Ariyadasa, and Shantha M. Egodage. "Development of Biodegradable Natural Rubber Latex Composites by Employing Corn Derivative Bio-Fillers." *Journal of Applied Polymer Science* (2020). https://doi.org/10.1002/app.49205

84. Da Costa, HM, RCR Nunes, LLY Visconte, and CRG Furtado. "Physical Properties and Swelling of Natural Rubber Compounds Containing Rice Husk Ash." *Raw Materials and Applications* 54, no. 5 (2001): 242-49

85. Boonmee, Anupong, Palida Sabsiriroht, and Kasama Jarukumjorn. "Preparation and Characterization of Rice Husk Ash for Using as a Filler in Natural Rubber." *Materials Today: Proceedings* 17 (2019): 2097-103.https://doi.org/10.1016/j.matpr.2019.06.259

86. Da Costa, HM, LLY Visconte, RCR Nunes, and CRG Furtado. "Rice Husk Ash Filled Natural Rubber. I. Overall Rate Constant Determination for the Vulcanization Process from Rheometric Data." *Journal of Applied Polymer Science* 87, no. 8 (2003): 1194-203.https://doi.org/10.1002/app.11452

87. Costa, Maria J., Arlete M. Marques, Lorenzo M. Pastrana, José A. Teixeira, Sanna M. Sillankorva, and Miguel A. Cerqueira. "Physicochemical Properties of Alginate-Based Films: Effect of Ionic Crosslinking and Mannuronic and Guluronic Acid Ratio." *Food Hydrocolloids* 81 (2018): 442-48.https://doi.org/10.1016/j.foodhyd.2018.03.014

88. Pocius, Alphonsus V, and David A Dillard. "Chapter 13 - Rubber Base Adhesives." In *Adhesion Science and Engineering: Surfaces, Chemistry and Applications*: Elsevier, 2002.

89. Kam, Ka-Wei, Pei-Leng Teh, Hakimah Osman, and Cheow-Keat Yeoh. "Comparison Study: Effect of Un-Vulcanized and Vulcanized Nr Content on the Properties of Two-Matrix Filled Epoxy/Natural Rubber/Graphene Nano-Platelets System." *Journal of Polymer Research* 25, no. 1 (2018): 1-

19.https://doi.org/10.1007/s10965-017-1418-x

90.   Ab Wahab, Mohd Kahar, Nadras Othman, and Hanafi Ismail. "Thermoplastic Elastomers from High-Density Polyethylene/Natural Rubber/Thermoplastic Tapioca Starch: Effects of Different Dynamic Vulcanization." *Natural Rubber Materials* 1 (2013): 242-64

91.   Khed, Veerendrakumar C, Bashar S Mohammed, MS Liew, and Noor Amila Wan Abdullah Zawawi. "Development of Response Surface Models for Self-Compacting Hybrid Fibre Reinforced Rubberized Cementitious Composite." *Construction and Building Materials* 232 (2020): 117191.https://doi.org/10.1016/j.conbuildmat.2019.117191

92.   Ab Rahman, M. F., N. S. Norfaizal, and A. R. Azura. "The Influence of Sago Starch Dispersion on Mechanical Properties of Biodegradable Natural Rubber Latex Films." *Materials Today: Proceedings* 17 (2019): 1040-46.https://doi.org/10.1016/j.matpr.2019.06.507

93.   Supanakorn, Goragot, Nanthaphak Varatkowpairote, Siriporn Taokaew, and Muenduen Phisalaphong. "Alginate as Dispersing Agent for Compounding Natural Rubber with High Loading Microfibrillated Cellulose." *Polymers* 13, no. 3 (2021): 468

94.   Turmanova, Sevdalina, Svetlana Genieva, and Lyubomir Vlaev. "Obtaining Some Polymer Composites Filled with Rice Husks Ash-a Review." *International Journal of Chemistry* 4, no. 4 (2012).https://doi.org/10.5539/ijc.v4n4p62

95.   Ismail, H., L. Mega, and H. P. S. Abdul Khalil. "Effect of a Silane Coupling Agent on the Properties of White Rice Husk Ash-Polypropylene/Natural Rubber Composites." *Polymer International* 50, no. 5 (2001): 606-11. https://doi.org/10.1002/pi.673

96.   Visakh, PM, Sabu Thomas, Kristiina Oksman, and Aji P Mathew. "Effect of Cellulose Nanofibers Isolated from Bamboo Pulp Residue on Vulcanized Natural Rubber." *Bioresources* 7, no. 2 (2012): 2156-68.https://doi.org/10.15376/biores.7.2.2156-2168

97.   Ismail, H, Salmah, and M Nasir. "The Effect of Dynamic Vulcanization on Mechanical Properties and Water Absorption of Silica and Rubberwood Filled Polypropylene/Natural Rubber Hybrid Composites." *International Journal of Polymeric Materials* 52, no. 3 (2003): 229-38.https://doi.org/10.1080/00914030304892

98.   Abraham, Eldho, Merin S Thomas, Cijo John, LA Pothen, O Shoseyov, and S Thomas. "Green Nanocomposites of Natural Rubber/Nanocellulose: Membrane Transport, Rheological and Thermal Degradation Characterisations." *Industrial Crops and Products* 51 (2013): 415-24.https://doi.org/10.1016/j.indcrop.2013.09.022

99.   Roy, Kumarjyoti, Subhas Chandra Debnath, Lazaros Tzounis, Aphiwat Pongwisuthiruchte, and Pranut %J Polymers Potiyaraj. "Effect of Various Surface Treatments on the Performance of Jute Fibers Filled Natural Rubber (Nr) Composites." *Polymers* 12, no. 2 (2020): 369. https://doi.org/10.3390/polym12020369

100.   Bhatt, Rachana, Dishma Shah, KC Patel, and Ujjval Trivedi. "Pha–Rubber Blends: Synthesis, Characterization and Biodegradation." *Bioresource technology* 99, no. 11 (2008): 4615-

20.https://doi.org/10.1016/j.biortech.2007.06.054

101. Ramasamy, Shamala, Hanafi Ismail, and Yamuna Munusamy. "Soil Burial, Tensile Properties, Morphology, and Biodegradability of (Rice Husk Powder)-Filled Natural Rubber Latex Foam." *Journal of Vinyl and Additive Technology* 21, no. 2 (2015): 128-33.https://doi.org/10.1002/vnl.21389

102. Yahya, Siti Rohana, Azura A. Rashid, and Baharin Azahari. "Soil Burial Studies for Biodegradation of Natural Rubber Latex Films." *Advanced Materials Research* 844 (2013): 406-09.https://doi.org/10.4028/www.scientific.net/AMR.844.406

103. Zaborski, Marian, Małgorzata Piotrowska, and Zofia Żakowska. "Hydrophilic-Hydrophobic Rubber Composites with Increased Susceptibility to Biodegradation." *Polimery* 51 (2006).https://doi.org/10.14314/polimery.2006.534

104. Kambale, RC, PA Shaikh, CH Bhosale, KY Rajpure, and YD Kolekar. "The Effect of Mn Substitution on the Magnetic and Dielectric Properties of Cobalt Ferrite Synthesized by an Autocombustion Route." *Smart Materials and structures* 18, no. 11 (2009): 115028.https://doi.org/10.1088/0964-1726/18/11/115028

105. Rajinder, Pal. *Electromagnetic, Mechanical, and Transport Properties of Composite Materials*. Vol. 158. United States: CRC Press, 2014.

106. Juntaro, J., S. Ummartyotin, M. Sain, and H. Manuspiya. "Bacterial Cellulose Reinforced Polyurethane-Based Resin Nanocomposite: A Study of How Ethanol and Processing Pressure Affect Physical, Mechanical and Dielectric Properties." *Carbohydrate Polymers* 87, no. 4 (2012): 2464-69.https://doi.org/10.1016/j.carbpol.2011.11.020

107. Wu, Haitao, and Eung Soo Kim. "Correlations between Crystal Structure and Dielectric Properties of High-Q Materials in Rock-Salt Structure Li 2 O–Mgo–Bo 2 (B= Ti, Sn, Zr) Systems at Microwave Frequency." *RSC advances* 6, no. 53 (2016): 47443-53.https://doi.org/10.1039/C6RA06624K

108. Samanta, B., P. Kumar, D. Nanda, and R. Sahu. "Dielectric Properties of Epoxy-Al Composites for Embedded Capacitor Applications." *Results in Physics* 14 (2019).https://doi.org/10.1016/j.rinp.2019.102384

109. Muhammad Abdul Jamal, E., P. A. Joy, Philip Kurian, and M. R. Anantharaman. "Synthesis of Nickel–Rubber Nanocomposites and Evaluation of Their Dielectric Properties." *Materials Science and Engineering: B* 156, no. 1-3 (2009): 24-31.https://doi.org/10.1016/j.mseb.2008.10.041

110. Sheykhnazari, S., T. Tabarsa, M. Mashkour, A. Khazaeian, and A. Ghanbari. "Multilayer Bacterial Cellulose/Resole Nanocomposites: Relationship between Structural and Electro-Thermo-Mechanical Properties." *Int J Biol Macromol* 120, no. Pt B (2018): 2115-22.https://doi.org/10.1016/j.ijbiomac.2018.09.047

111. Thomas, P Selvin, Adedigba A Abdullateef, Mamdouh A Al-Harthi, Muataz A Atieh, SK De, Mostafizur Rahaman, TK Chaki, D Khastgir, and Sri Bandyopadhyay. "Electrical Properties of Natural Rubber Nanocomposites: Effect of 1-Octadecanol Functionalization of Carbon Nanotubes." *Journal of Materials Science* 47, no. 7 (2012): 3344-49

112. Braunger, ML, CA Escanhoela Jr, I Fier, L Walmsley, and EC Ziemath. "Electrical Conductivity of Silicate Glasses with Tetravalent Cations

Substituting Si." *Journal of non-crystalline solids* 358, no. 21 (2012): 2855-61.https://doi.org/10.1016/j.jnoncrysol.2012.07.013

113. Kaklamani, Georgia, Diana Kazaryan, James Bowen, Fabrice Iacovella, Spiros H Anastasiadis, and George %J Regenerative biomaterials Deligeorgis. "On the Electrical Conductivity of Alginate Hydrogels." *Regenerative biomaterials* 5, no. 5 (2018): 293-301

114. Prunet, Geoffrey, Florent Pawula, Guillaume Fleury, Eric Cloutet, Anthony James Robinson, Georges Hadziioannou, and Amir Pakdel. "A Review on Conductive Polymers and Their Hybrids for Flexible and Wearable Thermoelectric Applications." *Materials Today Physics* (2021): 100402

115. Le, Thanh-Hai, Yukyung Kim, and Hyeonseok Yoon. "Electrical and Electrochemical Properties of Conducting Polymers." *Polymers* 9, no. 4 (2017): 150

116. Mohan, Sneha, Oluwatobi S Oluwafemi, Nandakumar Kalarikkal, Sabu Thomas, and Sandile P Songca. "Biopolymers–Application in Nanoscience and Nanotechnology." *Recent advances in biopolymers* 1, no. 1 (2016): 47-66.https://doi.org/10.5772/62225

117. Díez-Pascual, Ana María. "Synthesis and Applications of Biopolymer Composites." *Int. J. Mol. Sci.* 20, no. 9 (2019): 2321. https://doi.org/10.3390/ijms20092321

118. Sadasivuni, Kishor Kumar, John-John Cabibihan, Deepalekshmi Ponnamma, Mariam AlAli AlMaadeed, and Jaehwan Kim. *Biopolymer Composites in Electronics*: Elsevier, 2016.

119. Urbina, Leire, Ana Alonso-Varona, Ainara Saralegi, Teodoro Palomares, Arantxa Eceiza, María Ángeles Corcuera, and Aloña Retegi. "Hybrid and Biocompatible Cellulose/Polyurethane Nanocomposites with Water-Activated Shape Memory Properties." *Carbohydr Polym* 216 (2019): 86-96.https://doi.org/10.1016/j.carbpol.2019.04.010

120. Gu, Ruijun, Bohuslav V Kokta, Katrin Frankenfeld, and Kerstin Schlufter. "Bacterial Cellulose Reinforced Thermoplastic Composites: Preliminary Evaluation of Fabrication and Performance." *BioRes* 5, no. 4 (2010): 2195-207

121. Cañas-Gutiérrez, A, M Osorio, C Molina-Ramírez, D Arboleda-Toro, and C Castro-Herazo. "Bacterial Cellulose: A Biomaterial with High Potential in Dental and Oral Applications." *Cellulose* (2020): 1-18.https://doi.org/10.1007/s10570-020-03456-4

122. Wang, Jing, Javad Tavakoli, and Youhong Tang. "Bacterial Cellulose Production, Properties and Applications with Different Culture Methods–a Review." *Carbohydr Polym* 219 (2019): 63-76.https://doi.org/10.1016/j.carbpol.2019.05.008

123. Perrella, Frank W, and Anthony A Gaspari. "Natural Rubber Latex Protein Reduction with an Emphasis on Enzyme Treatment." *Methods* 27, no. 1 (2002): 77-86.https://doi.org/10.1016/S1046-2023(02)00055-5

124. Suwatthanarak, Thanawat, Bhumin Than-ardna, Duangkamol Danwanichakul, and Panu Danwanichakul. "Synthesis of Silver Nanoparticles in Skim Natural Rubber Latex at Room Temperature." *Mater Lett* 168 (2016): 31-35.https://doi.org/10.1016/j.matlet.2016.01.026

125. Than-ardna, Bhumin, Hiroshi Tamura, and Tetsuya Furuike. "Improving

Deproteinized Skim Natural Rubber Latex with a Further Leaching Process." *Eng Appl Sci Res* 46, no. 1 (2019): 64-71

126. Sriring, Manus, Adun Nimpaiboon, Nattanee Dechnarong, Sirirat Kumarn, Yuji Higaki, Ken Kojio, Atsushi Takahara, Chee Cheong Ho, and Jitladda Sakdapipanich. "Pre-Vulcanization of Large and Small Natural Rubber Latex Particles: Film-Forming Behavior and Mechanical Properties." *Macromol Mater Eng* 304, no. 9 (2019): 1900283.https://doi.org/10.1002/mame.201900283

127. Nimpaiboon, Adun, Sureerut Amnuaypornsri, and Jitladda Sakdapipanich. "Influence of Gel Content on the Physical Properties of Unfilled and Carbon Black Filled Natural Rubber Vulcanizates." *Polym Test* 32, no. 6 (2013): 1135-44.https://doi.org/10.1016/j.polymertesting.2013.07.003

128. Ramana, CH VV, Williem Clarke, J Jayaramudu, Rotimi Sadiku, and SS Ray. "Dielectric Properties of Polycarbonate Coated Natural Fabric Grewia Tilifolia." Paper presented at the 2011 INTERNATIONAL CONFERENCE ON RECENT ADVANCEMENTS IN ELECTRICAL, ELECTRONICS AND CONTROL ENGINEERING 2011.

129. Anju, VP, and Sunil K Narayanankutty. "Polyaniline Coated Cellulose Fiber/Polyvinyl Alcohol Composites with High Dielectric Permittivity and Low Percolation Threshold." *AIP Advances* 6, no. 1 (2016): 015109.https://doi.org/10.1063/1.4940664

130. Potivara, Kornkamol, and Muenduen Phisalaphong. "Development and Characterization of Bacterial Cellulose Reinforced with Natural Rubber." *Materials* 12, no. 14 (2019): 2323.https://doi.org/10.3390/ma12142323

131. Li, Guohui, Avinav G Nandgaonkar, Youssef Habibi, Wendy E Krause, Qufu Wei, and Lucian A Lucia. "An Environmentally Benign Approach to Achieving Vectorial Alignment and High Microporosity in Bacterial Cellulose/Chitosan Scaffolds." *RSC advances* 7, no. 23 (2017): 13678-88.https://doi.org/10.1039/C6RA26049G

132. Suratago, Theerawat, Siriporn Taokaew, Nitisak Kanjanamosit, Kijchai Kanjanaprapakul, Vorakan Burapatana, and Muenduen Phisalaphong. "Development of Bacterial Cellulose/Alginate Nanocomposite Membrane for Separation of Ethanol–Water Mixtures." *J Ind Eng Chem* 32 (2015): 305-12.https://doi.org/10.1016/j.jiec.2015.09.004

133. Lai, Cheng-Lee, Rey-May Liou, Shih-Hsiung Chen, Chi-Yu Shih, JS Chang, Cheng-Hsien Huang, Mu-Ya Hung, and Kueir-Rarn Lee. "Dehydration of Ethanol/Water Mixture by Asymmetric Ion-Exchange Membranes." *Desalination* 266, no. 1-3 (2011): 17-24.https://doi.org/10.1016/j.desal.2010.07.062

134. Sriring, Manus, Adun Nimpaiboon, Sirirat Kumarn, Atsushi Takahara, and Jitladda Sakdapipanich. "Enhancing Viscoelastic and Mechanical Performances of Natural Rubber through Variation of Large and Small Rubber Particle Combinations." *Polym Test* 81 (2020): 106225.https://doi.org/10.1016/j.polymertesting.2019.106225

135. Guidelli, Eder José, Ana Paula Ramos, Maria Elisabete D Zaniquelli, and Oswaldo Baffa. "Green Synthesis of Colloidal Silver Nanoparticles Using Natural Rubber Latex Extracted from Hevea Brasiliensis." *Spectrochim. Acta, Part A* 82, no. 1 (2011): 140-45.https://doi.org/10.1016/j.saa.2011.07.024

136. Kalapat, Nanticha, Ladawan Watthanachote, and Thirawan Nipithakul. "Extraction and Characterization of Proteins from Skim Rubber." *Agriculture and Natural Resources* 43, no. 5 (2009): 319-25

137. Nun-anan, Phattarawadee, Suwaluk Wisunthorn, Skulrat Pichaiyut, Chatchamon Daengkanit Nathaworn, and Charoen Nakason. "Influence of Nonrubber Components on Properties of Unvulcanized Natural Rubber." *Polym Adv Technol* 31, no. 1 (2020): 44-59.https://doi.org/10.1002/pat.4746

138. Azeredo, Henriette, Hernane Barud, Cristiane S Farinas, Vanessa M Vasconcellos, and Amanda M Claro. "Bacterial Cellulose as a Raw Material for Food and Food Packaging Applications." *Frontiers in Sustainable Food Systems* 3 (2019): 7. https://doi.org/10.3389/fsufs.2019.00007

139. Chen, Si-Qian, Patricia Lopez-Sanchez, Dongjie Wang, Deirdre Mikkelsen, and Michael J Gidley. "Mechanical Properties of Bacterial Cellulose Synthesised by Diverse Strains of the Genus Komagataeibacter." *Food Hydrocolloids* 81 (2018): 87-95.https://doi.org/10.1016/j.foodhyd.2018.02.031

140. Portela, Raquel, Catarina R Leal, Pedro L Almeida, and Rita G Sobral. "Bacterial Cellulose: A Versatile Biopolymer for Wound Dressing Applications." *Microb Biotechnol* 12, no. 4 (2019): 586-610.https://doi.org/10.1111/1751-7915.13392

141. Ahmad, Mohd Rozi, Nur Awatif Ahmad, Suraya Ahmad Suhaimi, Nor Azreen Abu Bakar, Wan Yunus Wan Ahmad, and Jamil Salleh. "Tensile and Tearing Strength of Uncoated and Natural Rubber Latex Coated High Strength Woven Fabrics." Paper presented at the 2012 IEEE Symposium on Humanities, Science and Engineering Research 2012.

142. Egbujuo, Wisdom Okechukwu, Placid Ikechukwu Anyanwu, and Henry Chinedu Obasi. "Utilization of Chitin Powder as a Filler in Natural Rubber Vulcanizates: In Comparison with Carbon Black Filler." *International Review of Applied Sciences and Engineering* 11, no. 1 (2020): 43-51.https://doi.org/10.1556/1848.2020.00006

143. Amnuaypornsri, Sureerut, Jitladda Sakdapipanich, and Yasuyuki Tanaka. "Green Strength of Natural Rubber: The Origin of the Stress–Strain Behavior of Natural Rubber." *J Appl Polym Sci* 111, no. 4 (2009): 2127-33. https://doi.org/10.1002/app.29226

144. Nun-anan, Phattarawadee, Suwaluk Wisunthorn, Skulrat Pichaiyut, Norbert Vennemann, and Charoen Nakason. "Novel Approach to Determine Non-Rubber Content in Hevea Brasiliensis: Influence of Clone Variation on Properties of Un-Vulcanized Natural Rubber." *Industrial crops products* 118 (2018): 38-47.https://doi.org/10.1016/j.indcrop.2018.03.011

145. Trovatti, Eliane, Antonio JF Carvalho, Sidney JL Ribeiro, and Alessandro Gandini. "Simple Green Approach to Reinforce Natural Rubber with Bacterial Cellulose Nanofibers." *Biomacromolecules* 14, no. 8 (2013): 2667-74.https://doi.org/10.1021/bm400523h

146. Saowapark, Thanunya, Ekrachan Chaichana, and Adisak Jaturapiree. "Properties of Natural Rubber Latex Filled with Bacterial Cellulose Produced from Pineapple Peels." *JMMM* 27, no. 2 (2017).DOI: 10.14456/jmmm.2017.12

147. Rosli, Noor Afizah, Ishak Ahmad, Farah Hannan Anuar, and Ibrahim Abdullah. "Effectiveness of Cellulosic Agave Angustifolia Fibres on the Performance of

Compatibilised Poly (Lactic Acid)-Natural Rubber Blends." *Cellulose* 26, no. 5 (2019): 3205-18.https://doi.org/10.1007/s10570-019-02262-x

148. Berthelot, Karine, Sophie Lecomte, Yannick Estevez, Vanessa Zhendre, Sarah Henry, Julie Thévenot, Erick J Dufourc, Isabel D Alves, and Frédéric Peruch. "Rubber Particle Proteins, Hbref and Hbsrpp, Show Different Interactions with Model Membranes." *Biochim Biophys Acta* 1838, no. 1 (2014): 287-99.https://doi.org/10.1016/j.bbamem.2013.08.025

149. Xu, Lili, Cheng Huang, Mingchao Luo, Wei Qu, Han Liu, Zhewei Gu, Liumei Jing, Guangsu Huang, and Jing %J Rsc Advances Zheng. "A Rheological Study on Non-Rubber Component Networks in Natural Rubber." *J Rsc Advances* 5, no. 111 (2015): 91742-50.https://doi.org/10.1039/C5RA07428B

150. Danwanichakul, Panu, and Bhumin Than-ardna. "Permeation of Salicylic Acid through Skim Natural Rubber Films." *Ind Crops Prod* 122 (2018): 166-73.https://doi.org/10.1016/j.indcrop.2018.05.066

151. Sintharm, Praewpakun, and Muenduen Phisalaphong. "Green Natural Rubber Composites Reinforced with Black/White Rice Husk Ashes: Effects of Reinforcing Agent on Film's Mechanical and Dielectric Properties." *Polymers* 13, no. 6 (2021): 882.https://doi.org/10.3390/polym13060882

152. Alvarez, Vera Alejandra, RA Ruseckaite, and A Vazquez. "Degradation of Sisal Fibre/Mater Bi-Y Biocomposites Buried in Soil." *Polym Degrad Stab* 91, no. 12 (2006): 3156-62.https://doi.org/10.1016/j.polymdegradstab.2006.07.011

153. Wan, YZ, Honglin Luo, F He, H Liang, Y Huang, and XL Li. "Mechanical, Moisture Absorption, and Biodegradation Behaviours of Bacterial Cellulose Fibre-Reinforced Starch Biocomposites." *Compos Sci Technol* 69, no. 7-8 (2009): 1212-17.https://doi.org/10.1016/j.compscitech.2009.02.024

154. Camargo, Michely Sayumi Alves, Ana Paula Cercal, Victoria Fonseca Silveira, Ketlin Critine Batista Mancinelli, Regina Maria Miranda Gern, Michele Cristina Formolo Garcia, Giannini Pasiznick Apati, Andrea Lima dos Santos Schneider, and Ana Paula Testa Pezzin. "Evaluation of Wet Bacterial Cellulose Degradation in Different Environmental Conditions." Paper presented at the Macromolecular Symposia 2020.

155. Schröpfer, Suellen Brasil, Marcia Karpinski Bottene, Liane Bianchin, Luiz Carlos Robinson, Viviane de Lima, Vanusca Dalosto Jahno, Hernane da Silva Barud, and Sidney José Lima Ribeiro. "Biodegradation Evaluation of Bacterial Cellulose, Vegetable Cellulose and Poly (3-Hydroxybutyrate) in Soil." *Polímeros* 25, no. 2 (2015): 154-60.https://doi.org/10.1590/0104-1428.1712

156. Bras, Julien, Mohammad L Hassan, Cecile Bruzesse, Enas A Hassan, Nahla A El-Wakil, and Alain Dufresne. "Mechanical, Barrier, and Biodegradability Properties of Bagasse Cellulose Whiskers Reinforced Natural Rubber Nanocomposites." *Industrial crops products* 32, no. 3 (2010): 627-33.https://doi.org/10.1016/j.indcrop.2010.07.018

157. Mastalygina, Elena, Ivetta Varyan, Natalya Kolesnikova, Maria Isabel Cabrera Gonzalez, and Anatoly Popov. "Effect of Natural Rubber in Polyethylene Composites on Morphology, Mechanical Properties and Biodegradability." *Polymers* 12, no. 2 (2020): 437.https://doi.org/10.3390/polym12020437

158. O-Rak, K, E Phakdeepataraphan, N Bunnak, S Ummartyotin, M Sain, and H Manuspiya. "Development of Bacterial Cellulose and Poly (Vinylidene Fluoride)

Binary Blend System: Structure and Properties." *Chem Eng J* 237 (2014): 396-402.https://doi.org/10.1016/j.cej.2013.10.032

159. Liu, Jie, Siwu Wu, Zhenghai Tang, Tengfei Lin, Baochun Guo, and Guangsu Huang. "New Evidence Disclosed for Networking in Natural Rubber by Dielectric Relaxation Spectroscopy." *Solf Matter* 11, no. 11 (2015): 2290-99.https://doi.org/10.1039/C4SM02521K

160. Shakun, Alexandra, Essi Sarlin, and Jyrki Vuorinen. "Energy Dissipation in Natural Rubber Latex Films: The Effect of Stabilizers, Leaching and Acetone-Treatment." *J Appl Polym Sci* 138, no. 1 (2021): 49609. https://doi.org/10.1002/app.49609

161. Kosumphan, Huda, Sahapong Somwong, and Mitchai Chongcheawchamnan. "Electrical Characteristics of Pure and Contaminated Latex Serum." *Songklanakarin Journal of Science Technology* 40, no. 3 (2018).10.14456/sjst-psu.2018.41

APPENDIX

Table A 1 Data for Figure 4.10, thickness of NR composites

Sample	Thickness (mm)	
	Average	S.D.
NR	0.21	0.02
NR-B20	0.48	0.00
NR-B60	0.55	0.03
NR-B100	0.58	0.02
NR-T20	0.46	0.03
NR-T60	0.51	0.02
NR-T100	0.63	0.03
NR-W20	0.42	0.02
NR-W60	0.54	0.02
NR-W100	0.66	0.01
NR-BC20	0.46	0.02
NR-BC60	0.55	0.03
NR-BC100	0.63	0.04
NR-TC20	0.46	0.01
NR-TC60	0.58	0.04
NR-TC100	0.65	0.04
NR-WC20	0.40	0.02
NR-WC60	0.52	0.02
NR-WC100	0.64	0.01
NR-BS100	0.65	0.08
NR-TS100	0.65	0.07
NR-WS100	0.64	0.07

Table A 2 Data for Figure 4.11, mechanical properties of NR composites

Sample	Young's modulus (MPA)		Tensile strength (Mpa)		Elongation at break (%)	
	Average	S.D.	Average	S.D.	Average	S.D.
NR	2.07	0.55	1.02	0.05	113.30	12.56
NR-B20	10.82	1.11	4.91	0.11	392.00	22.63
NR-B60	34.70	11.04	5.50	0.22	333.20	23.31
NR-B100	61.07	3.66	6.58	0.32	180.00	23.25
NR-T20	7.34	1.37	4.88	0.15	348.67	29.23
NR-T60	14.13	2.66	6.71	0.44	364.67	24.73
NR-T100	12.41	2.03	4.90	0.49	175.50	23.51
NR-W20	7.44	0.46	4.18	0.19	267.00	7.76
NR-W60	11.54	1.14	10.02	0.81	302.70	29.19
NR-W100	115.57	4.25	10.44	0.56	149.00	16.31
NR-BC20	4.29	0.19	2.44	0.28	348.00	14.24
NR-BC60	11.04	0.64	2.84	0.13	277.90	10.20
NR-BC100	58.43	4.45	3.24	0.22	173.53	10.28
NR-TC20	6.86	0.50	2.35	0.11	280.07	14.93
NR-TC60	13.90	1.72	5.47	0.36	338.00	36.11
NR-TC100	12.57	0.39	4.46	0.26	156.00	18.29
NR-WC20	14.03	0.61	4.44	0.08	221.13	8.17
NR-WC60	13.41	1.77	11.51	0.43	264.07	27.02
NR-WC100	108.57	3.48	13.07	0.35	199.10	9.20
NR-BS100	66.11	0.96	11.67	0.90	216.80	24.81
NR-TS100	57.90	4.38	11.37	0.51	192.80	23.82
NR-WS100	108.62	0.25	13.20	0.25	175.98	25.32

Table A 3 Data for Figure 4.12, water absorption capacity of NR composites

Day	NR		20 phr				60 phr	
	NR	S.D.	NR-B20	S.D.	NR-BC20	S.D.	NR-B60	S.D.
0	0.0000	0.0000	0.0000	0.0000	0.0000	0.0000	0.0000	0.0000
2	16.6031	1.6354	36.7196	1.8394	42.2484	0.4694	40.9679	3.8641
4	26.9349	1.5133	38.2922	1.9429	38.3761	1.1120	43.4319	2.4182
6	31.0902	2.2986	40.1543	2.2039	37.6979	0.0379	43.8380	2.2272
8	32.5459	1.6538	41.3860	2.5132	37.5090	1.3724	45.6843	2.5967
10	34.2682	1.1858	42.5701	2.4711	38.4520	1.0358	46.3231	2.3373
12	35.7389	1.0769	40.8325	1.1473	38.3624	1.7993	47.4715	1.3703
14	36.8337	1.1363	41.9172	1.1886	37.9068	1.6484	47.5385	1.3324
16	37.8005	1.0492	42.5698	1.4641	39.0617	1.7065	49.1882	0.4671
18	38.7776	1.2329	43.4716	2.1669	36.2867	1.2470	52.6822	2.3645

Day	60 phr		100 phr					
	NR-BC60	S.D.	NR-B100	S.D.	NR-BC100	S.D.	NR-BS100	S.D.
0	0.0000	0.0000	0.0000	0.0000	0.0000	0.0000	0.0000	0.0000
2	58.7158	0.5552	42.1199	2.0426	71.7267	1.9251	32.7536	1.9536
4	58.9781	0.4118	43.6926	2.4539	72.1974	1.8781	32.9028	1.8911
6	59.5819	0.2041	45.6794	1.4444	72.7243	2.2757	35.9327	1.7680
8	60.8354	1.3674	46.7864	1.7188	72.1681	1.6763	37.6430	1.6195
10	62.1299	1.8955	47.9705	1.7547	73.0949	2.5600	39.0756	2.0958
12	62.3478	2.1134	48.3110	1.7681	73.5177	0.5979	40.9607	1.0783
14	62.8697	1.8688	49.5221	1.1942	74.4391	1.0570	41.6500	0.7795
16	63.2721	1.1891	50.8240	1.1707	74.9053	2.2133	42.6861	0.0037
18	63.2236	0.9603	51.8350	0.2635	72.3137	1.2610	43.0504	0.2034

Day	20 phr				60 phr			
	NR-T20	S.D.	NR-TC20	S.D.	NR-T60	S.D.	NR-TC60	S.D.
0	0.0000	0.0000	0.0000	0.0000	0.0000	0.0000	0.0000	0.0000
2	40.7122	1.8597	43.0496	1.5492	55.7311	0.0795	65.3249	1.7964
4	51.0294	1.8032	42.5318	0.3019	57.8246	0.2206	61.5422	2.1875
6	52.5407	2.1719	43.7874	0.8932	59.8621	0.1778	68.3526	1.6428
8	54.8181	2.1816	46.1289	1.6426	62.6957	0.0702	74.5031	0.5393
10	57.4378	1.1377	47.2665	3.5972	63.7228	0.6244	80.2763	2.6151
12	58.4007	1.1747	50.3651	2.2052	67.4785	1.3881	81.0911	2.7222
14	60.6461	2.7144	50.0704	0.9161	69.8808	0.1335	88.3232	2.3887
16	61.0474	2.6078	50.3829	1.2151	72.4266	1.7484	91.2488	2.9287
18	62.2471	3.5122	53.5526	1.9503	74.9313	0.4632	93.8094	3.3774

Day	100 phr					
	NR-T100	S.D.	NR-TC100	S.D.	NR-TS100	S.D.
0	0.0000	0.0000	0.0000	0.0000	0.0000	0.0000
2	54.1772	0.3740	98.5725	0.4250	27.3280	0.6337
4	55.3809	0.3836	109.9637	1.4711	25.1139	3.5672
6	57.1214	0.8156	110.1518	1.3771	25.6941	3.4665
8	58.1197	0.4981	111.0605	0.8756	27.5025	3.8644
10	60.5545	1.9724	112.0946	0.0959	28.7087	4.0491
12	62.9328	1.0652	115.0553	2.1440	40.5772	5.8496
14	66.3116	1.2264	116.8726	2.2063	40.7461	5.8726
16	68.1134	0.3874	120.2256	0.0752	41.2551	5.6034
18	70.7951	1.6509	139.2137	1.3378	41.4000	5.6024

Day	20 phr				60 phr			
	NR-W20	S.D.	NR-WC20	S.D.	NR-W60	S.D.	NR-WC60	S.D.
0	0.0000	0.0000	0.0000	0.0000	0.0000	0.0000	0.0000	0.0000
2	29.6724	1.2001	38.0591	0.9427	40.5907	2.4966	7.3421	3.5685
4	31.6107	1.6107	39.4158	1.3729	44.2228	1.8877	6.0217	3.3712
6	33.0458	1.5180	39.5156	1.7044	45.0634	1.6046	6.4133	2.7745
8	37.2754	3.6642	41.0606	0.9911	48.6518	2.0000	6.9192	2.9659
10	38.3361	4.1695	41.1833	1.5770	50.5343	0.5974	7.1702	2.6329
12	39.4491	3.6158	41.0853	1.3053	51.9933	0.9341	7.5315	2.2306
14	40.2689	2.9078	41.9706	0.9746	53.4530	2.3464	8.6790	1.9854
16	41.8988	2.7321	44.2733	0.1506	53.8426	2.7482	7.5970	2.2061
18	44.3871	0.9149	42.0210	0.6777	54.2804	2.6432	8.8675	2.0841

Day	100 phr					
	NR-W100	S.D.	NR-WC100	S.D.	NR-WS100	S.D.
0	0.0000	0.0000	0.0000	0.0000	0.0000	0.0000
2	71.8670	1.6081	7.0179	0.3756	19.0516	0.5217
4	71.8950	1.6360	7.5841	0.4569	20.1595	0.3592
6	72.3127	1.2183	8.0044	0.4470	20.8976	0.2989
8	73.2341	1.3043	8.6115	0.1224	22.2772	0.2824
10	73.8902	1.3756	8.8928	0.3079	24.3848	0.9424
12	75.1887	1.5880	9.6712	0.3036	28.3495	0.3766
14	76.0107	0.9898	9.8291	1.0295	30.7895	0.7895
16	78.2416	0.0461	9.9456	0.7288	32.6863	1.2886
18	78.5072	0.2281	10.8193	1.0375	34.0371	0.7385

Table A 4 Data for Figure 4.13, Toluene uptake

Time (h)	NR		20 phr			
	NR	S.D.	NR-B20	S.D.	NR-BC20	S.D.
0	0.0000	0.0000	0.0000	0.0000	0.0000	0.0000
1	772.9218	58.4149	251.2075	16.2423	189.1916	14.4140
2	910.0965	48.2139	323.3476	15.0820	271.6824	30.1741
3	1207.5405	52.5124	480.9549	34.9043	399.2860	33.4269
4	1746.4370	32.5941	534.3663	51.0056	458.7393	64.4692
8	-	-	-	-	495.3936	80.0472

Time (h)	60 phr			
	NR-B60	S.D.	NR-BC60	S.D.
0	0.0000	0.0000	0.0000	0.0000
1	90.1199	8.9400	204.8128	31.7858
2	147.9511	17.5694	277.9815	25.9354
3	207.3744	40.9902	320.7285	20.1688
4	250.0026	35.1159	352.7449	16.2272
8	294.0361	37.0334	344.1946	15.6450

Time (h)	100 phr					
	NR-B100	S.D.	NR-BC100	S.D.	NR-BS100	S.D.
0	0.0000	0.0000	0.0000	0.0000	0.0000	0.0000
1	82.4485	4.2541	56.1408	13.0208	133.3828	13.3617
2	101.6862	11.1015	92.2788	28.5624	142.0260	18.0827
3	131.3138	59.2049	99.7991	4.8942	166.6563	21.7931
4	208.6028	19.7130	133.2478	25.7856	176.7340	17.7176
8	257.7231	13.4396	180.2885	33.1006	181.4120	21.8872

Time (h)	20 phr				60 phr			
	NR-T20	S.D.	NR-TC20	S.D.	NR-T60	S.D.	NR-TC60	S.D.
0	0.0000	0.0000	0.0000	0.0000	0.0000	0.0000	0.0000	0.0000
1	253.9924	13.9997	318.1039	4.9662	142.1502	18.8577	246.7489	3.6820
2	339.7323	8.3341	324.4066	32.4615	207.6059	5.3330	256.0314	8.9384
3	467.5145	40.4601	355.5246	5.3532	245.4336	8.7916	265.0169	5.3971
4	547.5176	28.2326	391.7236	7.4157	294.1065	10.3686	274.5239	4.7759
8	-	-	403.5177	4.7482	305.1011	11.2274	290.0994	6.1814

Time (h)	100 phr					
	NR-T100	**S.D.**	**NR-TC100**	**S.D.**	**NR-TS100**	**S.D.**
0	0.0000	0.0000	0.0000	0.0000	0.0000	0.0000
1	108.4812	10.0285	57.4813	17.7238	137.0057	4.7052
2	162.8344	19.8377	62.6734	22.3322	158.5227	5.3789
3	195.3348	7.2309	100.5892	25.1865	170.2141	3.8018
4	230.4826	19.4247	138.0385	22.8685	197.0433	8.6546
8	271.4991	4.1597	173.5976	15.7141	205.4659	4.8698

Time (h)	20 phr				60 phr			
	NR-W20	**S.D.**	**NR-WC20**	**S.D.**	**NR-W60**	**S.D.**	**NR-WC60**	**S.D.**
0	0.0000	0.0000	0.0000	0.0000	0.0000	0.0000	0.0000	0.0000
1	468.4671	33.8337	276.0483	70.1322	180.1761	34.6185	98.9730	24.4927
2	544.8595	34.8751	376.5668	41.8118	211.0376	17.9965	121.6531	17.9955
3	566.7988	42.2278	391.1162	39.5194	234.5213	15.3465	146.3868	21.8698
4	646.2335	50.7577	421.1785	45.0188	247.2943	9.2487	177.0394	16.8366
8	-	-	665.6520	28.1944	253.6398	13.2576	215.1795	7.7853

Time (h)	100 phr					
	NR-W100	**S.D.**	**NR-WC100**	**S.D.**	**NR-WS100**	**S.D.**
0	0.0000	0.0000	0.0000	0.0000	0.0000	0.0000
1	95.5010	2.3140	67.8792	16.0885	86.8400	37.9792
2	162.3772	13.2823	133.3241	12.0742	98.4164	39.0785
3	191.9265	17.4032	150.7026	10.5882	111.8697	44.5034
4	220.3242	13.9926	163.0388	9.2858	172.1540	29.6922
8	297.7411	6.8104	169.7255	8.8168	181.9419	19.4205

Table A 5 Data for Figure 4.14, weight loss of biodegradation in soil test

Sample	% Weight loss					
	1 month		2 months		3 months	
	Average	S.D.	Average	S.D.	Average	S.D.
NR	2.0814	0.4811	3.8891	0.5369	5.3162	0.2471
NR-B20	3.2708	0.5337	6.4982	0.6728	7.5727	0.4598
NR-B60	4.9364	0.7686	7.9902	1.1086	10.0472	0.7192
NR-B100	5.8158	0.4362	8.3184	0.4181	11.0320	0.1411
NR-BC20	2.6826	0.0423	6.0901	0.4947	8.2254	0.9143
NR-BC60	3.9628	0.3983	6.0901	0.7091	11.6707	0.1411
NR-BC100	4.9501	0.5887	11.1457	0.8566	13.0131	0.3267
NR-BS100	2.6826	0.1791	6.4495	0.4715	9.0252	0.7075
NR-T20	3.9998	0.5458	5.0918	0.2381	8.0888	0.7531
NR-T60	5.9769	0.3627	8.4132	0.6745	10.4910	0.1028
NR-T100	6.6614	0.7977	9.0598	0.3086	13.4341	0.2970
NR-TC20	2.9424	0.7419	7.5029	0.3048	9.9729	0.6273
NR-TC60	5.6095	0.1571	7.5029	0.7941	12.8143	0.2970
NR-TC100	6.3819	0.6514	10.2811	0.6785	14.5567	0.2913
NR-TS100	3.8636	0.1571	5.5107	0.5903	9.8436	0.2872
NR-W20	4.5299	1.2827	6.3603	0.2544	7.5570	0.4297
NR-W60	5.4603	1.1061	8.1506	0.2247	9.4170	0.2334
NR-W100	11.2526	0.4540	15.8581	0.2478	18.3704	0.3533
NR-WC20	6.5934	0.2627	7.2748	1.3421	11.5609	0.1893
NR-WC60	5.2253	0.7579	7.2748	1.1340	15.8173	0.3533
NR-WC100	3.1494	0.2164	6.1310	0.5781	13.2289	0.9541
NR-WS100	1.4834	0.4366	4.4818	0.5313	7.5533	0.9648

Table A 6 Data for Figure 5.4, thickness of BC, SNR-BC and FNR-BC composites

Samples	Thickness (mm)		Samples	Thickness (mm)	
	Average	S.D.		Average	S.D.
BC	0.0217	0.0024	BC	0.0217	0.0024
1SNR-BC50	0.0400	0.0032	1SNR-BC60	0.0500	0.0021
2.5SNR-BC50	0.0620	0.0027	2.5SNR-BC60	0.0670	0.0045
5SNR-BC50	0.1117	0.0029	5SNR-BC60	0.1250	0.0051
1FNR-BC50	0.0338	0.0022	1FNR-BC60	0.0400	0.0019
2.5FNR-BC50	0.0390	0.0025	2.5FNR-BC60	0.0583	0.0029
5FNR-BC50	0.0563	0.0041	5FNR-BC60	0.0675	0.0023

Table A 7 Data for Figure 5.5, dry weight of BC composite films

Samples	Dry weight (g)				Samples	Dry weight (g)	
	BC	S.D.	NR	S.D.		NR	S.D.
BC	0.2488	0.00985	0.0000	0.0000	BC	0.0000	0.0000
1SNR-BC50	0.2488	0.00985	0.1673	0.0087	1SNR-BC60	0.2910	0.0248
2.5SNR-BC50	0.2488	0.00985	0.7500	0.0392	2.5SNR-BC60	0.6500	0.0144
5SNR-BC50	0.2488	0.00985	1.4413	0.0976	5SNR-BC60	1.6201	0.0605
1FNR-BC50	0.2488	0.00985	0.0885	0.0307	1FNR-BC60	0.2375	0.0000
2.5FNR-BC50	0.2488	0.00985	0.1168	0.0336	2.5FNR-BC60	0.3575	0.0204
5FNR-BC50	0.2488	0.00985	0.2028	0.0090	5FNR-BC60	0.6636	0.0077

Table A 8 Data for Figure 5.5, elongation at break of BC composite films

Samples	Elongation at break (%)		Samples	Elongation at break (%)	
	Average	S.D.		Average	S.D.
BC	1.482	0.152	BC	1.482	0.152
1SNR-BC50	1.872	0.336	1SNR-BC60	1.820	0.093
2.5SNR-BC50	15.063	1.288	2.5SNR-BC60	14.550	1.853
5SNR-BC50	17.620	0.965	5SNR-BC60	28.033	2.120
1FNR-BC50	1.613	0.052	1FNR-BC60	1.635	0.057
2.5FNR-BC50	2.417	0.224	2.5FNR-BC60	2.847	0.056
5FNR-BC50	3.340	0.279	5FNR-BC60	3.763	0.427

Table A 9 Data for Figure 5.5, tensile strength of BC composite films

Samples	Tensile strength (Mpa)		Samples	Tensile strength (Mpa)	
	Average	S.D.		Average	S.D.
BC	107.033	7.380	BC	107.033	7.380
1SNR-BC50	119.267	4.833	1SNR-BC60	79.725	5.101
2.5SNR-BC50	123.120	8.839	2.5SNR-BC60	66.133	12.209
5SNR-BC50	52.150	7.234	5SNR-BC60	86.633	1.159
1FNR-BC50	100.638	6.652	1FNR-BC60	67.667	6.527
2.5FNR-BC50	127.533	11.029	2.5FNR-BC60	120.150	7.850
5FNR-BC50	177.467	5.682	5FNR-BC60	83.650	1.450

Table A 10 data for Figure 5.5, young' s modulus of BC composite films

Samples	Young's modulus (MPa)		Samples	Young's modulus (MPa)	
	Average	S.D.		Average	S.D.
BC	11201.333	521.376	BC	11201.33	521.376
1SNR-BC50	6935.667	664.166	1SNR-BC60	5722.000	220.697
2.5SNR-BC50	1871.667	44.432	2.5SNR-BC60	2347.250	326.273
5SNR-BC50	721.333	140.479	5SNR-BC60	1067.333	3.300
1FNR-BC50	5595.667	411.270	1FNR-BC60	4823.333	723.653
2.5FNR-BC50	7921.667	724.540	2.5FNR-BC60	8777.667	529.002
5FNR-BC50	13323.000	238.130	5FNR-BC60	6129.500	428.303

Table A 11 Data for Figure 5.8, water absorption capacity of BC composite films

Day	Water absorption capacity (%)							
	BC	S.D.	SNR	S.D.	1SNR-BC50	S.D.	2.5SNR-BC50	S.D.
0	0.0000	0.0000	0.0000	0.0000	0.0000	0.0000	0.0000	0.0000
2	442.6282	32.3718	29.6034	0.7698	247.0429	2.2429	132.3939	20.0651
4	680.1113	18.5729	36.1795	2.7829	261.1857	7.6143	141.9829	10.4761
6	695.6646	16.1775	39.6711	4.4223	269.3000	4.3000	179.2144	3.8045
8	706.0897	18.9103	40.2202	4.5942	309.2665	7.2941	181.1011	5.6913
10	742.1559	3.9980	40.4987	4.8184	326.3815	17.0252	190.8599	7.2533
12	771.4238	0.3711	40.5618	4.8425	388.1717	4.6855	190.0103	6.2017
14	801.5013	15.6039	40.6131	4.8501	413.1000	21.9000	218.8637	10.6445
16	809.8853	11.1673	40.6327	4.8335	427.5286	20.3286	228.1608	14.4622

Day	Water absorption capacity (%)							
	5SNR-BC50	S.D.	1SNR-BC60	S.D.	2.5SNR-BC60	S.D.	5SNR-BC60	S.D.
0	0.0000	0.0000	0.0000	0.0000	0.0000	0.0000	0.0000	0.0000
2	116.3373	5.9364	180.2451	8.4170	179.9237	29.3355	158.7178	7.0229
4	128.5079	0.7851	237.4774	1.7631	204.8529	20.1471	169.9780	11.5035
6	141.5992	9.9160	255.3345	16.0940	247.1122	3.5937	176.3026	14.4382
8	143.5894	20.4179	273.0741	9.7830	258.6656	3.3715	183.1607	9.4319
10	152.0452	4.5205	280.9132	6.2297	275.0599	3.7636	214.6657	21.4454
12	169.0869	8.6909	328.4177	18.4177	295.0327	6.1438	229.4335	25.1962
14	177.0777	7.7708	350.7685	15.0542	304.1558	8.7854	240.7721	31.4501
16	187.0887	8.8709	373.6528	25.0814	308.8824	8.8824	247.1751	36.1582

Day	Water absorption capacity (%)							
	FNR	S.D.	1FNR-BC50	S.D.	2.5FNR-BC50	S.D.	5FNR-BC50	S.D.
0	0.0000	0.0000	0.0000	0.0000	0.0000	0.0000	0.0000	0.0000
2	25.7655	3.6659	292.0500	17.4738	160.0098	8.0908	152.9836	7.0299
4	35.8634	4.2091	419.5735	2.1132	179.1894	26.8118	163.6999	17.5628
6	41.2708	7.7622	498.5099	9.9557	183.5865	31.3542	168.9509	16.2109
8	37.7356	6.5307	545.6381	17.3249	192.4364	36.1343	174.1298	17.3876
10	37.7521	6.0417	557.8568	15.6881	202.9908	33.7043	178.0543	16.1381
12	37.8321	5.9953	599.7275	4.4894	210.4546	37.6569	185.8385	12.9709
14	37.9089	6.0130	612.0707	1.4887	211.0662	37.5856	186.7491	12.8813
16	37.9866	6.0132	618.9535	3.0804	211.7903	37.3683	187.6742	12.7102

Day	Water absorption capacity (%)					
	1FNR-BC60	S.D.	2.5FNR-BC60	S.D.	5FNR-BC60	S.D.
0	0.0000	0.0000	0.0000	0.0000	0.0000	0.0000
2	210.9725	27.7702	158.9060	30.9490	90.0255	12.4974
4	215.9735	25.3106	170.6483	25.4870	147.3003	14.2728
6	230.9457	12.7228	179.0595	20.4574	150.9422	13.3275
8	247.8828	6.0014	190.0421	24.4507	167.3469	7.4845
10	255.4133	13.0277	212.2682	8.5048	178.5875	18.2664
12	261.5144	17.0615	218.4744	6.6464	180.3969	18.9290
14	273.9115	30.3487	226.6363	11.0449	193.7342	24.4681
16	281.2306	37.0237	228.4089	11.2046	195.1010	24.0001

Table A 12 Data for Figure 5.9, toluene uptake of BC composite films

Time (h)	Toluene uptake (%)							
	SNR	S.D.	BC	S.D.	1SNR-BC50	S.D.	2.5SNR-BC50	S.D.
0	0.0000	0.0000	0.0000	0.0000	0.0000	0.0000	0.0000	0.0000
1	4167.4771	54.5565	3.1979	0.9165	14.0580	0.7246	18.9795	0.6010
2	4924.4350	134.7692	6.4996	0.5434	20.0828	1.8219	24.3981	1.5858
3	-	-	9.9469	2.1804	22.7743	1.0352	30.7919	1.6104
4	-	-	14.6051	1.3618	23.7694	1.4480	31.1919	0.7704
8	-	-	17.5954	1.0152	25.9783	0.9783	37.9819	1.6829

Time (h)	Toluene uptake (%)							
	5SNR-BC50	S.D.	1SNR-BC60	S.D.	2.5SNR-BC60	S.D.	5SNR-BC60	S.D.
0	0.0000	0.0000	0.0000	0.0000	0.0000	0.0000	0.0000	0.0000
1	28.9930	1.4313	10.5596	1.0953	24.1501	0.7643	31.9574	1.8841
2	37.1595	1.4769	17.8493	0.1775	33.1986	0.7675	44.0937	1.9077
3	48.0157	0.1751	21.8523	0.9984	37.8296	1.0965	54.5248	0.3823
4	58.3228	1.2342	25.1090	0.9346	40.5965	0.8449	66.3034	1.7964
8	68.3959	1.2337	29.4166	0.7335	50.1819	1.5374	72.8449	0.6923

Time (h)	Toluene uptake (%)							
	FNR	S.D.	1FNR-BC50	S.D.	2.5FNR-BC50	S.D.	5FNR-BC50	S.D.
0	0.0000	0.0000	0.0000	0.0000	0.0000	0.0000	0.0000	0.0000
1	4621.4452	109.9219	6.4517	0.0297	16.4966	0.1701	21.5552	1.3020
2	5445.6099	152.6730	15.6685	0.0722	21.4097	1.0393	45.3874	1.4480
3	-	-	19.3552	0.0892	30.6784	1.9747	64.8542	0.2973
4	-	-	23.2902	0.5630	40.4214	0.3193	75.8535	0.0959
8	-	-	37.8367	0.7997	45.5499	1.6723	86.8527	0.4891

Time (h)	Toluene uptake (%)					
	1FNR-BC60	S.D.	2.5FNR-BC60	S.D.	5FNR-BC60	S.D.
0	0.0000	0.0000	0.0000	0.0000	0.0000	0.0000
1	15.0093	1.4291	16.3463	1.6929	29.5304	0.5838
2	25.2917	0.6342	25.1890	1.4777	50.1557	0.6508
3	31.8705	1.0063	40.3669	0.7442	75.5688	0.0747
4	34.4749	1.1416	46.0538	1.7239	82.7330	1.9706
8	40.9860	1.4798	54.5819	0.9737	94.2130	0.1418

VITA

NAME	Praewpakun Sintharm
DATE OF BIRTH	2 November 1988
PLACE OF BIRTH	Bangkok
INSTITUTIONS ATTENDED	King Mongkut's Institute of Technology Ladkrabang Chulalongkorn university
HOME ADDRESS	70 Moo 3, Pak Chan Sub-district, Nakhon Luang District, Ayutthaya 13260 Thailand
PUBLICATION	Sintharm, Praewpakun, and Muenduen Phisalaphong. "Green Natural Rubber Composites Reinforced with Black/White Rice Husk Ashes: Effects of Reinforcing Agent on Film's Mechanical and Dielectric Properties." Polymers 13.6 (2021): 882.
AWARD RECEIVED	-

จุฬาลงกรณ์มหาวิทยาลัย
CHULALONGKORN UNIVERSITY